# DETERMINATION OF THE CHANGES OF DROUGHT OCCURRENCE IN MIDDLE EAST AND NORTH AFRICA USING REGIONAL CLIMATE MODELING

by

Fatma Sibel Saygılı

B.S., Physics, Middle East Technical University, 2013

Submitted to the Institute for Graduate Studies in
Science and Engineering in partial fulfillment of
the requirements for the degree of
Master of Science

Graduate Program in Computational Science and Engineering

Boğaziçi University

2017

DETERMINATION OF THE CHANGES OF DROUGHT OCCURRENCE IN MIDDLE EAST AND NORTH AFRICA USING REGIONAL CLIMATE MODELING

APPROVED BY:

Prof. M. Levent Kurnaz .....
(Thesis Supervisor)

Assoc. Prof. Osman Börekçi .....

Assist. Prof. Tuğba Öztürk .....

DATE OF APPROVAL: 17.08.2017

# ACKNOWLEDGEMENTS

I would like to start with expressing my deepest appreciation and respect to my thesis advisor, Prof. M. Levent Kurnaz, who has been the source of my motivation from day one through his infinite love, passion and enthusiasm for his job. I am immeasurably grateful for his generous guidance and support through my master's and his understanding towards his students. It has been a great pleasure studying with him and I thank him from the bottom of my heart.

I thank my İKLİMBU family, Kamil Çöllü, Tuğba Öztürk, M. Tufan Turp, Nazan An, Abdullah Akbaş, Cemre Kassara, Alkor Ezer, and my dearest, closest friend F. Büşra Deler for walking with me on this road to contribute saving our only home yet, the cutest planet ever, lovely Earth.

I thank The Turkish Foundation for Combating Soil Erosion, for Reforestation and the Protection of Natural Habitats (Türkiye Erozyonla Mücadele, Ağaçlandırma ve Doğal Hayatı Koruma Vakfı) for their support for my thesis and expess my appreciation for all their activities in Turkey.

I would like to thank my dearest family Hüseyin Saygılı, Nurcan Saygılı, Serdar Saygılı and Simge Saygılı who have always supported and been there for me through my life. My love for them is indescribable.

I would also like to thank my lovely people Aycan Aracı, Çağrı Kemal Tüzer, Didem Tek, İlknur Özçakıroğlu, Ahu Senem Demiröz, Ahu Senem Demiröz, Didem Bozkurt, Merve Yavuz, Ali Sinanoğlu, Can Kayabek, Berk Aydın and my lovely creatures Kahve and Bulut for their support and friendship.

Life makes me a very happy person thanks to all of you in my life.

# ABSTRACT


## DETERMINATION OF THE CHANGES OF DROUGHT OCCURRENCE IN MIDDLE EAST AND NORTH AFRICA USING REGIONAL CLIMATE MODELING

The Middle East and North Africa (MENA) region has many nations which are among the most vulnerable to drought and any possible reduction in precipitation. Along with the growing populations in the region, the need for freshwater both for domestic and agricultural uses increase tremendously. However, with the unprecedented $CO_2$ increase in the atmosphere since the industrial revolution, the climate of the Earth is changing and MENA region is foreseen to face even worse problems in terms of lack of freshwater.

This study is aimed to determine the future changes of the intensity and frequency of drought occurrences and to provide an early warning system for the countries in the region to better prepare for the possible severe drought conditions. Therefore, firstly the outputs of the MPI-ESM-MR global climate model of the Max Planck Institute for Meteorology are downscaled to 50km for the MENA region by using the Regional Climate Model (RegCM4.4) of the Abdus Salam International Centre for Theoretical Physics (ICTP). To make the future projections for the period 2071-2100 with respect to the 1971-2000 reference period, the worst case emission scenario RCP8.5 is used. Thereafter, the two most useful indices in terms of drought probabilities, the Standardized Precipitation Index (SPI) and Standardized Precipitation Evapotranspiration Index (SPEI) values are calculated to create the spatial distribution maps, which show the changes of drought probabilities.

# ÖZET

## BÖLGESEL İKLİM MODELLEME KULLANILARAK ORTA DOĞU VE KUZEY AFRİKA KURAKLIK DEĞİŞİMLERİNİN BELİRLENMESİ

Orta Doğu ve Kuzey Afrika (MENA) kuraklığa ve yağışta meydana gelebilecek azalmalara en hassas olan uluslara sahip bölgedir. Bölgede artan nüfusla birlikte hane ve tarımsal kullanım için tatlı su ihtiyacı muhteşem ölçüde artmaktadır. Endüstri devriminden itibaren atmosferdeki emsalsiz $CO_2$ artışıyla Dünya'nın iklimi değişmekte ve MENA bölgesinin tatlı su anlamında daha da kötü problemlerle karşılaşacağı öngörülmektedir.

Bu çalışmayla kuraklık oluşumlarının şiddeti ve frekansındaki gelecek değişimlerin belirlenmesi ve bölgedeki ülkelerin olası şiddetli kuraklık koşullarına daha iyi hazırlanabilmesi için erken bir uyarı sistemi sağlanması amaçlanmıştır. Bu sebeple ilk olarak Max Planck Enstitüsü'nün MPI-ESM-MR küresel iklim modelinin çıktıları Abdus Salam Uluslararası Teorik Fizik Merkezi (ICTP)'nin Bölgesel İklim Modeli (RegCM4.4) kullanılarak 50 km çözünürlüğe düşürülmüştür. 1971-2000 referans dönemine göre 2071-2100 dönemi gelecek projeksiyonları için en karamsar emisyon senaryosu RCP8.5 kullanılmıştır. Daha sonra kuraklık olasılıkları anlamında en kullanışlı iki indis olan Standartlaştırılmış Yağış İndisi (SPI) ve Standartlaştırılmış Yağış Evapotiranspirasyon İndisi (SPEI) değerleri hesaplanarak kuraklık olasılıklarındaki değişimleri gösteren alansal dağılım haritaları çizilmiştir.

# TABLE OF CONTENTS

# LIST OF FIGURES

# LIST OF TABLES

# LIST OF ACRONYMS/ABBREVIATIONS

| | |
|---|---|
| AR4 | IPCC Fourth Assessment Report, 2007 |
| AR5 | IPCC Fifth Assessment Report, 2014 |
| ARWR | Actual Renewable Water Resources |
| BAU | Business as Usual |
| CDO | Climate Data Operator |
| CFCs | Chlorofluorocarbons |
| CORDEX | Coordinated Regional Climate Downscaling Experiment |
| ESP | Earth System Physics |
| FAO | Food and Agriculture Organization |
| GCC | Gulf Cooperation Council |
| GCM | General Circulation Model |
| GDP | Gross Domestic Product |
| GrADS | Grid Analysis and Display System |
| ICTP | The Abdus Salam International Centre for Theoretical Physics |
| IPCC | The Intergovernmental Panel on Climate Change |
| MENA | The Middle East North Africa |
| MPI | Max Planck Institute |
| NCAR | National Center for Atmospheric Research |
| NDMC | National Drought Mitigation Center |
| NMHSs | National Meteorological and Hydrological Services |
| NOAA | National Oceanic and Atmospheric Administration |
| PDSI | Palmer Drought Severity Index |
| PET | Potential Evapotranspiration |
| ppm | parts per million |
| RCD | Regional Climate Downscaling |
| RCM | Regional Climate Model |
| RCPs | Representative Concentration Pathways |

| | |
|---|---|
| RegCM4 | Regional Climate Modeling 4 |
| sc-PDSI | Self Calibrated Palmer Drought Severity Index |
| SNR | School of Natural Resources |
| SPEI | Standardized Precipitation Evapotranspiration Index |
| SPI | Standardized Precipitation Index |
| SRES | Special Report on Emissions Scenarios |
| TRWR | Total Renewable Water Resources |
| UNCCD | United Nations Framework Convention to Combat Desertification |
| UNEP | United Nations Environment Programme |
| USDA | United States Department of Agriculture |
| WCRP | World Climate Research Program |
| WMO | World Meteorological Organization |

# 1. INTRODUCTION

Climate change is one of the most significant problems human beings have ever encountered with. After the industrial revolution, greenhouse gas emissions have reached the highest levels of at least 800,000 years with an unprecedented speed. This speed made it almost impossible to adapt to this change for almost all living things. Due to the rising greenhouse gas emissions, the atmosphere and the oceans are warming, the glaciers are shrinking almost worldwide, the total amount of snow and ice in Greenland and Antarctic is diminishing and the sea level is rising. While the warming of the climate system is unequivocal, it has been affecting biosphere in every possible way and therefore affecting all ecological, social and economic systems.

Coming along with the global warming, climate change shows its effects differently in different locations on Earth. While some regions get warmer, some regions get colder. While precipitation increases to dangerous levels leading to floods in some regions, some regions face the threat of severe droughts and some experience both. Since drought is a direct threat to all vital activities, it is crucial to determine the location, duration and severity of the drought and to take the necessary measures in a way that the particular region needs.

Drought events are categorized in the literature depending on their severity and duration. The first one of these is the meteorological drought, which is the beginning of all drought events, and it starts with a decline in precipitation, continues till the groundwater decreases with the rise in evaporation due to the elevated temperatures. Then agricultural drought starts with a decline in soil moisture and pressure on agricultural products arises due to the inadequacy of the minimum water capacity needed by plants. The part where the drought reaches really dangerous levels is when the hydrological drought occurs and its economic, social and environmental consequences are inevitable. As a result of hydrological drought, severe

degradations in supply-demand balances may arise and then lead to socio-economic drought.

Since drought is a disaster that starts slowly and continues slowly, it is difficult to detect and monitor the drought and to determine its severity. Throughout the years, scientists have discussed which drought index could be used for which application in a particular climate. In 2009, 54 delegates representing 22 countries met at the Inter-Regional Workshop on indices and Early Warning Systems for Drought held at the University of Nebraska in the United States with the joint sponsorship of the United States Department of Agriculture (USDA), the United Nations Framework Convention to Combat Desertification (UNCCD), University of Nebraska-Lincoln, School of Natural Resources (SNR), the National Drought Mitigation Center (NDMC), the World Meteorological Organization (WMO), National Oceanic and Atmospheric Administration (NOAA). They reviewed the drought indices used to describe meteorological, agricultural and hydrological droughts in different parts of the world and agreed on the need for a standardized index describing different droughts. The scientists at the workshop recommended the use of Standardized Precipitation Index (SPI) by all National Meteorological and Hydrological Services (NMHSs) to identify the characteristics of the drought along with the other drought indices [1]. Along with the fact that WMO recommended the use of SPI to be able to analyze and monitor drought, Trenberth *et al.* (2014) noted that SPI is useful as a measure of precipitation deficiencies or meteorological drought, but it is limited since it only uses precipitation data and is not interested in evapotranspiration [2]. Therefore, in this study, along with the SPI, Standardized Precipitation Evapotranspiration Index (SPEI), which is a relatively new drought index, is used. SPEI uses the basis of SPI, however, it takes temperature data as well as precipitation data as input, which ensures the index to account for the effect of temperature on drought development.

SPI and SPEI values can be calculated for a month using the monthly total precipitation data from the previous 1 to 72 months. For example, to calculate the 36-month SPI values for a particular month, the average of the total precipitation data of the 36 months prior to that particular month is used. In this way, SPI and SPEI values can be calculated in different time scales, such as 1-month, 3-month 12-month, etc. Guttmann (1994, 1999) reported that the 1-month to 24-month are statistically the best practical range for the application [3, 4]. SPI and SPEI are applicable for all climate regimes and also the results are comparable since they are standardized. They both require at least 30 years of complete dataset for robust outputs.

Therefore, in this study, the outputs of the MPI-ESM-MR global climate model of the Max Planck Institute for Meteorology are downscaled to 50km for the MENA region by using the Regional Climate Model (RegCM4.4) of the Abdus Salam International Centre for Theoretical Physics (ICTP) and then to make the future projections for the period 2071-2100 with respect to the 1971-2000 reference period, the worst case emission scenario that is Representative Concentration Pathway 8.5 (RCP8.5) of the Inter-governmental Panel on Climate Change (IPCC) is used. Thereafter, by using the SPI and SPEI packages of R programing language, the two most useful indices in terms of drought probabilities, the Standardized Precipitation Index (SPI) [5] and Standardized Precipitation Evapotranspiration Index (SPEI) [6] values are calculated in 2 time scales, that are 6-month and 12-month, to create the spatial distribution maps, which show the changes of drought probabilities.

# 2. CLIMATE CHANGE

Climate is the average weather conditions for a place over a long period of time. Changing of a climate for a certain place can take hundreds, thousands of years. UK MET Office defines climate change for Earth as the large scale, long term shift in the planet's weather patterns or average temperatures [7].

During the Earth's 4.5 billion years of history, it has gone through many major climate changes none of which were human induced until the industrial revolution. The major problem of today's climate change lies under the fact that human beings are forcing climate to change and this change is happening with an unprecedented speed.

The last ice age of Earth started about 120000 years ago and started to come to an end about 20000 years ago. During the recovery period from this last glacial maximum, that is between 20000 and 10000 years ago, the average warming rate of Earth was about 0.2°C per century over Greenland, with lower rates for other regions. When we compare this with the temperature rise in the twentieth century which is about 0.6°C, we come to realize that the warming is reaching to dangerous levels and it is happening very fast. For at least 45 years, global surface temperature rose at an average rate of about 0.17°C per decade. This is more than twice as fast as the 0.07°C per decade increase observed for the entire period of recorded observations which started in 1850. Even though the Earth's climate changed before, it has never happened with this extremely high rate of temperature change and all living things are having difficulties adapting this fast change in today's world.

It is stated by the UK Met Office that there are seven main sources of evidence for climate change: "Higher temperatures, changing rainfall, changes in nature, sea level rises, retreating glaciers, sea ice, and ice sheets." [7]

It is not possible for the warming to be uniform across the planet but the upward trend in the globally averaged temperature shows that more areas warming than cooling. Since 1880, surface temperature has risen at an average rate of 0.07°C per decade, giving a net warming of 0.95°C [8]. In this 137-year period, warming is greater over land than over the oceans since water is slower to absorb and release heat.

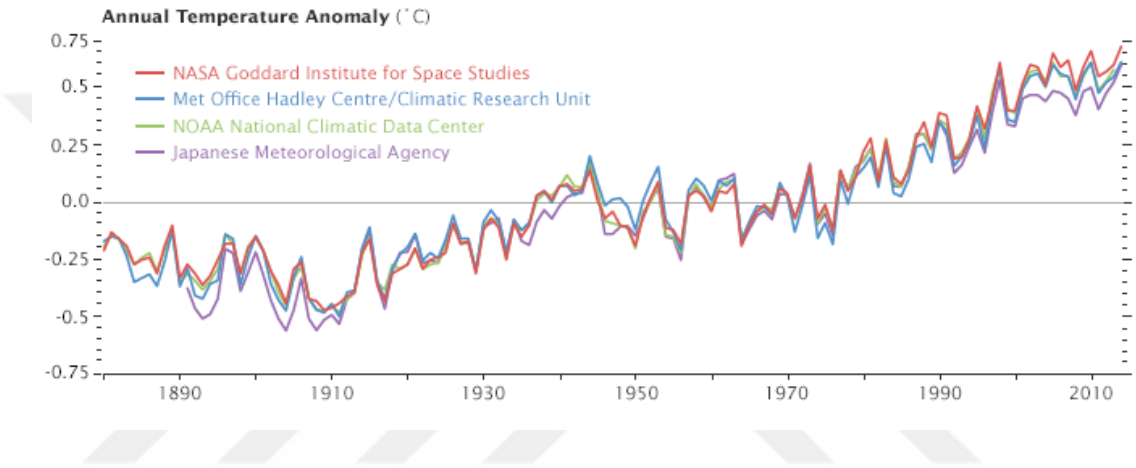


Figure 2.1. Annual temperature anomaly as recorded by NASA, NOAA, the Japan Meteorological Agency, and the Met Office Hadley Centre [9].

As can be seen from the Figure 2.1, all four records show rapid warming in the past few decades and all agree that the last decade as the warmest.

The precipitation conditions have changed almost worldwide leaving some nations on the edge of the water scarcity as mentioned before, and some regions faced floods. The rate of extreme events related to precipitation increased unequivocally.

Changes in the seasons (such as spring starting earlier than it is supposed to or autumn starting later than it is supposed to) are bringing changes in the behavior of many species, for example, butterflies appearing earlier in the year and birds shifting their migration patterns.

Because of the rapidly melting glaciers and ice sheets, sea level is rising very fast, making the coastal regions where today's marginal population lives very dangerous to survive. The Figure 2.2 shows the ground data of sea level changes, however, satellite data by NASA since 1993 shows good agreement with ground data and the rate of change is 3.4 mm per year [10].

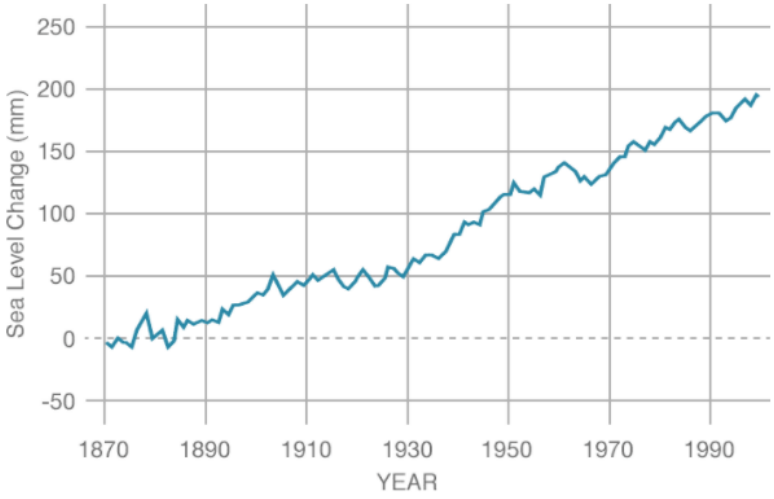


Figure 2.2. Sea Level Change by Coastal tide gauge records [10].

Glaciers all over the world - in the Alps, Rockies, Andes, Himalayas, Africa and Alaska - are melting and the rate of shrinkage has increased in recent decades according to all measurements that have been done.

Arctic sea-ice has been declining since the late 1970s as can be seen from Figure 2.3, reducing by about 4%, or 0.6 million square kilometers (an area about the size of Madagascar) per decade. At the same time Antarctic sea-ice has increased, but at a slower rate of about 1.5% per decade. Arctic sea ice reaches its minimum each September and September Arctic sea ice is now declining at a rate of 13.3% per decade relative to the 1981-2010 average [11].

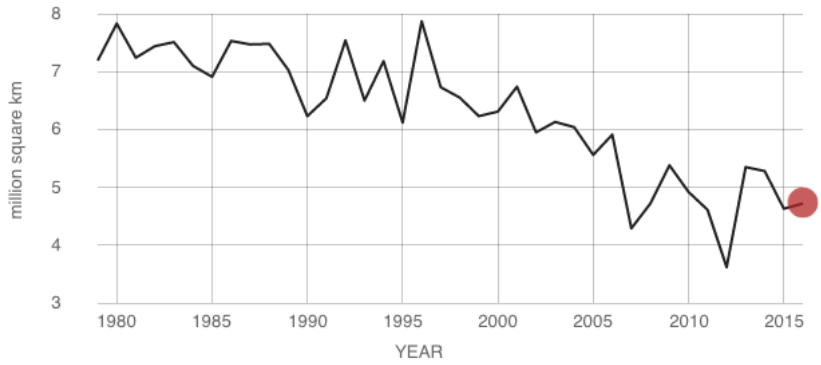


Figure 2.3. Average monthly Arctic sea ice minimum since 1979, derived from satellite observations [11].

The Greenland and Antarctic ice sheets, which store the majority of the world's fresh water, are both shrinking at an accelerating rate. The Figures 2.4 and 2.5 show the heartbreaking mass variations of the Earth's two ice sheets. The rate of change for the Antarctica is 125 gigatons per year and for the Greenland, it is 287 gigatons per year [12].

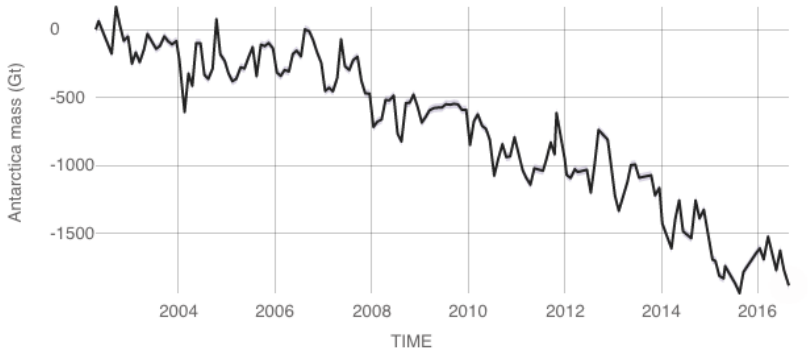


Figure 2.4. Antarctica mass variation since 2002 measured by NASA's GRACE satellites [12].

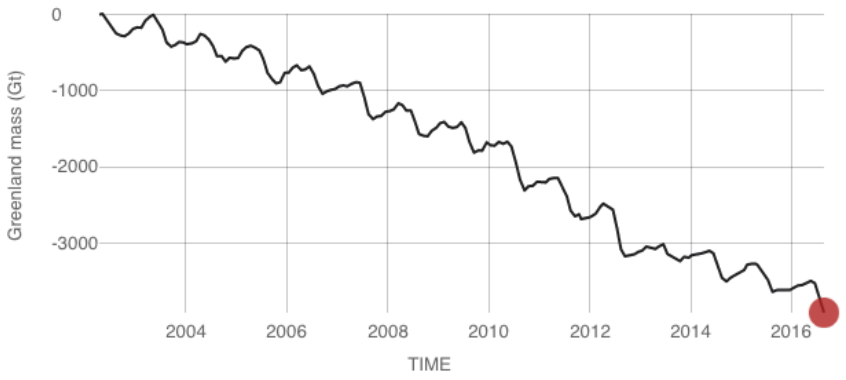


Figure 2.5. Greenland mass variation since 2002 measured by NASA's GRACE satellites [12].

All these changes, as stated by the UK Met Office, are the sources of evidence that the climate is changing without a doubt. At this point, there comes another debate among society, whether it is human induced or not.

## 2.1. The Cause of Today's Climate Change

Climate change can be due to many reasons as there were examples in the past.

In the seventeenth century, during the Maunder Minimum when almost no sunspots were recorded, the solar output was lower by a few tenths of a watt per square meter than its value today. This brought relatively colder climate to Earth.

In April 1815, Tambora volcano in Indonesia erupted and since volcanic eruptions are negative feedbacks for a warming planet, this brought two exceptionally colder years, and 1816 was regarded in New England and Canada as the 'year without a summer'.

Moreover, the Earth's position changes with respect to the Sun due to its elliptical orbit. Even though the total quantity of solar radiation reaching the Earth varies very little, the distribution of that radiation with latitude and season changes considerably. There are three regular variations in the orbit of the Earth around the Sun. The first one is related to the eccentricity of the ellipse, that is the ration between the greatest and the least diameters, varies with a period of 100000 years, which is the slowest of three variations. The second is due to the spinning of Earth on its own axis and the axis of spin is being tilted with respect to the axis of the Earth's orbit. The angle of tilt varies between 21.6° and 24.5° with a period of about 41000 years. The last variation is the Earth's perihelion, which is the time of year when the Earth is closest to the Sun. The time of perihelion moves through the months of the year with a period of about 23000 years. All these variations affect the Earth's climate tremendously. It is suggested by James Croll, a British Scientist, in 1867 that the major ice ages may be linked to these variations. Then in 1920, his ideas were developed by Milutin Milankovitch, a Serbian climatologist [13].

All these and some other natural events were the causes of Earth's climate change in the past.

The problem of today's climate change is that human beings are the cause of it. After the industrial revolution, the energy need of human beings increased tremendously. As the world globalised rapidly, our use of trains, cars, airplanes increased rapidly as well. Not just for transportation, but for almost all our energy need we have been using oil, coal and natural gas. The use of fossil fuels and also the use of chlorofluorocarbons(CFCs) for cooling purposes resulted in excessive accumulation of greenhouse gases in the atmosphere. These gases such as carbon dioxide ($CO_2$), methane ($CH_4$), nitrous oxide ($N_2O$) act like a blanket for the Earth and while they allow the solar radiation to pass and reach the Earth, they scatter the thermal radiation emitted by the Earth, which is supposed to go into space,

back to Earth, into the atmosphere and into space. This situation disrupts the energy balance of the Earth. As can be seen from Figure 2.6, while the average power falling on one square meter of a level surface outside the atmosphere is about 342 watts, about 6% is scattered back into space by atmospheric molecules, about 10% is reflected back to space by land and ocean surface, and the remaining 84% which is about 288 watts per square meter remains to actually heat the surface. The amount of thermal radiation emitted by the Earth's surface due to its temperature is supposed to balance the incoming energy. The Earth's temperature was high enough to keep the energy balanced a few centuries ago, however today with the presence of greenhouse gases not enough energy can leave the Earth, and therefore the Earth is warming to increase its thermal radiation.

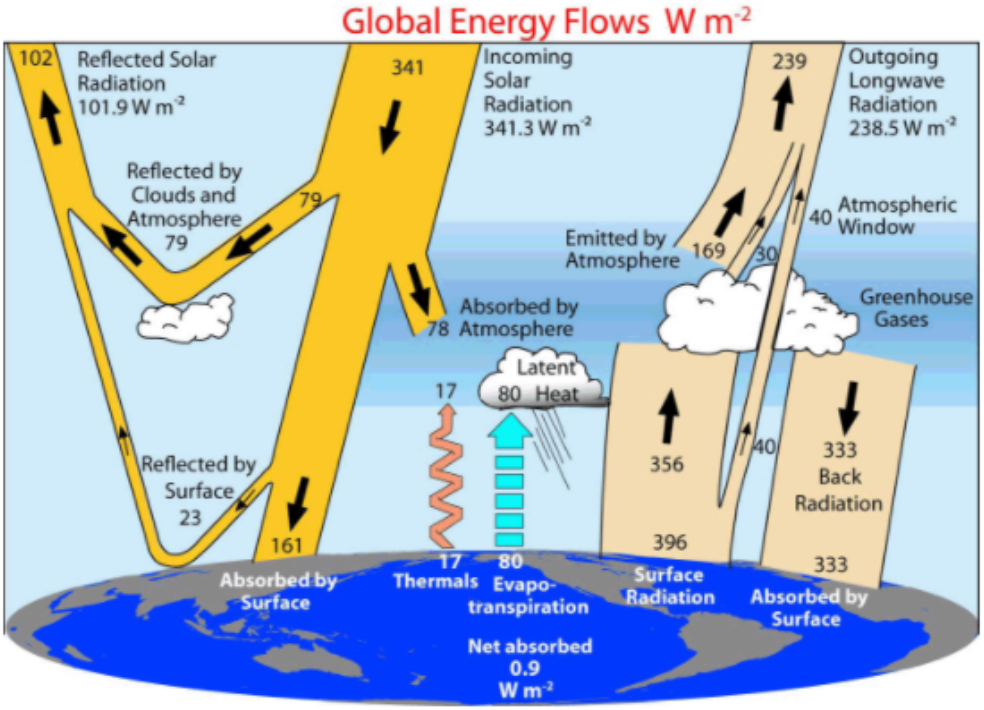


Figure 2.6. Earth's energy budget [14].

Intergovernmental Panel on Climate Change (IPCC) has been doing extensive studies on climate change and whether it is human induced or not. In their first report in 1990, it is explained that even though the size of the observed warming

was consistent with the projections of climate models, it was also in the range of natural climate variability, therefore an unequivocal statement on the detection of anthropogenic climate change could not be done.

In the second report of IPCC in 1995, there was more evidence available, however, IPCC was still very cautious about the attribution of the climate change and they reached a conclusion as follows.

"Our ability to quantify the human influence on global climate is currently limited because the expected signal is still emerging from the noise of natural climate variability, and because there are uncertainties in key factors. These include the magnitude and patterns of long term natural variability and the time-evolving pattern of forcing by, and response to, changes in the concentrations of greenhouse gases and aerosols, and land surface changes. Nevertheless, the balance of evidence suggests a discernible influence on global climate. [15]"

From 1995 to 2001, until their third report, better estimates of natural variability have been made and by the use of models IPCC concluded that the warming over the last century can not be only due to natural variability. Their conclusion in the third assessment report is as follows.

"In the light of new evidence and taking into account the remaining uncertainties, most of the observed warming over the last 50 years is *likely* to have been due to the increase in greenhouse gas concentrations. [16]"

In their fourth assessment report in 2007, their conclusions strengthened and they stated as follows.

"It is *very likely* that anthropogenic greenhouse gas increases caused most of the observed increase in globally averaged temperatures since the mid-20th century. Discernible human influences now extend to other aspects of climate, including

continental-average temperatures, atmospheric circulation patterns and some types of extremes. [17]"

Finally in their most up-to-date report released in 2014, IPCC clearly admitted that the climate change in our era is due to the anthropogenic greenhouse gas emissions with following words.

"Anthropogenic greenhouse gas emissions have increased since the preindustrial era, driven largely by economic and population growth, and are now higher than ever. This has led to atmospheric concentrations of carbon dioxide, methane and nitrous oxide that are unprecedented in at least the last 800000 years. Their effects, together with those of other anthropogenic drivers, have been detected throughout the climate system and are *extremely likely* to have been the dominant cause of the observed warming since the mid-20th century. [18]"

This concludes that we are responsible for the heart wrenching condition of our planet, therefore we must do what ever should be done to save our home.

## 2.2. IPCC

The Intergovernmental Panel on Climate Change (IPCC) is the leading international body for the assessment of the science related to climate change. It was established in 1988 by the United Nations Environment Programme (UNEP) and the World Meteorological Organization (WMO) to provide the world with a clear scientific view on the current state of knowledge in climate change and its potential environmental and socio-economic impacts, and also to provide policymakers with assessments of the scientific basis of climate change, its impacts and future risks, and options for adaptation and mitigation.

The IPCC reviews and assesses the most recent scientific, technical and socio-economic information produced worldwide relevant to the understanding of climate change. IPCC assessments offer a scientific basis for governments to develop climate related policies, they present projections of future climate change based on different scenarios and the risks that climate change brings, however, they do not tell policymakers what actions to take.

All member countries of the WMO and United Nations can participate in IPCC and currently IPCC has 195 members. The assessments are written by hundreds of leading scientists who volunteer their expertise and time as Coordinating Lead Authors and Lead Authors of the reports.

Their most up-to date report, which is Assessment Report 5 (AR5) was released in 2014 and their next report, that is Assessment Report 6 (AR6) is anticipated to be finalized in 2022 [19].

# 3. METHODOLOGY

## 3.1. Global Circulation Models (GCMs)

General Circulation Models (GCMs) are numerical models that represent physical precesses in the atmosphere, ocean, cryosphere and land surface. They are currently the most advanced tools to simulate the response of global climate system to increasing greenhouse gas concentrations. They use a three dimensional grid over the globe, usually having a horizontal resolution of between 250-600 km, 10 to 20 vertical layers in the atmosphere and up to 30 layers in the oceans. Their time resolution is around 6 hours. They use the power coming from the sun, land use, topography and atmospheric composition as input. They project the climate according to these inputs. Since their time and spatial resolutions are quite coarse, they can not give very detailed results.

A numerical model of the atmosphere contains descriptions of the basic dynamics and physics of the different components and their interactions. When a physical process is described in terms of an algorithm (a process of step- by-step calculation) and simple parameters (the quantities that are included in a mathematical equation), the process is said to have been parameterised.

The dynamical equations are:

- The horizontal momentum equations (Newton's Second Law of Motion). In these, the horizontal accel- eration of a volume of air is balanced by the horizontal pressure gradient and the friction. Because the Earth is rotating, this acceleration includes the Coriolis acceleration. The 'friction' in the model mainly arises from motions smaller than the grid spacing, which have to be parameterised.

- The hydrostatic equation. The pressure at a point is given by the mass of the atmosphere above that point. Vertical accelerations are neglected.
- The continuity equation. This ensures conservation of mass.

The model's physics consists of:

- The equation of state. This connects the quantities of pressure, volume and temperature for the atmosphere.
- The thermodynamic equation (the law of conservation of energy).
- Parameterisation of moist processes (such as evaporation, condensation, formation and dispersal of clouds).
- Parameterisation of absorption, emission and reflection of solar radiation and of thermal radiation.
- Parameterisation of convective processes.
- Parameterisation of exchange of momentum (in other words, friction), heat and water vapour at the surface.

Most of the equations in the model are differential equations, which means they describe the way in which quantities such as pressure and wind velocity change with time and with location. If the rate of change of a quantity such as wind velocity and its value at a given time are known, then its value at a later time can be calculated. Constant repetition of this procedure is called integration. Integration of the equations is the process whereby new values of all necessary quantities are calculated at later times, providing the model's predictive powers [13].

### 3.1.1. MPI-ESM-MR Global Climate Model

In this study, the outputs of the Earth System model MPI-ESM-MR of the Max Planck Institute for Meteorology (MPI-M) have been used. This model is an improved version of the well-known ECHAM5/MPIOM climate model and available

for use by the scientific community. The main improvement to the previous model is the coupled carbon cycle, which allows studying feedbacks of climate change on the carbon cycle itself. The representation of shortwave radiative transfer, surface albedo and aerosol has also been improved. The representation of the middle atmosphere as well as the land surface with interactive vegetation dynamics and the possibility of using different resolutions depending on the different questions were also incorporated into the design of the MPI-ESM [20].

### 3.2. RegCM4

Since the resolution of the GCMs is quite coarse, scientists developed Regional Climate Models (RCMs), which take the input data from GCMs and increase the resolution so that more comprehensive and detailed studies could be done on a regional basis. RCMs use the outputs of GCMs as input, they also use a finer resolution topography, geopotential height, temperature, relative humidity, wind velocity in 3 dimensions as input.

In this study one of the regional climate models RegCM4.4 is used. The first version RegCM was built in 1989 at the National Center for Atmospheric Research (NCAR) - Pennsylvania State University (PSU) and maintained in the Earth System Physics (ESP) section of the ICTP. Since then, it has undergone major updates in 1993 (RegCM2), 1999 (RegCM2.5), 2006 (RegCM3) and most recently 2010 (RegCM4). The latest version of the model, RegCM4, is now fully supported by the ESP, while previous versions are no longer available. This version includes major upgrades in the structure of the code and its pre- and post- processors, along with the inclusion of some new physics parameterizations. The model is flexible, portable and easy to use. One of the best properties of RegCM is that it can be applied to any region in the world with grid spacing of up to 10 km, which is the hydrostatic limit, and for a wide range of studies, from process studies to paleoclimate and future climate simulation [21]. At this hydrostatic limit, model assumes that air

parcel moves only horizontal and vertical, not diagonally.

### 3.2.1. Model Components

The RegCM modeling system has four components, that are Terrain, ICBC, RegCM, and Postprocessor. Terrain and ICBC are the two components of RegCM preprocessor. Terrestrial variables (including elevation, landuse and sea surface temperature) and three-dimensional isobaric meteorological data are horizontally interpolated from a latitude longitude mesh to a high-resolution domain on either a Rotated (and Normal) Mercator, Lambert Conformal, or Polar Stereographic projection. Vertical interpolation from pressure levels to the $\sigma$ coordinate system -which is defined below- of RegCM is also performed. $\sigma$ surfaces near the ground closely follow the terrain, and the higher-level $\sigma$ surfaces tend to approximate isobaric surfaces.

Since the vertical and horizontal resolution and domain size can vary, the modeling package programs employ parameterized dimensions requiring a variable amount of core memory, and the requisite hard-disk storage amount is varied accordingly.

### 3.2.2. The RegCM Model Horizontal and Vertical Grid

It is useful to first introduce the model's grid configuration. The modeling system usually gets and analyzes its data on pressure surfaces, but these have to be interpolated to the model's vertical coordinate before input to the model. The vertical coordinate is terrain-following (Figure 3.1) meaning that the lower grid levels follow the terrain while the upper surface is flatter. Intermediate levels progressively flatten as the pressure decreases toward the top of the model.

The Hydrostatic solver uses a dimensionless $\sigma$ coordinate to define the model levels where p is the pressure, $p_t$ is a specified constant top pressure, $p_s$ is the surface

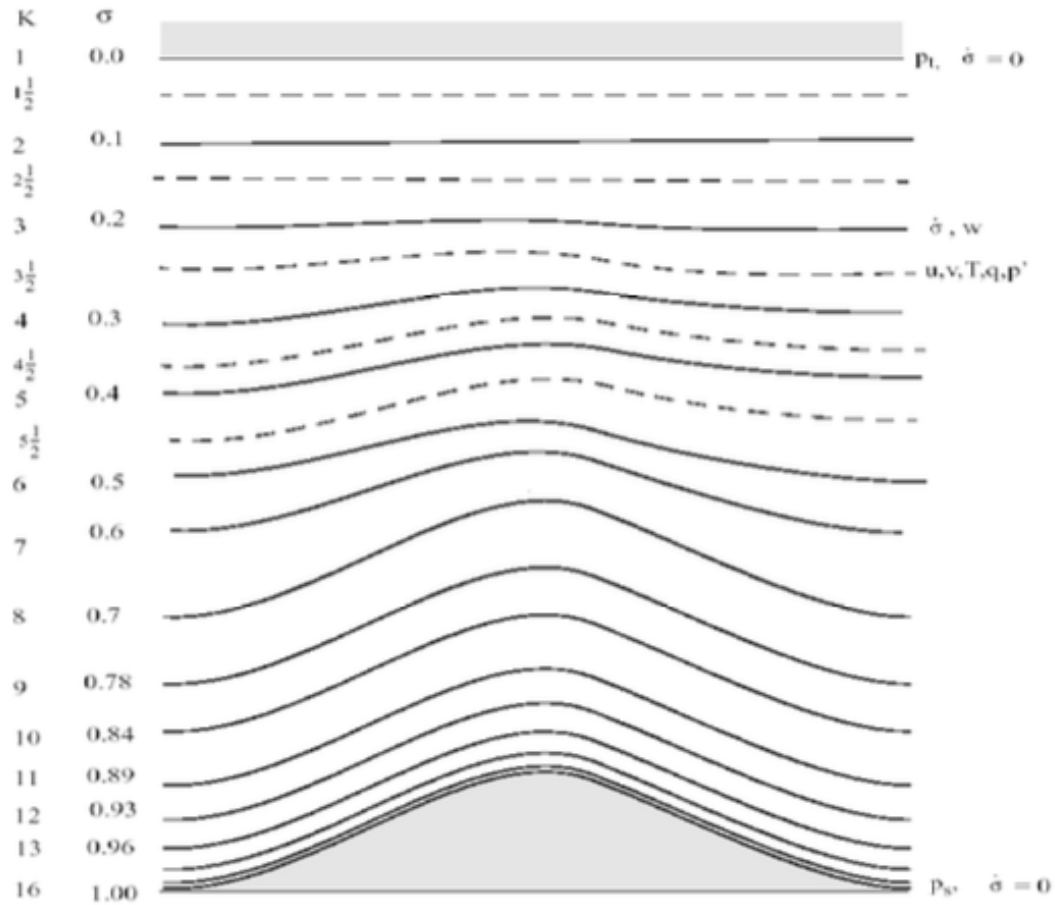


Figure 3.1. Schematic representation of the vertical structure of the model. This example is for 16 vertical layers. Dashed lines denote half-sigma levels, solid lines denote full-sigma levels [22].

pressure.

$$\sigma = \frac{p - p_{\mathrm{t}}}{p_{\mathrm{s}} - p_{\mathrm{t}}} \tag{3.1}$$

where we can define:

$$p^{*}(x, y) = p_{\mathrm{s}}(x, y) - p_{\mathrm{t}} \tag{3.2}$$

For the non-hydrostatic solver a similar dimensionless coordinate is used, but it is defined entirely from the reference pressure. Given a reference atmospheric profile:

$$p(x, y, z, t) = p_0(z) - p'(x, y, z, t) \tag{3.3}$$

$$T(x, y, z, t) = T_0(z) - T'(x, y, z, t) \tag{3.4}$$

$$\rho(x, y, z, t) = \rho_0(z) - \rho'(x, y, z, t) \tag{3.5}$$

the vertical sigma coordinate is defined as:

$$\sigma = \frac{p_0 - p_{\mathrm{t}}}{p_{\mathrm{s}} - p_{\mathrm{t}}} \tag{3.6}$$

where $\mathrm{p_s}$ is the surface pressure, $\mathrm{p_t}$ is a specified constant top pressure and $\mathrm{p_0}$ is the reference pressure profile. The total pressure at each grid point is thus given as:

$$p = p^{*}\sigma + p_{\mathrm{t}} + p' \tag{3.7}$$

with $\mathrm{p}^{*}$ defined as in the hydrostatic solver.

It can be seen from the Equation 3.1 and Figure 3.1 that $\sigma$ is zero at the top and one at the surface, and each model level is defined by a value of $\sigma$. The model vertical resolution is defined by a list of values between zero and one that do not necessarily have to be evenly spaced. Commonly the resolution in the boundary layer is much finer than above, and the number of levels may vary upon the user demand.

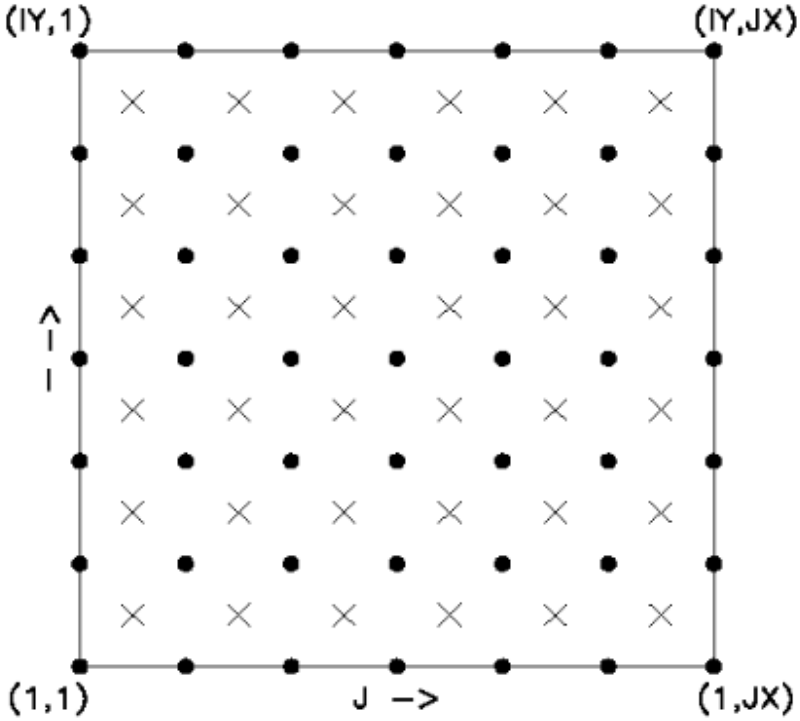


Figure 3.2. Schematic representation showing the horizontal Arakawa B-grid staggering of the dot and cross grid points [22].

The horizontal grid has an Arakawa-Lamb B-staggering of the velocity variables with respect to the scalar variables. This is shown in Figure 3.1 where it can be seen that the scalars (T, q, p, etc.) are defined at the center of the grid box, while the eastward (u) and northward (v) velocity components are collocated at the corners. The center points of grid squares will be referred to as cross points,

and the corner points are dot points. Hence horizontal velocity is defined at dot points. Data is input to the model, the preprocessors do the necessary interpolation to assure consistency with the grid.

All the above variables are defined in the middle of each model vertical layer, referred to as half-levels and represented by the dashed lines in Figure 3.1. Vertical velocity is carried at the full levels (solid lines). In defining the sigma levels it is the full levels that are listed, including levels at $\sigma = 0$ and 1. The number of model layers is therefore always one less than the number of full sigma levels.

The finite differencing in the model is, of course, crucially dependent upon the grid staggering wherever gradients or averaging are represented terms in the equation.

Detailed information is given in the Reference Manual of RegCM4.4 by ICTP [22].

### 3.2.3. RCP Scenarios

Climate models are computer models which describe the components, processes and interactions in the climate system. In order to be able to see how human activities could affect the system, scientists insert greenhouse gas concentrations, pollution, changes in the land use, etc. into the models. to be able to do future projections, a variety of approaches to scenarios in climate research have been used over time. Representative Concentration Pathways (RCPs) are four greenhouse gas concentration trajectories adopted by the IPCC for its Fifth Assessment Report (AR5) in 2014. It supersedes Special Report on Emissions Scenarios (SRES) projections published in 2000.

In Table 3.1 an overview of most prominent sets of emissions scenarios is shown.

Table 3.1. History of Scenarios

| Year | Name | Used in |
|---|---|---|
| 1990 | SA90 | First Assessment Report |
| 1992 | IS92 | Second Assessment Report |
| 2000 | SRES-Special Report on Emissions and Scenarios | Third and Fourth Assessment Reports |
| 2009 | RCPs-Representative Concentration Pathways | Fifth Assessment Report |

The pathways are used for climate modeling and research. They describe four possible climate futures, all of which are considered possible depending on how much greenhouse gases are emitted in future years depending on the actions to be taken against climate change. The four RCPs, RCP2.6, RCP4.5, RCP6, and RCP8.5, are named after a possible range of radiative forcing values in the year 2100 relative to pre-industrial values (+2.6, +4.5, +6.0, and +8.5 W/$m^2$, respectively) [23].

Table 3.2. Overview of RCP Scenarios

| Scenario | Description | Citation |
|---|---|---|
| RCP 8.5 | Rising radiative forcing pathway leading to 8.5 W/$m^2$ in 2100 | Riahi *et al.* (2007) [24]<br>Rao and Riahi (2006) [25] |
| RCP 6 | Stabilization without overshoot pathway to 6 W/$m^2$ at stabilization after 2100 | Fujino *et al.* (2006) [26]<br>Hijioka *et al.* (2008) [27] |
| RCP 4.5 | Stabilization without overshoot pathway to 4.5 W/$m^2$ at stabilization after 2100 | Smith and Wigley (2006) [28]<br>Clarke *et al.* (2007) [29]<br>Wise *et al.* (2009) [30] |
| RCP 2.6 | Peak in radiative forcing at 3 W/$m^2$ before 2100 and decline | van Vuuren *et al.* (2006; 2007) [31], [32] |

In Table 3.2, the overview of the RCP Scenarios and related publications are given.

RCP 8.5 scenario is consistent with a future with no policy to reduce emissions, therefore it is also referred as the business as usual (BAU) scenario. In this scenario, it is foreseen that there will be rapid increase in $CO_2$ and $CH_4$ emissions, the world population will reach 12 billion by 2100 and therefore the use of croplands and

grassland will increase, there will be heavy reliance on fossil fuels, and the rate of technology development will decrease. Today, $CO_2$ concentration in the atmosphere is about 410 ppm, which is consistent for now with the RCP 8.5 scenario. Therefore, in this study, RCP 8.5 scenario is used for the reliability of the future predictions which state that the $CO_2$ concentration in the atmosphere will exceed the maximum predicted concentration level before 2100 [33].

### 3.3. SPI

Over the years, many drought indices were developed and used by scientists around the world to be able to detect and monitor drought. However, scientists from the United States thought that an index is supposed to be simple, easy to calculate, statistically relevant and meaningful. With this purpose, scientists McKee, Doesken and Kleist developed the Standardized Precipitation Index in 1993. This index is rather simple and easy to calculate since it uses only monthly total precipitation data as input [34]. Ideally, to be able to get robust results from the index, at least 30 years of monthly precipitation data is needed [1]. Therefore in this study, monthly precipitation data of the 1971-2000 and 2071-2100 periods have been used. The program can be run with missing data but this will affect the robustness of the results depending on the distribution of the missing data in relation to the length of the record.

The SPI can be calculated for multiple timescales such as 3-, 6-, 12-, 24- and 48-month. These timescales reflect the impact of drought on the availability of the different water resources. For example, soil moisture conditions respond to relatively short scaled precipitation anomalies whereas groundwater, stream-flow and reservoir storage respond to longer term precipitation anomalies. In this study 3-month and 12-month SPI values are calculated so that both the short-term meteorological and long-term hydrological drought can be analyzed by the use of the index. 3-month SPI uses the previous 3 months' monthly average precipitation data successively

and 12-month SPI uses the previous 12 months' monthly average precipitation data successively. If SPI value is between 0.49 and -0.49 that means the precipitation is in the normal class of McKee drought classification. Since the SPI is standardized, more positive values of SPI means the precipitation is more than the normal, and more negative values mean that the precipitation is less than the normal. Therefore, to monitor and analyze the meteorological drought for MENA, 3-month SPI has been used and to monitor and analyze the long-term hydrological drought 12-month SPI has been used in this study.

One of the main advantages of SPI is that it allows cross-regional comparisons even if the regions have very different climates, and by standardization of the index it allows the determination of frequency of drought. Developers of SPI, McKee *et al.* (1993), classify the water availability into seven classes as shown in Table 3.3. These seven classes are derived from standard normal (Gaussian) distributed precipitation data. The long-term precipitation precipitation record input is fitted to a probability distribution and then it is transformed into a normal distribution so that the mean SPI for the location and desired period is zero [1]. Consequently, positive SPI values indicate greater than median precipitation and negative values indicate less than median precipitation, which means that the index can be used to monitor the wet periods as well as dry periods.

Other advantages of the SPI are that it is flexible, that it is spatially consistent and that shorter timescale SPIs can provide early warning of drought and help assess drought severity. In addition, its probabilistic nature gives it historical context so that it is well suited for decision making [1].

There are also some weaknesses of the SPI. It is both a weakness and reason of simplicity of the SPI that it is based only on precipitation. Secondly, since there is no soil water-balance component, no ratios of evapotranspiration/potential evapotranspiration can be calculated.

Table 3.3. McKee Drought Classifications

| **SPI Values** | **Classification** |
|---|---|
| 2.00 and more | Extremely Wet |
| 1.50 to 1.99 | Very Wet |
| 1.00 to 1.49 | Moderately Wet |
| -0.99 to 0.99 | Near Normal |
| -1.00 to -1.49 | Moderately Dry |
| -1.50 to -1.99 | Severely Dry |
| -2.00 and less | Extremely Dry |

Procedure and formula for computation of the SPI is as follows. Firstly SPI drought classes are derived from standard normal (Gaussian) distributed precipitation data, however, the probability distribution function of precipitation does not correlate well with the normal distribution [35]. Thom (1966) noted that the gamma distribution is the best probability distribution fit for standard normal distributed precipitation data [36]. Therefore, it is needed to convert probability distribution function of the total precipitation to gamma probability distribution function [4, 34, 37–39]. Gamma probability density function is given in Equation 3.8.

$$f(y) = \frac{\frac{y}{\beta}^{\alpha-1} e^{(-y/\beta)}}{\beta\Gamma(\alpha)} \tag{3.8}$$

where

$$y, \alpha, \beta > 0 \tag{3.9}$$

In this definition $\alpha$ is the shape parameter and $\beta$ is the scale parameter of the gamma probability density function. $\Gamma(\alpha)$ is the gamma function itself and it is

given in the Equation 3.10.

$$\Gamma(\alpha) = \int_0^\infty t^{\alpha-1} e^{-t} dt \tag{3.10}$$

Shape and scale parameters are obtained by calculating the $\bar{y}$ and $\bar{g}$, the arithmetic mean and geometric mean of the precipitation data respectively are shown below.

$$D = \ln \frac{\bar{y}}{\bar{g}} \tag{3.11}$$

$$\hat{\alpha} = \frac{1 + (1 + \frac{4D}{3})^{1/2}}{4D} \tag{3.12}$$

$$\beta = \frac{\bar{y}}{\hat{\alpha}} \tag{3.13}$$

By the numerical integration method recommended by Press *et al.* (1992), the precipitation probability distribution functions are obtained and by the use of reverse-standard normal function these functions are transformed into standardized precipitations [35, 40]. Thereafter, drought is classified into classes shown in Table 3.3.

## 3.4. SPEI

In recent years, there has been many studies to develop new drought indices or to improve existing ones [41–44]. Most of the studies carried out to analyze and monitor drought have been conducted by using either Palmer Drought Severity Index(PDSI) which is based on a soil water balance equation [45], or aforementioned SPI.

The main criticism about SPI is that it is based only on precipitation data and it does not consider other variables, such as temperature, evapotranspiration and soil water holding capacity.

The PDSI is based on the supply and demand concept of the water balance equation therefore it incorporates precipitation, moisture supply, runoff and evaporation demand. The calculation procedure is explained in a number of studies [46–48]. Nevertheless, PDSI has several deficiencies [46, 48–50]. Other than the strong influence of calibration period, it has problems in spatial comparability. These problems were solved by the development of self-calibrated PDSI (sc-PDSI) [43]. Sc-PDSI is spatially comparable and detects extreme wet and dry events. However, the main shortcomings of this index are its fixed temporal scale (between 9 and 12 months) and its autoregressive characteristics as well as its complexity during calculation. Moreover, drought is accepted as a multiscalar phenomenon and sc-PDSI has no such characteristics.

In their study of "A Multiscalar Drought Index Sensitive to Global Warming: The Standardized Precipitation Evapotranspiration Index" Vicente-Serrano *et al.* (2010) proposed a new climatic drought index [6]. The SPEI uses both precipitation and temperature data, moreover, it has the advantage of combining multiscalar character with the capacity to include the effects of temperature variability on drought assessment. Since SPI and SPEI identify different drought types due to their multiscalar character, they are both superior to sc-PDSI [6].

The calculation of SPEI is very easy compared to sc-PDSI and it is based on the original SPI calculation procedure mathematically. While SPI is calculated by the use of monthly precipitation data, SPEI is calculated by the use of monthly difference between precipitation and Potential Evapotranspiration (PET). There are a number of methods to calculate PET indirectly, such as Penmann-Monteith (PM) method, which requires large amounts of data since its calculation involves solar radiation, temperature, wind speed and relative humidity [6]. Thornthwaite

method [51], however, is rather simple and widely preferred by scientists since it has the advantage of requiring only monthly-mean temperature data. By this method, PET is calculated as in Equation 3.14 where T is the monthly-mean temperature in °C. I is a heat index, calculated as the sum of 12 monthly index values i, which are derived from Equation 3.15. m is a coefficient which depends on I and K is a correction coefficient computed from Equation 3.16.

$$PET = 16K(\frac{10T}{I})^m \tag{3.14}$$

$$i = (\frac{T}{5})^{1.514} \tag{3.15}$$

$$K = (\frac{N}{12})(\frac{NDM}{30}) \tag{3.16}$$

In Equation 3.16, NDM is the number of days of the month and N is the maximum number of sun hours, which is calculated as in Equation 3.17, for which $\omega_s$ is calculated as in Equation 3.18.

$$N = (\frac{24}{\pi})(\omega_s) \tag{3.17}$$

$$(\omega_s) = \arccos(-\tan(\varphi)\tan(\delta)) \tag{3.18}$$

$\varphi$ is the latitude in radians and $\delta$ is the solar declination in radians, calculated using Equation 3.19.

$$\delta = 0.4093sin(\frac{2\pi J}{365} - 1.405) \tag{3.19}$$

J is the average Julian day of the month. As the SPEI uses the difference between precipitation and PET, $D_{\mathrm{i}}$ is defined as follows.

$$D_{\mathrm{i}} = P_{\mathrm{i}} - PET_{\mathrm{i}} \tag{3.20}$$

The calculated $D_{\mathrm{i}}$ values are aggregated at different time scales, following the same procedure as that for the SPI. In spite of having similar calculations, SPI can be calculated using two-parameter gamma distribution, whereas SPEI is needed to be calculated using three-parameter gamma distribution [6]. The detailed calculations about the L skewness and L kurtosis to be able to create the L-moment ratio diagrams can be found in the paper of "A Multiscalar Drought Index Sensitive to Global Warming: The Standardized Precipitation Evapotranspiration Index" by the developers of the index [6].

The probability density function of a three-parameter log-logistic distributed variable is expressed as in Equation 3.21 where a, b, and g are scale, shape, and origin parameters, respectively, for D values in the range $\gamma > D < \infty$.

$$f(x) = \frac{\beta}{\alpha}(\frac{x-y}{\alpha})^{\beta-1}[1 + (\frac{x-y}{\alpha})^{\beta}]{-}2 \tag{3.21}$$

The probability distribution function of the D series, according to the log-logistic distribution is given by Equation 3.22.

$$F(x) = [1 + (\frac{\alpha}{x-y})^{\beta}]^{-1} \tag{3.22}$$

Hereafter the SPEI can easily be obtained as the standardized values of F(x). By the classical approximation of Abramowitz and Stegun (1965) [52],

$$SPEI = W - \frac{C_0 + C_1 W + C_2 W^2}{1 + d_1 W + d_2 W^2 + d_3 W^3} \tag{3.23}$$

where

$$W = \sqrt{-2\ln(P)} \tag{3.24}$$

for $P \leq 0.5$/ Here P is the probability of exceeding a determined D value, $P = 1 - F(x)$. If $P \leq 0.5$, then P is replaced by $1 - P$ and the sign of the resultant SPEI is reversed. The constants are $C_0 = 2.515517$, $C_1 = 0.802853$, $C_2 = 0.010328$, $d_1 = 1.432788$, $d_2 = 0.189269$, $d_3 = 0.001308$.

The mean value of SPEI is 0, and the standard deviation is 1. The SPEI is a standardized variable, and it can therefore be compared with other SPEI values over time and space as in SPI.

## 3.5. Coordinated Regional Climate Downscaling Experiment (CORDEX)

Coordinated Regional Climate Downscaling Experiment (CORDEX) has been established by World Climate Research Program (WCRP) in 2009 to further develop a framework to evaluate Regional Climate Downscaling (RCD) techniques and to produce a new generation of RCD-based fine-scale climate projections for identified regions worldwide. The CORDEX framework also offers the potential for better coordination of RCD-related research and modelling activities within the regional climate modelling and downscaling communities and further to bridge the gap between the climate modelling community and end users of climate information across the globe.

To be able to research and provide more detailed information in a much smaller scale than the global circulation models (GCMs) with a global partnership, CORDEX has divided world into 14 regions. These regions are listed below and shown in Figure 3.3.

- Region 1: South America
- Region 2: Central America
- Region 3: North America
- Region 4: Europe (EURO)
- Region 5: Africa
- Region 6: South Asia
- Region 7: East Asia
- Region 8: Central Asia
- Region 9: Australasia
- Region 10: Antarctica
- Region 11: Arctic
- Region 12: Mediterranean (MED)
- Region 13: Middle East and North Africa (MENA)
- Region 14: South East Asia (SEA)

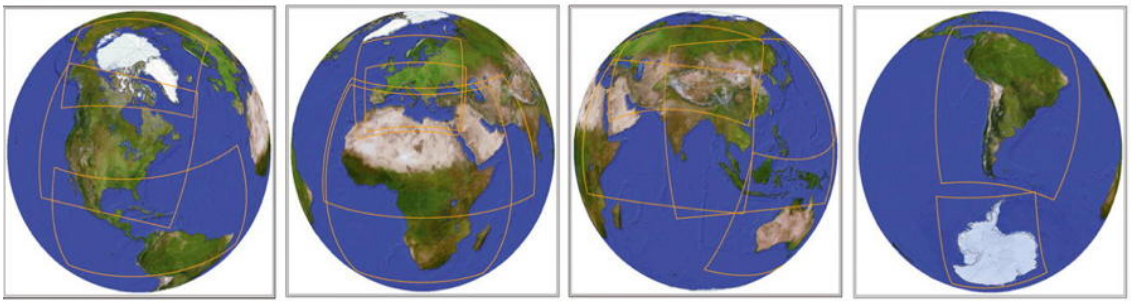

Figure 3.3. CCORDEX Global Domains [53].

Thanks to these CORDEX domains, scientists around the world are studying the same regions which allow the comparison of the studies and evaluation of the regional climate downscaling techniques.

## 3.6. MENA Region

MENA, being CORDEX Region 13, covers an extensive region extending from Morocco to Iran, including all the Middle Eastern and Maghreb countries.

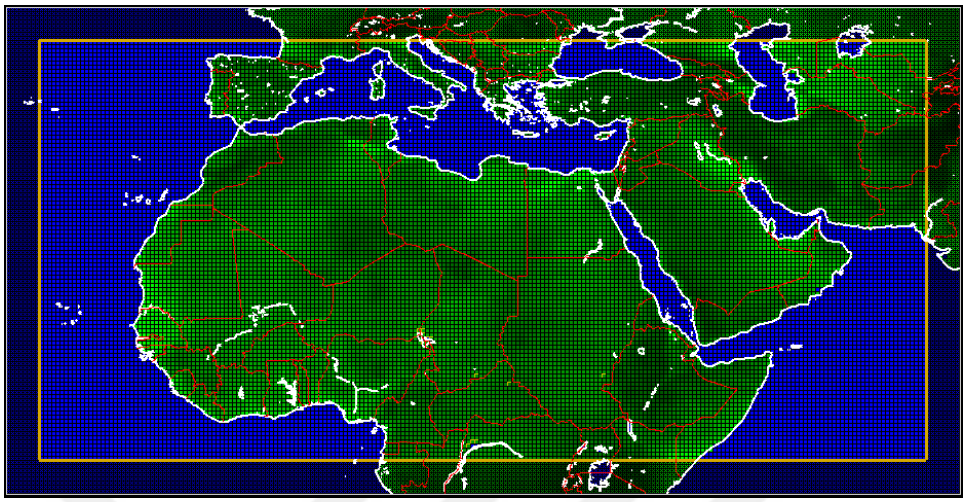

Figure 3.4. CORDEX Region 13: MENA [54].

As stated by World Bank, in 2015 population of the region was about 424 million, with 1.8% annual population growth, therefore the population is about 500 million today. The vast majority of the population lives in middle-income countries [55]. It is stated in the World Bank 2016 annual report, economic growth in MENA is projected to remain at 2.9% in 2016, with lower than average growth in the Gulf Cooperation Council (GCC) countries and in Lebanon, Morocco and Tunisia (1,8%) and higher than average growth in the developing countries of the region(4.4%), and the growth in 2017 is projected to rise to 4.2% with the assumption that oil production increases in Libya and Iran. Almost 3% of the population live in extreme poverty, however, the vulnerability is high since 53% of the population live on $4.00 a day or less [56].

Due to the population growth, water demand has been increasing in the region and along with the growing economies and land-use changes major stresses on freshwater resources came into existence [57]. It has been very difficult for almost all the countries in the region to cope with freshwater stress.

MENA is the most water scarce region in the world, and its water stress is foreseen to get worse in the future. It is stated by World Bank that renewable water resources per capita in the region has been reduced to one-fourth of its level in 1950 and by 2050 the natural water resources in the region will drop even further and may reach to 11 times less than the global average [58].

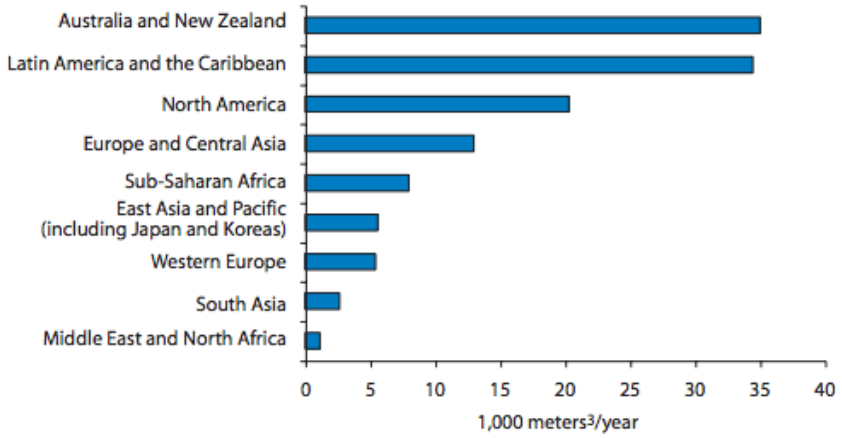


Figure 3.5. Actual Renewable Water Resources per Capita, by Region [59].

As shown in Figure 3.5, MENA region has the least actual renewable water resources (ARWR) per capita in the world. ARWR is the sum of internal and external renewable water resources. It corresponds to the maximum theoretical amount of water actually available for a country at a given moment. Moreover, it is shown in the Figure 3.6 that the region has the highest percentage of total renewable water resources withdrawn. These figures, taken from world bank, refer to the period of 1998 - 2002 and the figures may vary with time.

Figure 3.7 prepared by the Food and Agriculture Organization (FAO) shows the spatial distribution of total renewable water resources (TRWR) per capita for the year 2014. We can confidentially say that MENA region has the least ARWR in the world reaching to the levels of absolute water scarcity. The countries Algeria, Libya, Saudi Arabia, Yemen and Oman have less than 500 $m^3$/year/person TRWR per inhabitant which is regarded as absolute water scarcity. Morocco, Egypt, Sudan, Burkina Faso, Kenya and South Africa follow with TRWR per inhabitant values

between 500 to 1000 $m^3$/year which is considered as chronic water scarcity. There are no places on Earth which have worse TRWR problems.

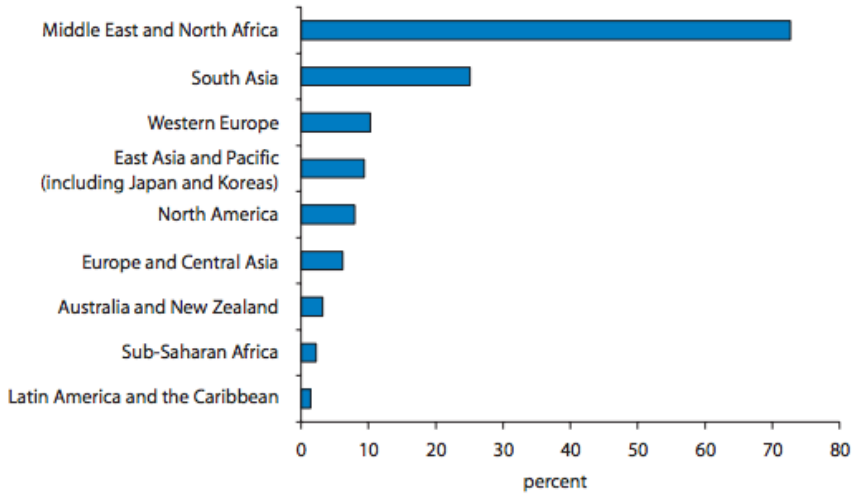


Figure 3.6. Percentage of Total Renewable Water Resources Withdrawn, by Region [59].

Figure 3.8 shows the average annual precipitation map of the world in mm/year for 2016, prepared by FAO. The first thing that captures the attention is the high correlation between the TRWR and average annual precipitation. It is clearly seen that MENA Region has the countries which get the least average annual precipitation worldwide. The countries Morocco, Algeria, Libya, Egypt, Mali, Niger, Sudan, Oman and south east part of Saudi Arabia are seen to get precipitation less than 100mm/year in the figure.

As much as droughts hit the region regularly threatening the human welfare and economic development, the opposite, floods also pose a significant danger in the region as well. For example, the 2008 floods in Yemen caused $1.6billion of damage which corresponds to 6% of the country's gross domestic product (GDP), the 2009 floods in Jeddah, Saudi Arabia caused $1.4 billion dollars worth of damage, the 2004 floods in Djibouti caused 230 deaths and $11.1 million in losses [58]. For all these reasons, it is very crucial to do studies on early warning systems about the

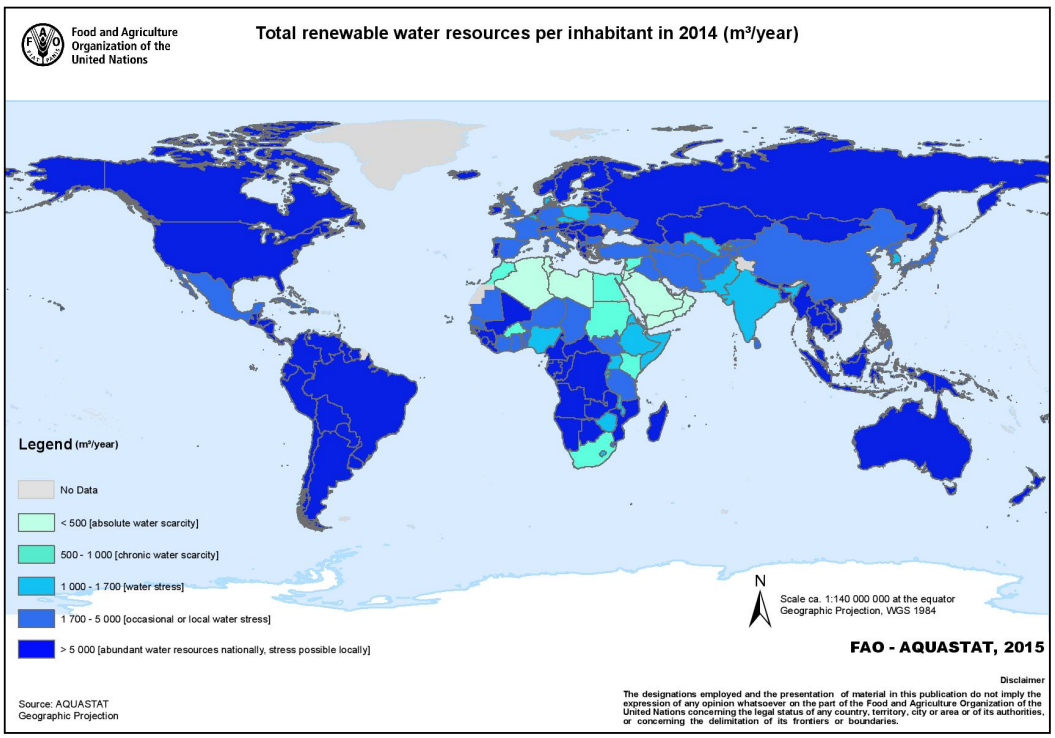


Figure 3.7. Total renewable water resources per inhabitant in 2014 [60].

precipitation conditions for the region.

### 3.6.1. Subdomains Used In This Study

Since the domain of this study, MENA, is very large and it contains very different climate zones, it is divided into 6 subdomains, which are tried to be chosen to have similar climates within themselves. These subdomains are shown on a topography map of MENA in Figure 3.9 which is drawn by the use of Grid Analysis and Display System (GrADS). Then spatial averages of the regions are taken by the use of Climate Data Operator (CDO) to be able to draw the SPI and SPEI time series for the historical and future periods of the regions. The latitudes and longitudes of the subdomains and a brief information about their climates are listed below.

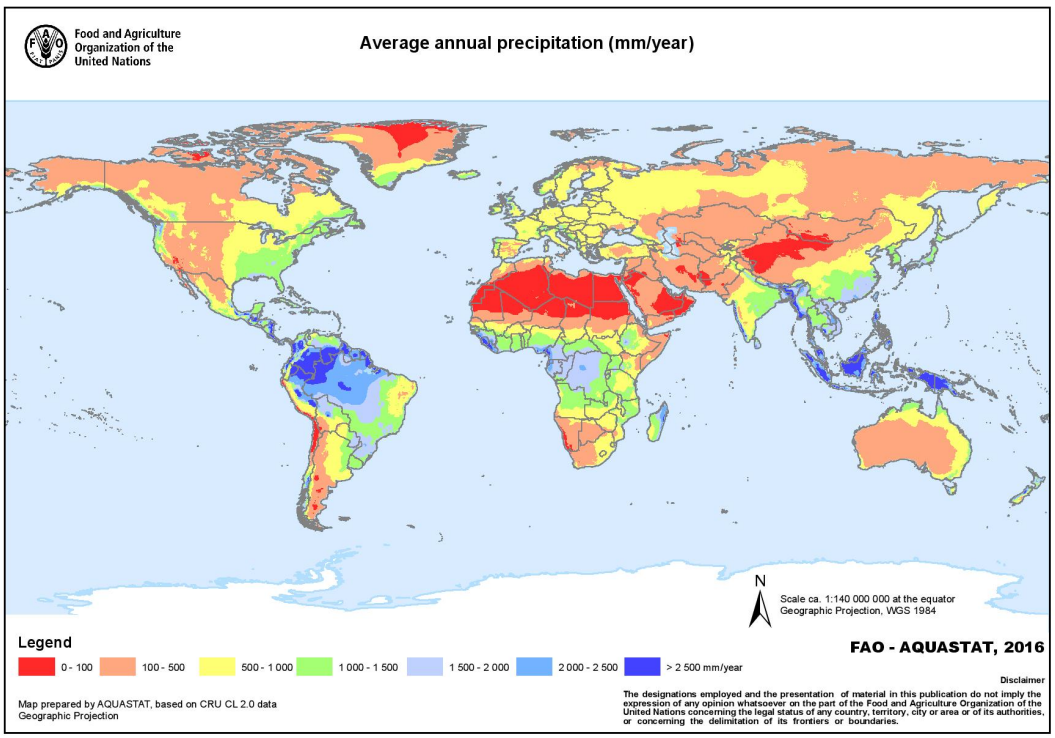


Figure 3.8. Average annual precipitation [61].

- Region A is shown with the red lined rectangle in Figure 3.9. It has the latitudes of 35°N - 43°N and longitudes of 24°E - 45°E. It contains Turkey. The region is in the dry class of the Köppen's Climatic Classification System, which means there is deficient precipitation most of the year and potential evaporation and transpiration exceeds precipitation [62]. Region A also have the moist, severe winter climate in the east part according to the Köppen's Climatic Classification System, which means that the east part has warm summers and cold winters. The average temperature of the warmest month exceeds 10°C, and the coldest monthly average drops below -3°C.

- Region B is shown with the green lined rectangle in Figure 3.9. It has the latitudes of 0°N -30°N and longitudes of 25°E - 45°E. The Region contains the Red Sea, North-East part of Saudi Arabia, Egypt, Sudan and South Sudan, Uganda and East part of Ethiopia and the Red Sea. Region B is again in the dry class of the Köppen's Climatic Classification System.

- Region C is shown with the dark blue lined rectangle in Figure 3.9. It has the latitudes of 25°N - 35°N and longitudes of 10°W - 25°E. The Region is actually the Northern Africa and it includes Morocco, Northern Algeria, Tunisia and Libya. Region C contains Sahara Desert to some extent and it is again in the dry class of the Köppen's Climatic Classification System

- Region D is shown with the light blue lined rectangle in Figure 3.9. It has the latitudes of 4°N - 15°N and longitudes of 15°W - 40°E. It has the countries Guinea, Sierra Leone, Liberia, Cote d'Ivorie, Ghana, Burkina Faso, Togo, Benin, Nigeria, North-East part of Cameroun, Southern Tchad, Central African Republic, South Sudan and Western Ethiopia. Region D is in the dry and tropical classes of the Köppen's Climatic Classification System. In the tropical moist climates, all months have an average temperature above 18°C and since all months are warm, there is no real winter season. Region D is one of the regions in MENA that gets affected most from the El Niño and La Niña events. El Niño events make the region drier and La Niña events make the region cooler and wetter.

- Region E is shown with the magenta lined rectangle in Figure 3.9. It has the latitudes of 5°S - 12°N and longitudes of 20°E - 50°E. It has the Horn of Africa and the countries Somalia, Ethiopia, South Sudan, Eastern part of Central African Republic, Rwanda and North-East part of Democratic Republic of Congo. Region E is in the tropical and dry classes of the Köppen's Climatic Classification System. The droughts in the Horn of Africa is thought to be the result of La Niña episodes and strong El Niños are correlated with high precipitation and floodings.

- Region F is shown with the yellow lined rectangle in Figure 3.9. It has the latitudes of 12°N - 35°N and longitudes of 30°E - 62°E. The region contains the

Arabian Peninsula and the countries Oman, Yemen, United Arab Emirates, Saudi Arabia, Jordan, Israel, Lebanon, Southern part of Syria, Iraq and Iran. Region F is in the dry class of the Köppen's Climatic Classification System. It contains the Arabian Desert, therefore SPI and SPEI results are expected to be in the extremely dry and extremely wet classes mostly.

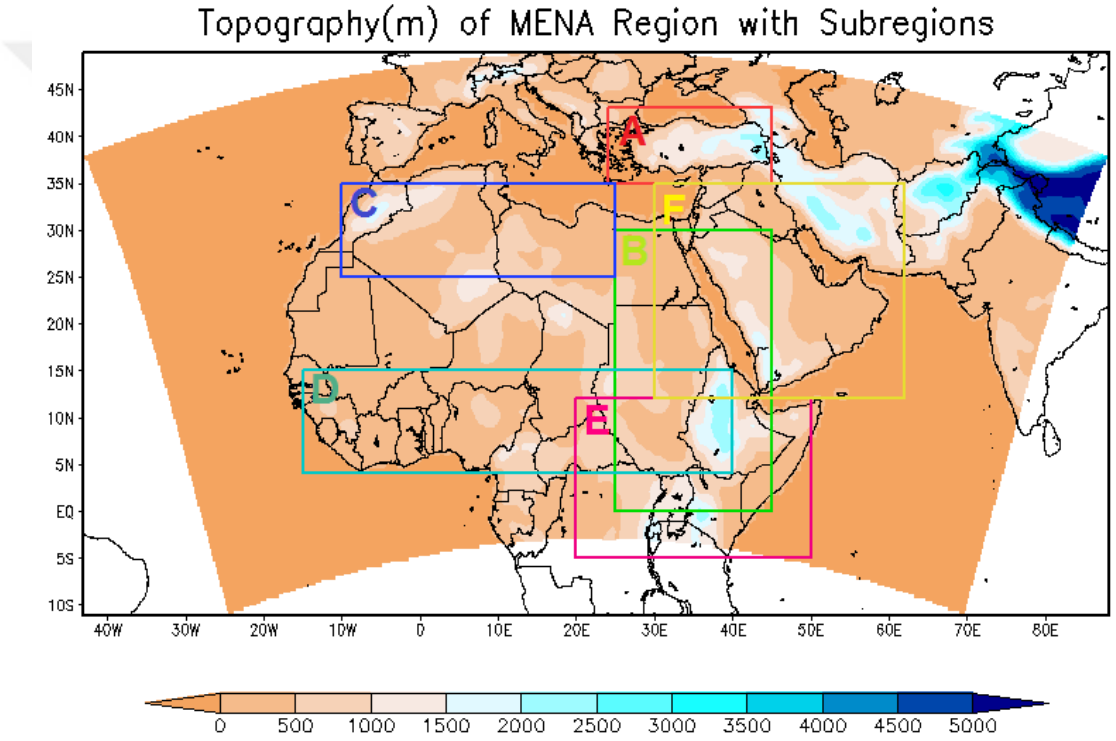


Figure 3.9. Subdomains used in this study.

# 4. RESULTS

## 4.1. SPI

### 4.1.1. SPI Results of Region A

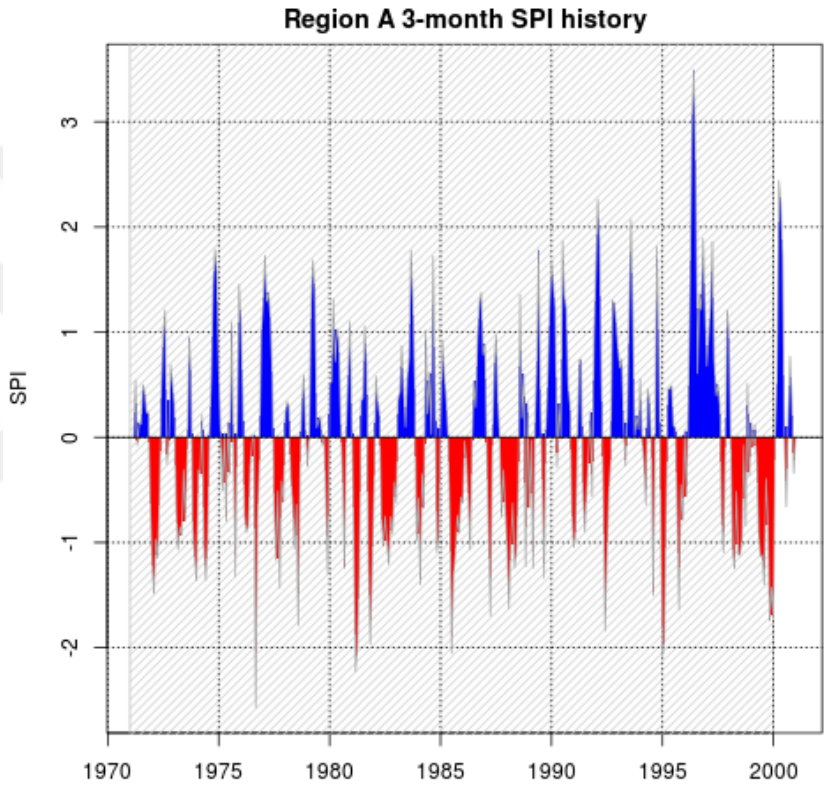


Figure 4.1. 1971-2000 period time series of 3-month SPI for Region A.

In Figure 4.1, SPI fluctuates as expectedly according to the seasons in Region A, which surrounds Turkey. However, while the trend is very consistent for about the first 25 years of the period, the durations of the wet and dry conditions get longer during the last 5 years of the period. Turkey had an above normal year in terms of precipitation in 1996, 1997 and 1998 [63]. 1999 and 2000 were below normal in terms of precipitation, and SPI captures these facts with the data taken from RegCM4.4.

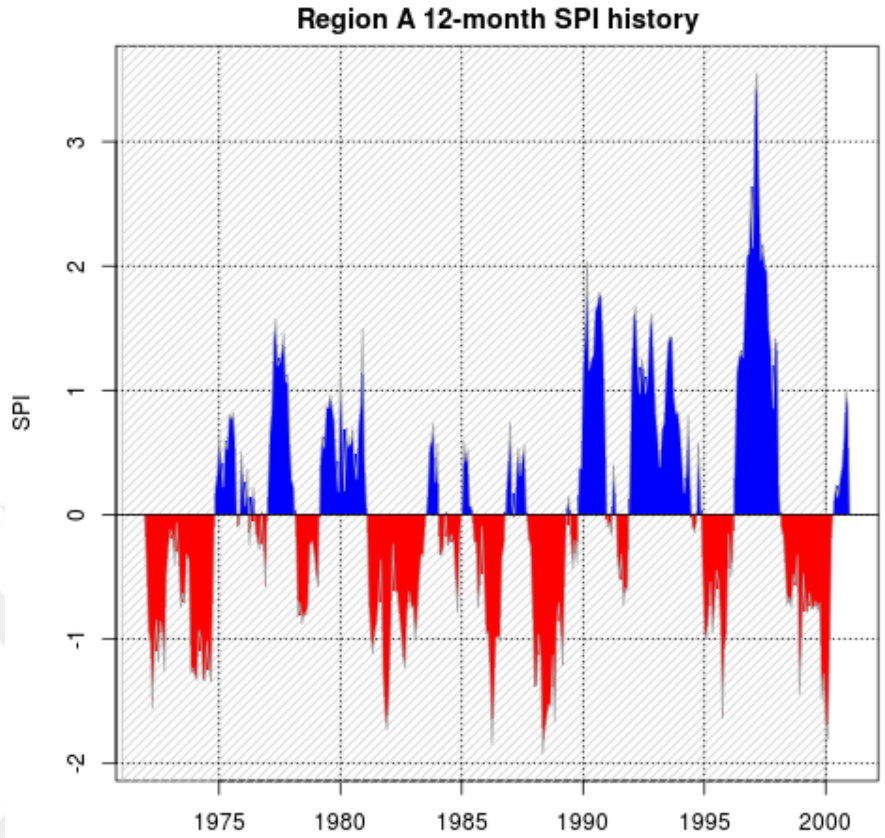


Figure 4.2. 1971-2000 period time series of 12-month SPI for Region A.

In Figure 4.2, the lines are thicker compared to 3-month SPI since the 12-month SPI uses the data from the previous 12 months. We can again see the wet years 1996, 1997, 1998 and the dry years 1999, 2000 as we saw in the 3-month SPI. The reason for the time series overflowing the 2000 threshold is that our input starts from the first month of 1971 and ends at the last month of 2000 and SPI uses the last 12 months of the input and calculates till 2001. Because of the same reason, the graph starts from 1972. The same situation is valid for all 12-month graphs and also 3-month graphs accordingly.

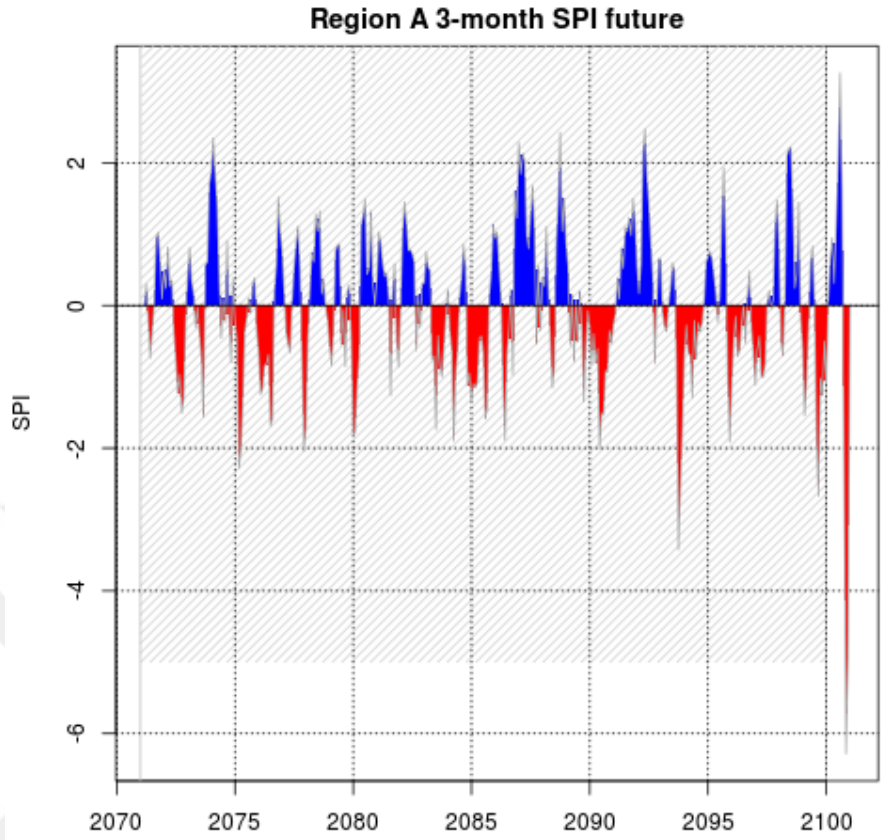


Figure 4.3. 2071-2100 period time series of 3-month SPI for Region A.

In Figure 4.3, we see the 3-month SPI results for the period 2071-2100 for Region A. Again the time series fluctuates because of the seasons, however we can see that after the year 2090, Region A will face a relatively long drought which is in the moderately dry class. After this drought a wet period is seen which is in the moderately wet class. We see that during the latter half of the future period, the region will be facing longer dry and wet events compared to the past according to these results. At the end of the century SPI makes a peak for both wet and dry conditions. The wet period do not seem to last very long but making a comment for the dry period would be injudicious since the time series ends at that point.

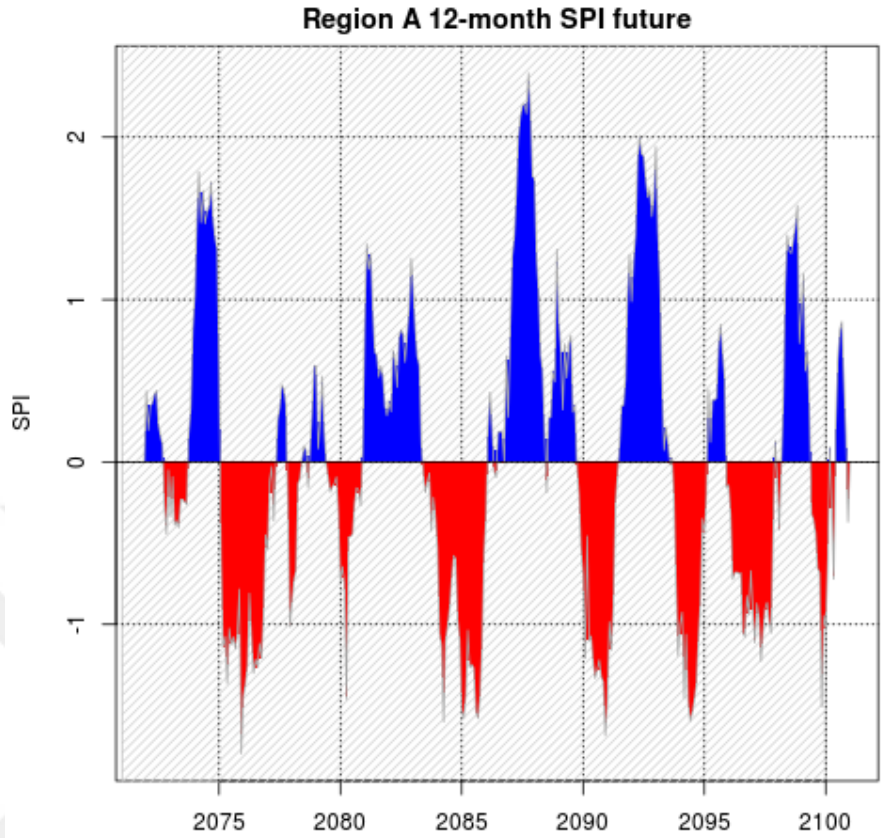


Figure 4.4. 2071-2100 period time series of 12-month SPI for Region A.

Figure 4.4 shows the 12-month SPI results for Region A. The lines are again thicker because of the reason explained at Figure 4.2. Here, the drought around the year 2085 seems more severe and longer than the drought around the year 2090. This is because the 12-month SPI adds together all the short term droughts seen in 3-month SPI around 2085. Still, the drought around this year is in the moderately dry class according the McKee drought classification. In the year 2087, there seems to be a extremely wet and very wet period and its duration does not seem to be very short. At the end of the century, we do not see a peak as we did in the 3-month SPI results. This is again because 12-month SPI adds together the previous 12 months' data.

### 4.1.2. SPI Results of Region B

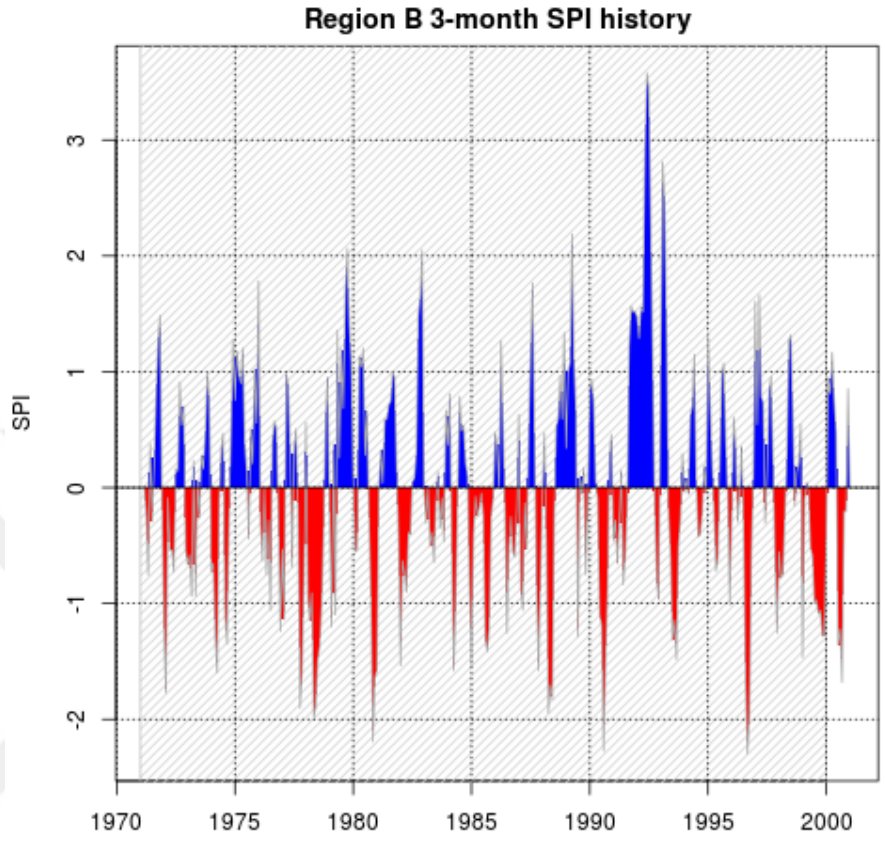


Figure 4.5. 1971-2000 period time series of 3-month SPI for Region B.

Figure 4.5 shows 3-month SPI results for the historical period of Region B. The first thing that captures the attention in the time series is the peak of the wet conditions around the years 1991, 1992. SPI value around these years is above 3, which is in the extremely wet class. This can be explained by the Active Red Sea Trough (ARST) which is an infrequent weather phenomenon that is associated with extreme precipitation, flash floods, and severe societal impacts in the Middle East. This phenomenon occurred in 1979, whose effect can also be seen from the graph, and in 1991 [64]. SPI drops below -2 a few times, which means extreme drought. Around late 1970s and late 1990s, the duration of the drought seems to be the longest. During 1979-1985 and 1990-1991 Sudan had drought events because of El Niño and the graph shows these drought events clearly [65].

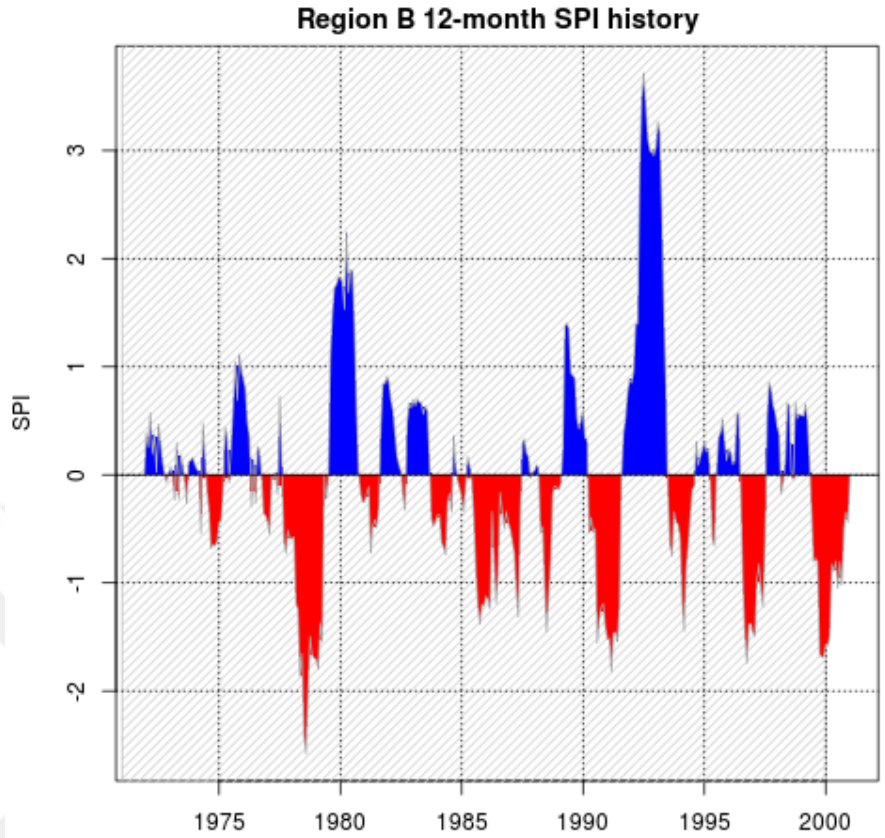


Figure 4.6. 1971-2000 period time series of 12-month SPI for Region B.

In Figure 4.6, we see clearly that the droughts in the late 1970s and late 1990s were the two of the longest droughts. During the late 1970s there was a drought recorded for the Western Africa (Sahel Region), and the graph may be showing a peak due to that drought. The drought starting around 1984 was not very severe, however it was long, which makes it a danger. The drought recorded around 1999 was severe and prolonged in northwest Africa. Additionally, 1991-1992 drought is also seem to be one of the longest droughts and even if it is not as severe as the aforementioned droughts, it was in fact continental in nature and stand unique in the available records [66].

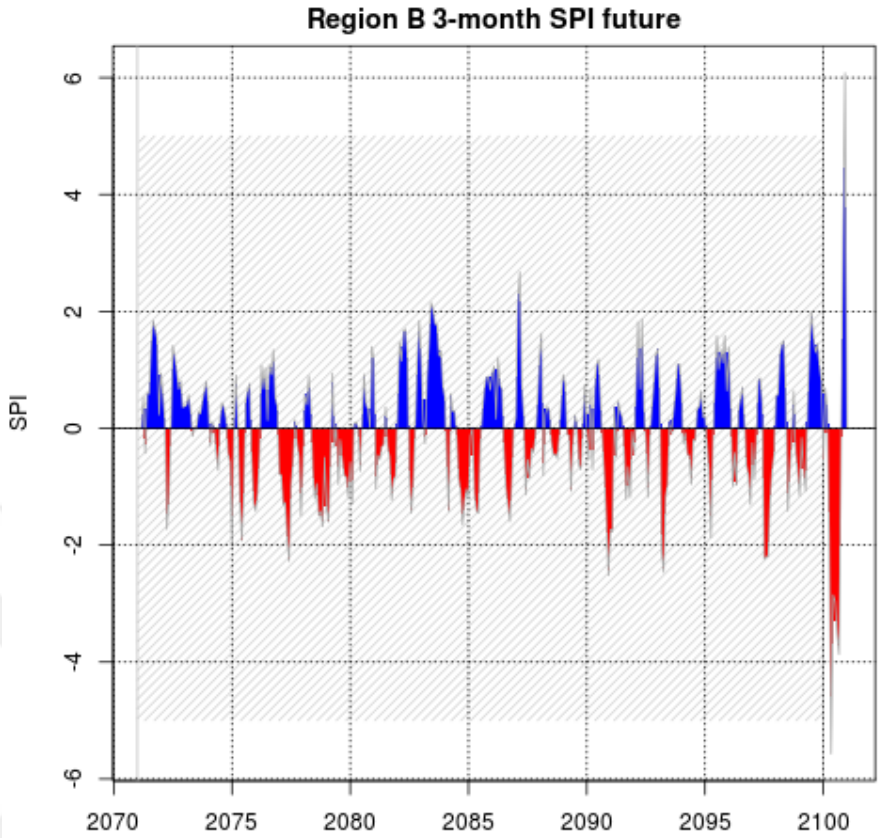


Figure 4.7. 2071-2100 period time series of 3-month SPI for Region B.

Figure 4.7 shows the SPI results of the future period for Region B. The Region B will be facing prolonged and extreme droughts and precipitations in the future as well according to these results. At the end of the century, the graph shows an extreme drought, whose SPI value reaches -4, and it is followed by an extremely wet period, whose SPI value reaches almost 5. These two events will be the most extreme events that the region will be facing during the future period according to these results. The drought at the end of the century seems to be a very severe one, however it does not seem to last a year. The duration of the extremely wet period is not shown in the graph.

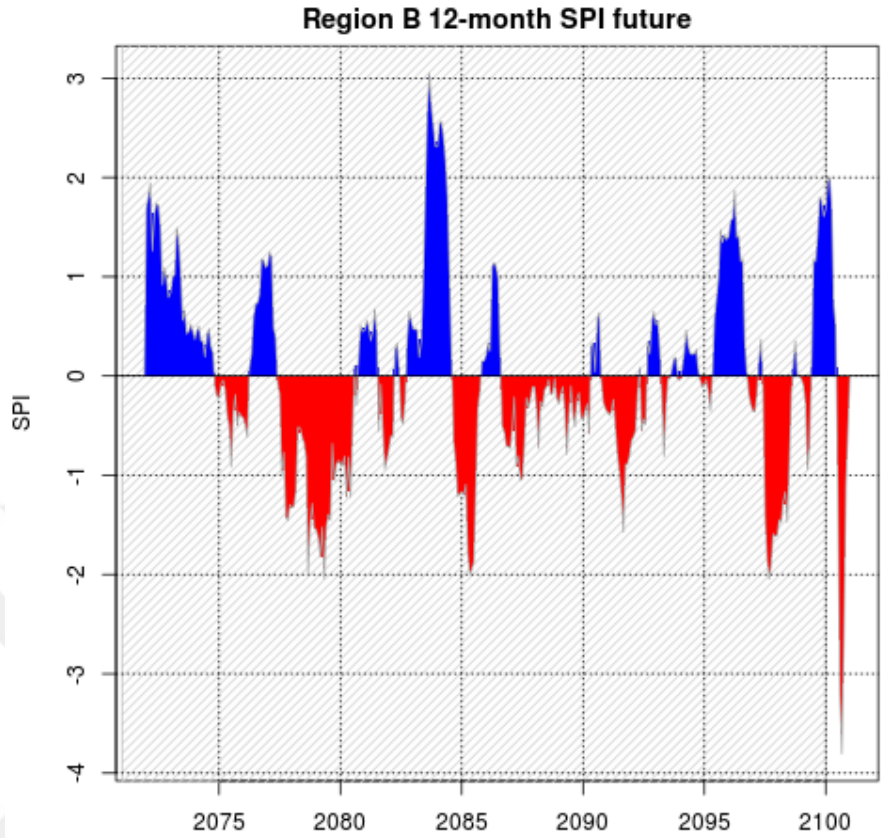


Figure 4.8. 2071-2100 period time series of 12-month SPI for Region B.

Figure 4.8 shows the 12-month SPI results of the Region B for the future period.There are two events that capture the attention in these results. The first one is the duration of the drought between 2077 and 2081. In the 3-month SPI graph there are several drought events during this period and 12-month SPI adds them together, showing us clearly the danger of the situation. The same is valid for the wet conditions in the early 2070s. The second event is the extremely wet conditions around the years 2083-2084. Here, the wet conditions seem to be both prolonged and also very severe since the SPI value is above 2. The drought shown starting from around 2087 is not severe as others however it seems to be the longest which makes it again a great danger for Region B.

### 4.1.3. SPI Results of Region C

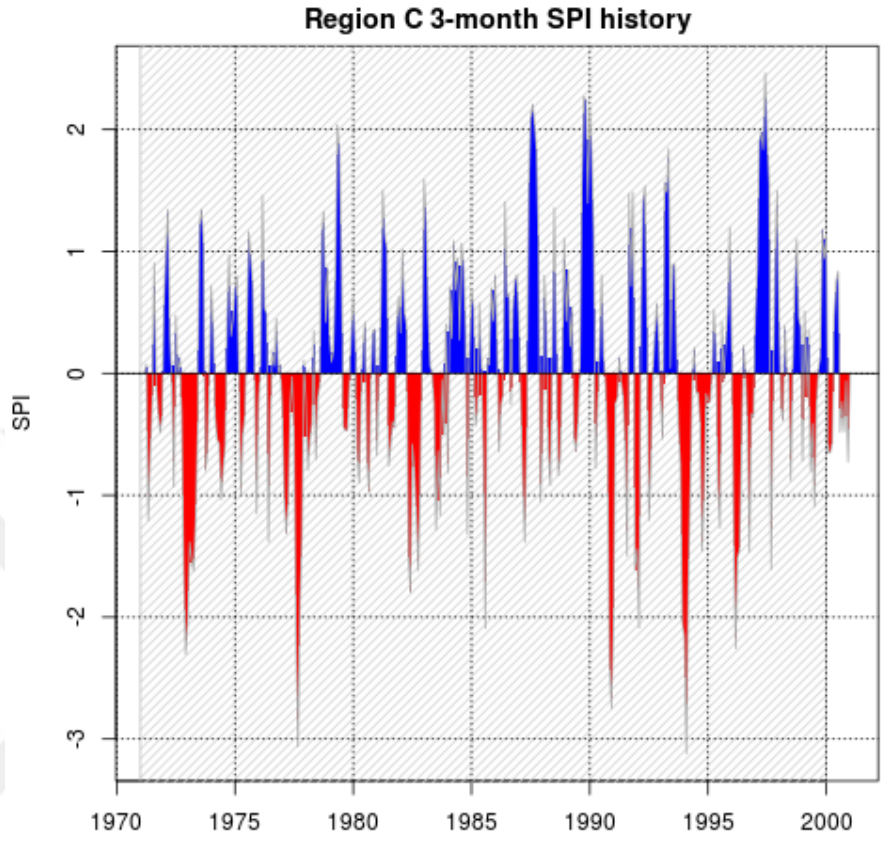


Figure 4.9. 1971-2000 period time series of 3-month SPI for Region C.

Figure 4.9 shows the SPI results of Region C for the 1971-2000 period. Since the Region contains some of the Sahara Desert, and because of the climatic conditions of the desert, the extreme events in the Region is frequent. Therefore we see very severe wet and very severe dry events in the results, which is consistent with the actual events. The severity of the aforementioned extreme drought events taken place in the late 1970s and in 1991-1992 can be seen clearly in this figure. Extremely wet conditions were also severe in the region.

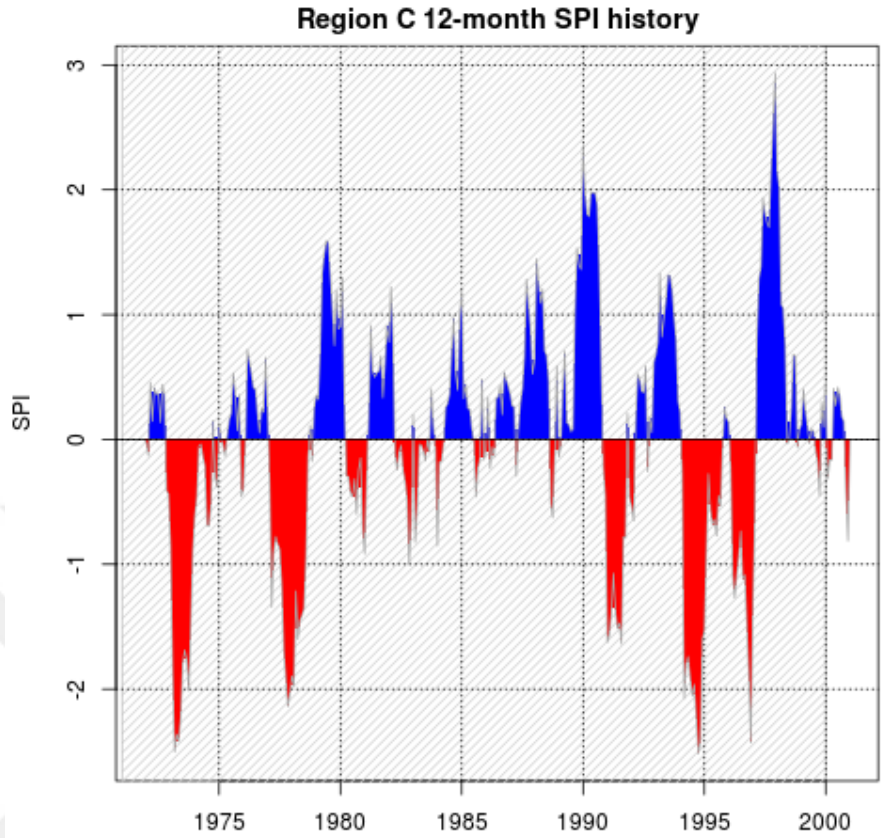


Figure 4.10. 1971-2000 period time series of 12-month SPI for Region C.

In Figure 4.10 we see the 12-month SPI results of Region C for the 1971-2000 period. Again we see the duration of the extreme events more clearly in the 12-month SPI results compared to the 3-month SPI results. In the literature, it is stated that Morocco had droughts in the years 1981-1984, 1986-1987, 1991-1993, 1994-1995 and in 1999-2003 [67]. It is also stated that Western Algeria and Tunisia had droughts in 1999-2002 [68]. However, we see droughts around 1973-1974, 1977-1978, 1994-1996 and this may be due to Sahara Desert being in Region C to some extent.

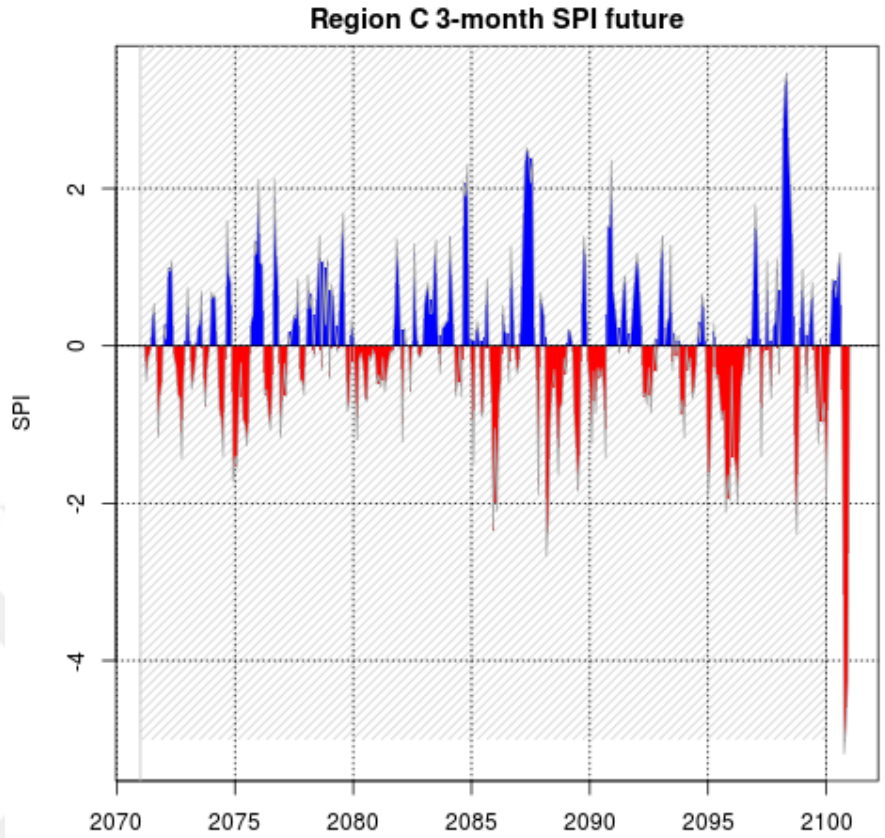


Figure 4.11. 2071-2100 period time series of 3-month SPI for Region C.

Figure 4.11 shows the future period SPI results for Region C. According to these results, the region will be facing extremely wet and extremely dry conditions in the future period as in the past. There will be a prolonged dry period for the region starting from 2087 lasting till 2091. This drought is in the extremely dry class of the McKee drought classification in the beginning, however towards the end, its severity decreases. Still, it is a long-term drought, therefore it is dangerous for the countries in Region C. A similar dry event is seen starting from the year 2094 and lasting till the year 2097 and it is followed by an extremely wet event. At the end of the century, we see a peak in the dry conditions whose SPI value exceeds -4.

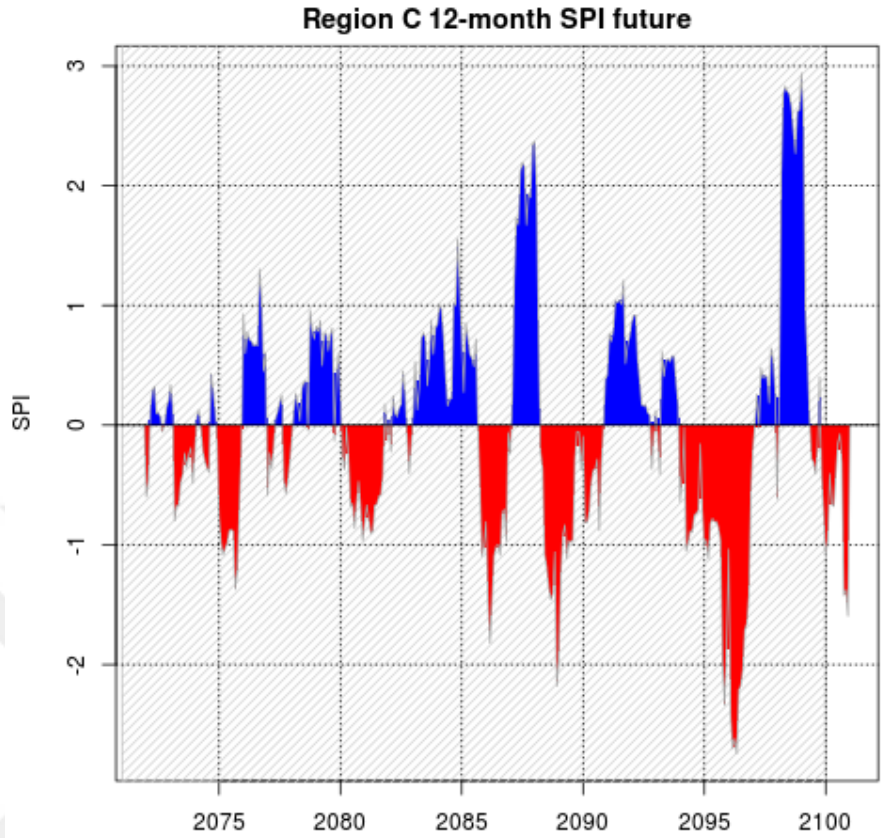


Figure 4.12. 2071-2100 period time series of 12-month SPI for Region C.

In Figure 4.12, we see the 12-month SPI results of Region C for the future period. Again, we see the extremely wet conditions at the end of the century and we see that the event is prolonged. Here we do not see the extreme drought at the end of the century as in 3-month SPI graph, since the 12-month SPI adds together the previous 12 months' data successively. However, the results show that the drought starting from 2094 will last almost 4 years and since the SPI value reaches to almost -3, it will be extremely severe.

### 4.1.4. SPI Results of Region D

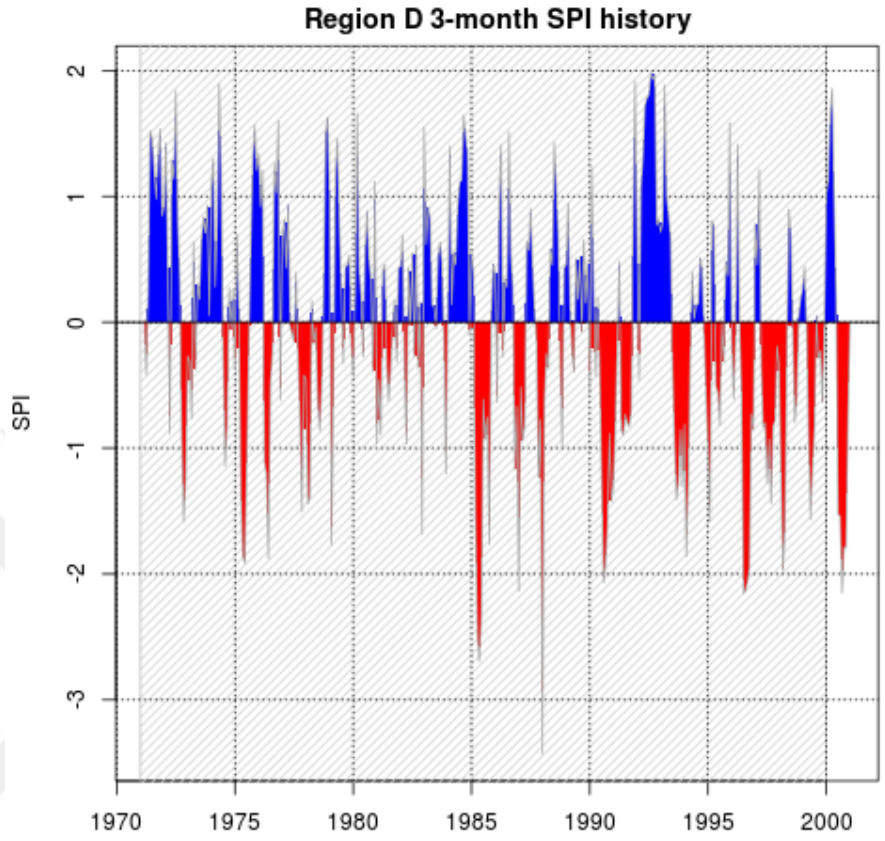


Figure 4.13. 1971-2000 period time series of 3-month SPI for Region D.

Figure 4.13 shows the 3-month SPI results of Region D for the historical period. The region has no winters but it has precipitation almost in a regular manner. SPI gives a severe drought around 1986 and a very long drought starting from 1994 lasting almost to the end of the century. There seems very little precipitation during this period. We know that Sudan had a drought in 1996, Chad, Niger had droughts in 1997, Ethiopia had droughts in 1997, 1998 and 1999, Burkina Faso, Guinea had droughts in 1998 [66]. 1982-1983 and 1997-1998 were the very strong El Niño years, and El Niño episodes make the region drier. Here we see that at the end of the historical period, the region is severely dry. 1973-1974, 1975-1976 and 1988-1989 were the strong La Niña years, and during these years the region has wet periods. Therefore we can say that SPI results are consistent with the actual events.

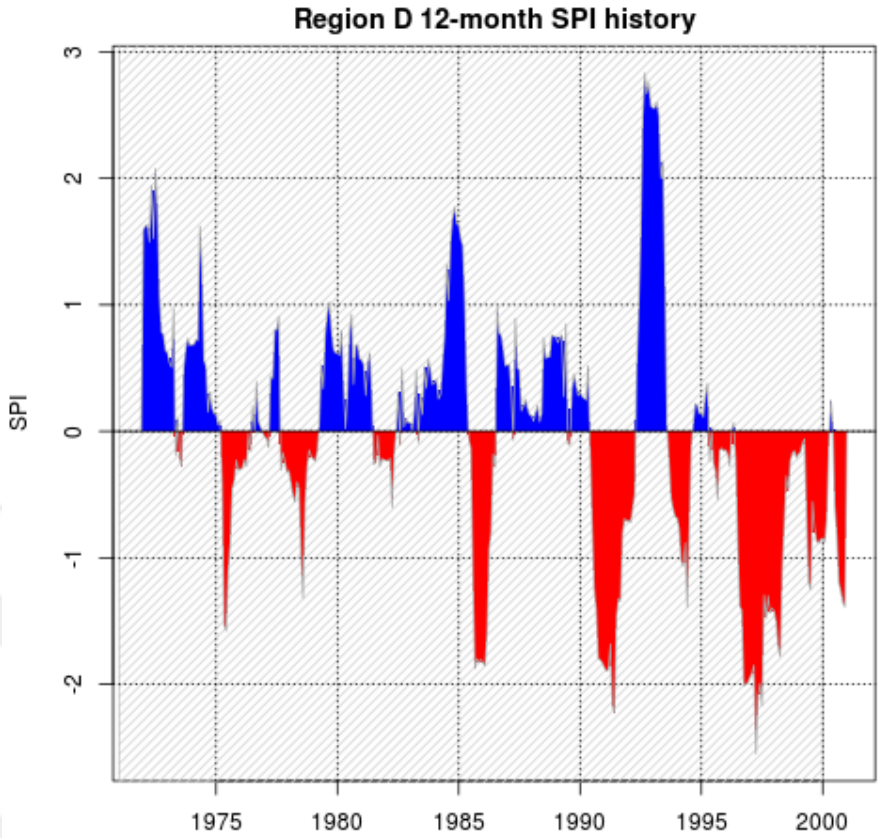


Figure 4.14. 1971-2000 period time series of 12-month SPI for Region D.

In Figure 4.14, we see the 12-month SPI results of Region D for the period 1971-2000. Here, we see the duration of the drought at the end of the century more clearly compared to the 3-month SPI results. This drought came after an extremely wet period according to the results. After the year 1985, Region D struggled with a lot of drought events as mentioned before. Again, we see the effects of El Niño and La Niña episodes on the region. It is crystal clear that the frequency, severity and duration of the droughts increased towards the end of the century which is consistent with the actual events as mentioned before.

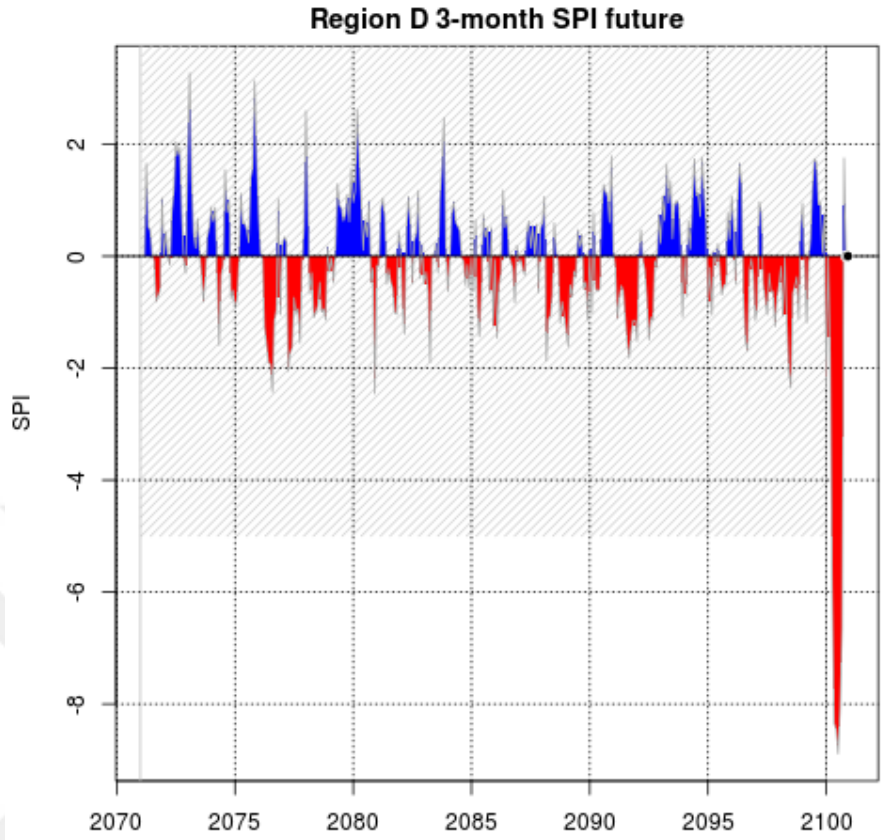


Figure 4.15. 2071-2100 period time series of 3-month SPI for Region D.

In Figure 4.15, we see the 3-month SPI results of Region D for the future period. During the first few years of the future period, there seems extreme precipitations followed by a long lasting drought between the years 2076-2079 whose SPI value almost reaches to extremely dry class. Another two drought events are seen after the year 2090 and the second one, that is between the years 2096-2099, the duration of the dry event is long which makes it a danger for the region. Again there is a peak at the end of the century whose duration can not be known from these results. However, SPI value reaches to -8 which is extremely extreme.

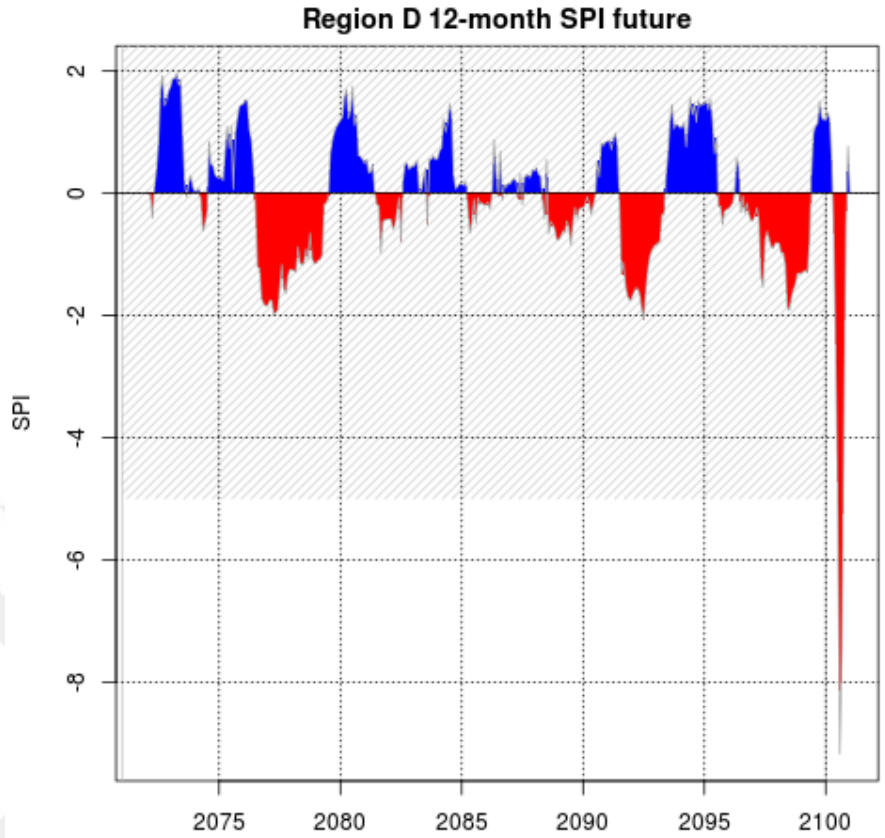


Figure 4.16. 2071-2100 period time series of 12-month SPI for Region D.

In Figure 4.16, we see the 12-month SPI results of Region D for the period of 2071-2100. As in the 3-month SPI results, we see severely and moderately wet periods according to McKee drought classification, then a very long lasting severely dry period. Towards the end of the century we see two more severely dry periods which are again prolonged. Between the years 2093-2096 we see a long wet period whose SPI value is in the moderately wet and severely wet classes. At the end of the century, we again see the peak that we saw in the previous graph and its value reaches to -8 as it did in the previous graph.

### 4.1.5. SPI Results of Region E

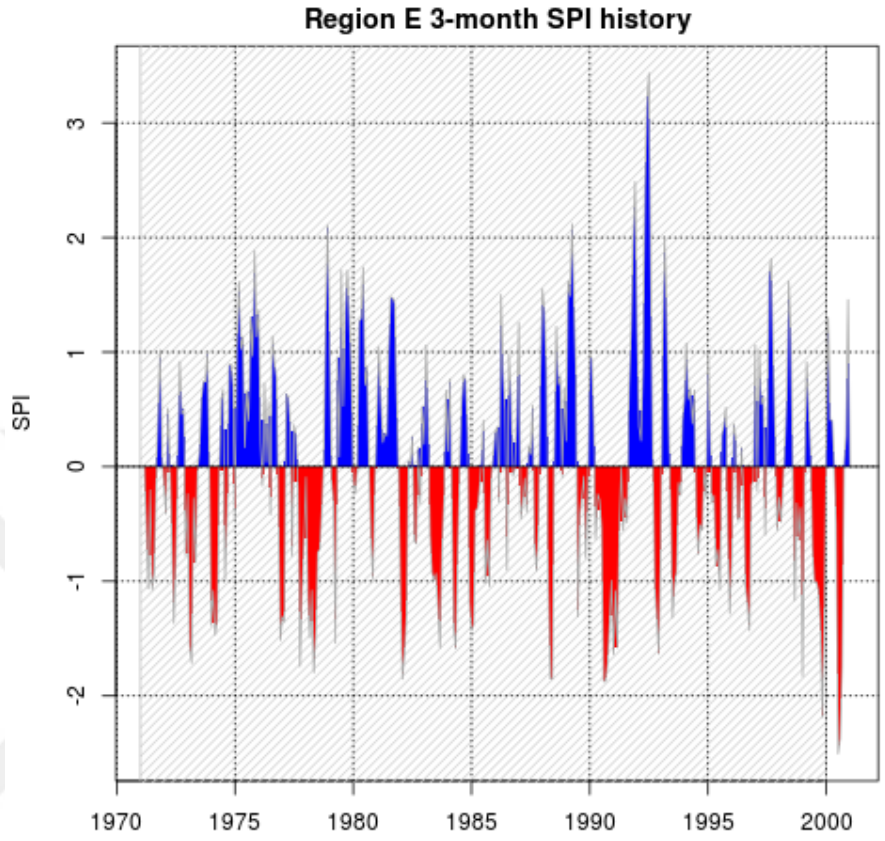


Figure 4.17. 1971-2000 period time series of 3-month SPI for Region E.

In Figure 4.17, we see the 3-month SPI results of Region E for the historical period. According to these results, the region had a prolonged wet period between 1975-1977 and then another wet period between 1979-1982. Later in 1990 and 1991 it had a severely dry period continued by an extremely wet period around 1993. Then around 1999 and 2000 the region had an extremely dry period. To verify these results, it is recorded in the literature that Ethiopia had droughts in 1989 and 1999, South Africa had a drought in 1990, Somalia, Kenya and Uganda had droughts in 1999 [66]. Somalia had floods in 1977, 1981 and 1993, South Eastern part of Ethiopia, where is exactly the part of the country in Region E, had a flood in 1993 as well and all these caused major economic damages [69, 70].

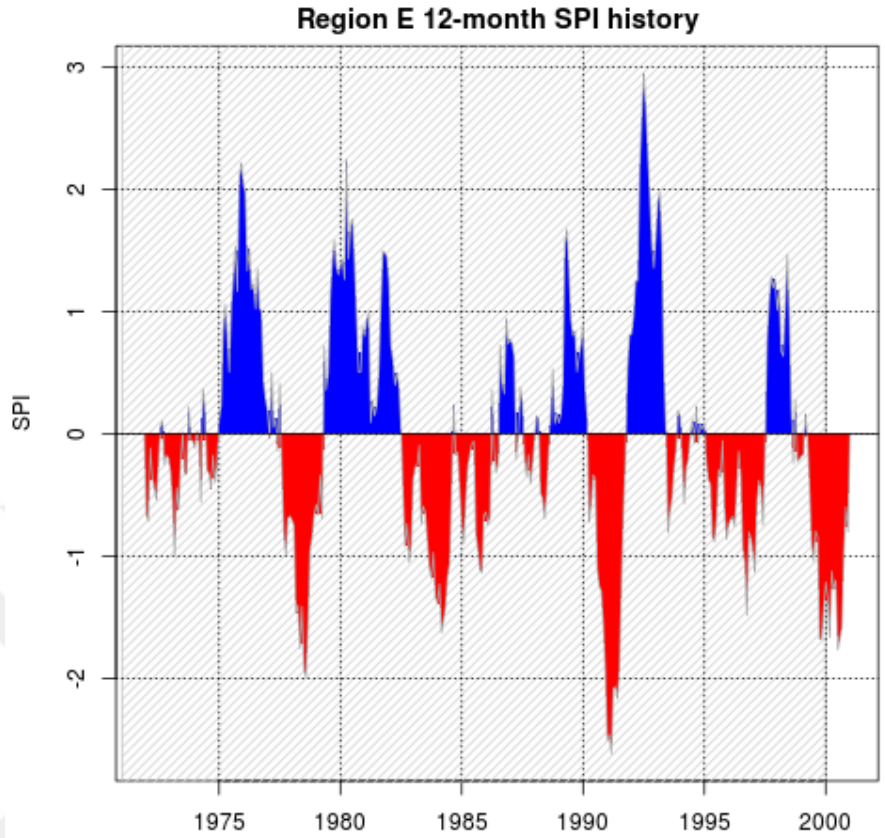


Figure 4.18. 1971-2000 period time series of 12-month SPI for Region E.

In Figure 4.18, we see the 12-month SPI results of Region E for the historical period. Again, we can see the duration of the dry and wet periods conspicuously in the 12-month SPI results. From the 3-month SPI results, we see that the year 1991 is in the severely dry class, however in 12-month SPI results it is seen to be in the extremely dry class of the McKee Drought Classification. This again because 12-month results add together the previous 12 months' data and this affects the severity of the dry and wet periods. Similarly, the drought at the end of the century is in the extremely dry class in the 3-month SPI results, however in 12-month results, it is in the severely dry class. The wettest period in 1993 is in the extremely wet class in both of the results. Region E gets affected by the El Niño events. Due to the 1982-1983 and 1997-1998 very strong El Niño episodes, the region was wetter and this effect can be seen in the results.

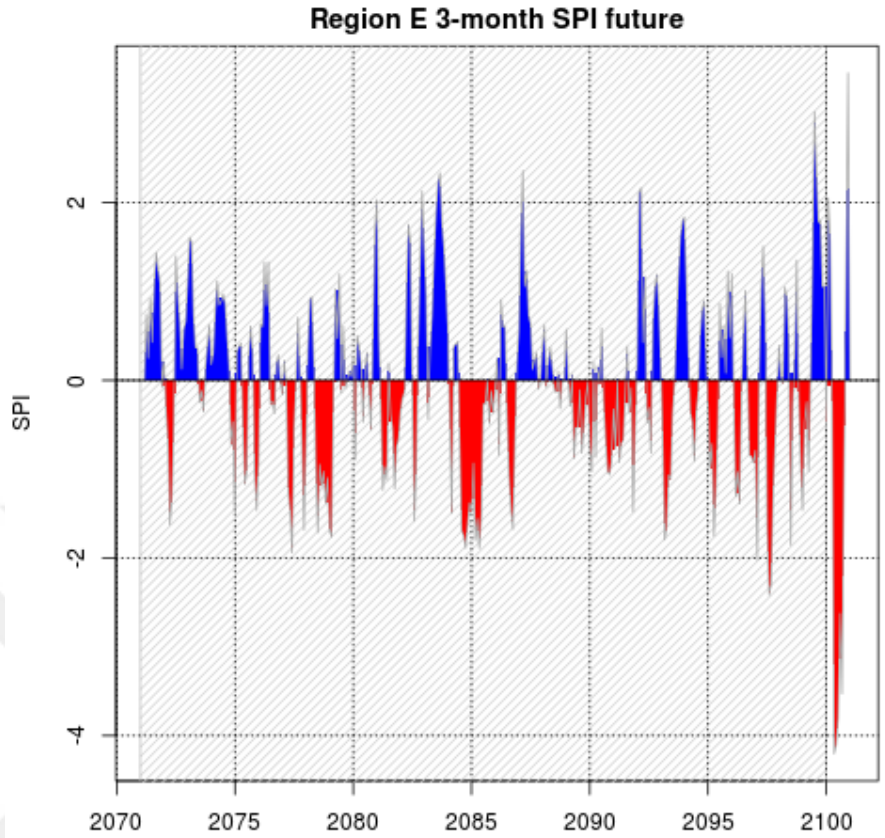


Figure 4.19. 2071-2100 period time series of 3-month SPI for Region E.

In Figure 4.19, we see the future period 3-month SPI results for Region E. The region continues to have both wet and dry periods changing in duration and severity. It seems to have a very long wet period between 2070 and 2075, an extremely wet period around 2084, a severely dry period around 2085 which may last about 2 years, a moderately dry period between 2089 and 2092. The results show peaks at the end of the century. Around 2099, the Region E will have an extremely wet period whose SPI value reaches 3, and then an extremely dry period whose SPI value reaches -4 according to these results.

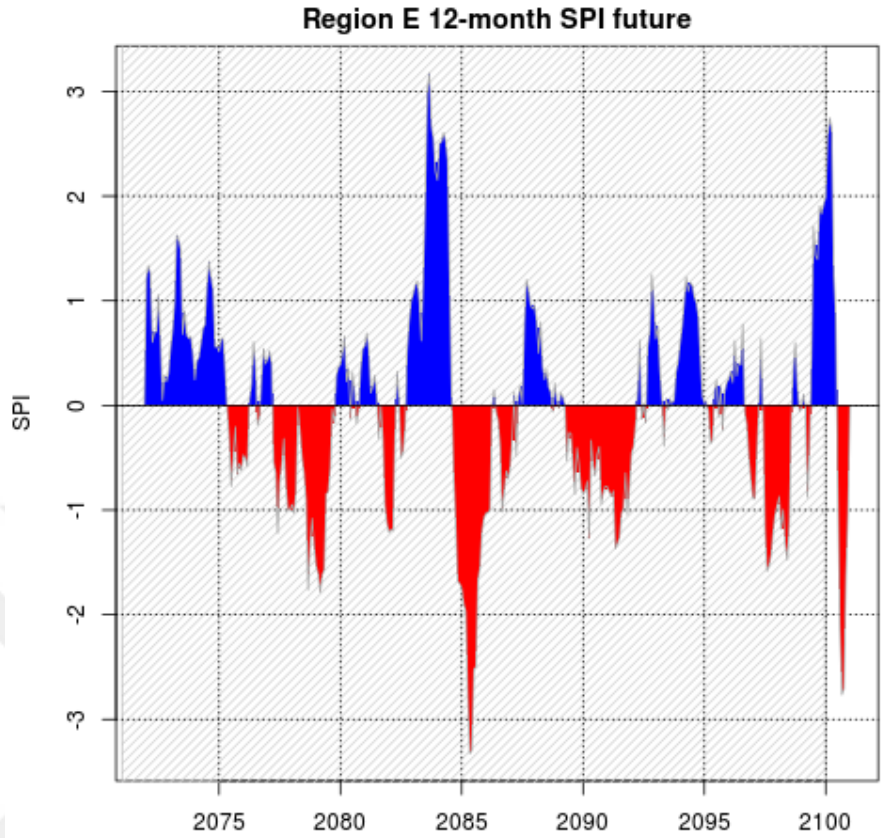


Figure 4.20. 2071-2100 period time series of 12-month SPI for Region E.

In Figure 4.20, we see 12-month SPI results of Region E for the future period. Here in these results, the severity of the situation can be seen more clearly. Aforementioned wet and dry periods seem to be more severe in the 12-month SPI results. There are two events that capture the attention in these results. The SPI value of the wet period around the year 2084 reaches to 3, and for dry period around the year 2085 it reaches to -3, which are both extreme. According to the results, the region will be facing rapid climate transitions, which will be very difficult for all livings to adapt in the region.

### 4.1.6. SPI Results of Region F

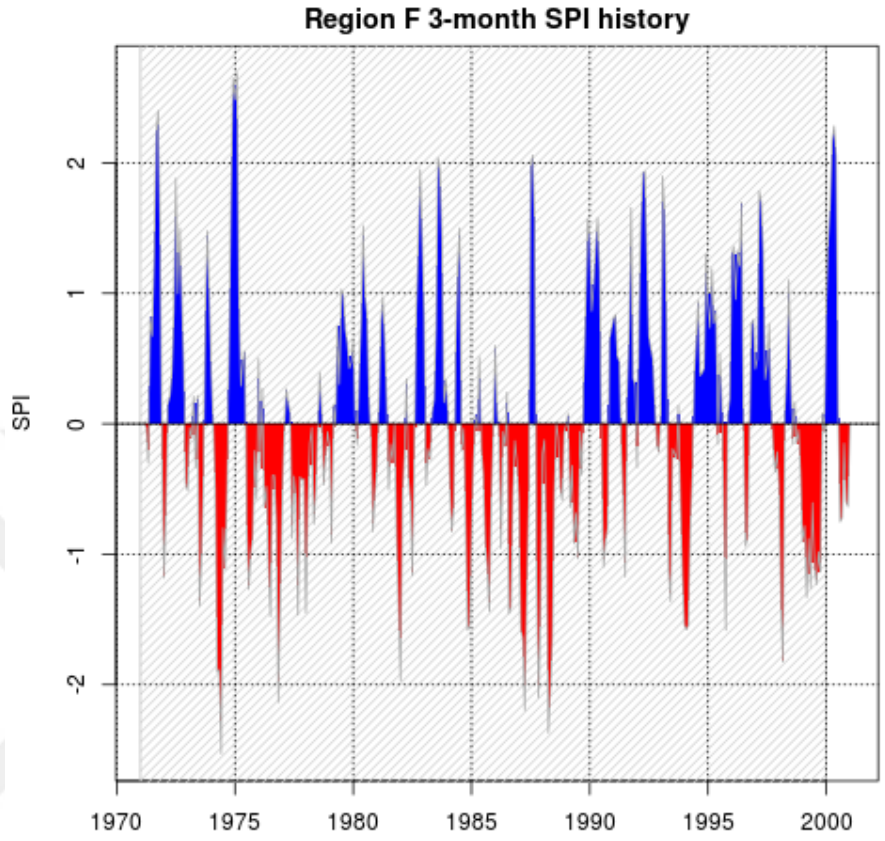


Figure 4.21. 1971-2000 period time series of 3-month SPI for Region F.

In Figure 4.21, we see that the Region F had severely wet and severely dry periods continuously since it contains a desert. The drought between the years 1985-1990 and then the wet period between the years 1990-1998 capture the attention. In the literature, there is a powerful cyclone that hit Masirah Island and progressed onto the Omani mainland in 1977. It was the most powerful storm to strike the Arabian Peninsula until Cyclone Gonu in 2007. The rainfall in the island reached 430.6mm in 24 hours which is more than six times the average annual precipitation in the area [71]. This cyclone was considered the worst disaster in Oman during the 20th century. There are other storms recorded in Region F in the years 1992, 1993, 1994, 1995, 1996 [72]. Almost all of them left heavy rainfall in the region, which is consistent with the SPI results.

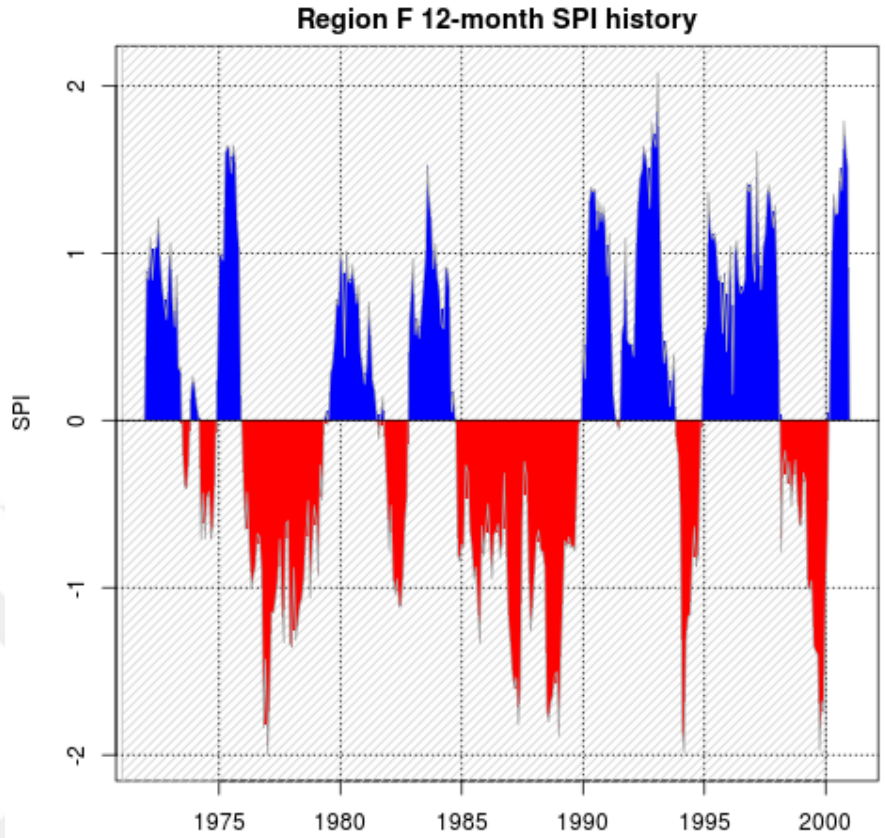


Figure 4.22. 1971-2000 period time series of 12-month SPI for Region F.

Figure 4.22 shows the 12-month SPI results of Region F for the period 1971-2000. The durations of the dry and wet events seems longer because they have no interruption since the 12-month SPI uses the previous 12 months' precipitation averages successively. The severity of the events seems milder compared to the 3-month SPI results. We see the effects of 1992, 1993, 1994, 1995, 1996 storms more clearly in the 12-month SPI results. The timing and the severity of the major events are consistent with the actual events mentioned in the 3-month SPI results of this region.

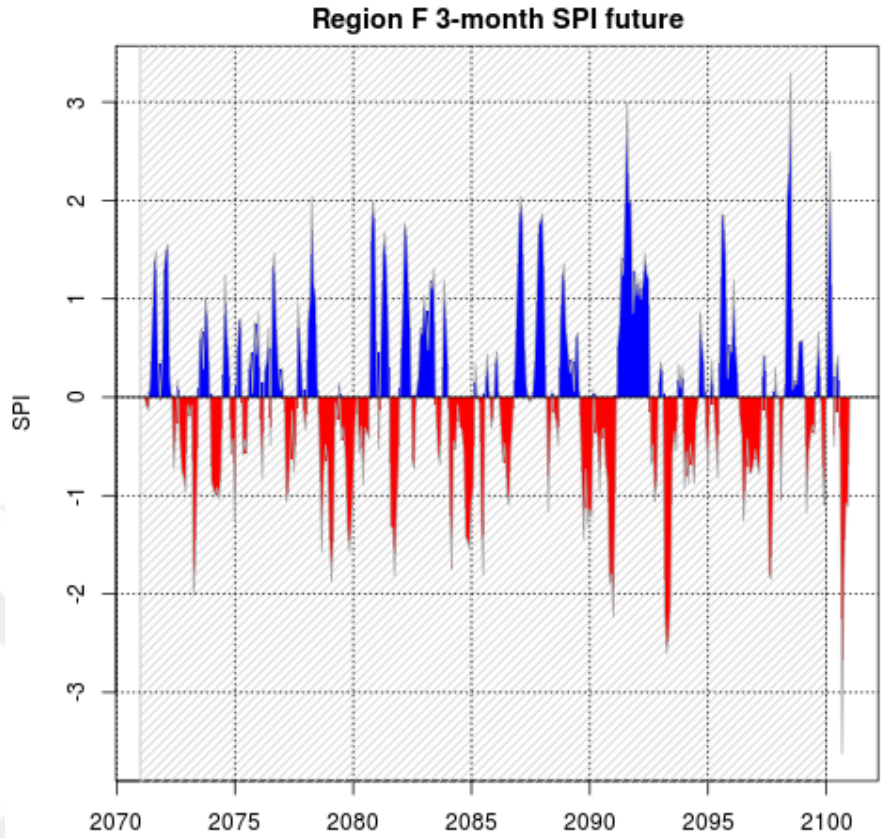


Figure 4.23. 2071-2100 period time series of 3-month SPI for Region F.

Figure 4.23 shows the 3-month SPI results of Region F for the future period. Here, we see that the severities of both the dry and wet events decrease compared to the historical period until the year 2092. Till this year, almost none of the events reach the extremely dry of extremely wet classes. Then around 2092 we see an extremely wet period followed by an extremely dry period both of which seem to last more than a year. This situation pose a threat for the region, however, these extreme events can be related to the fact that the region contains a desert. Toward the end of the century, we see a peak for both wet conditions and dry conditions, whose SPI values reach to 3 and -3 respectively.

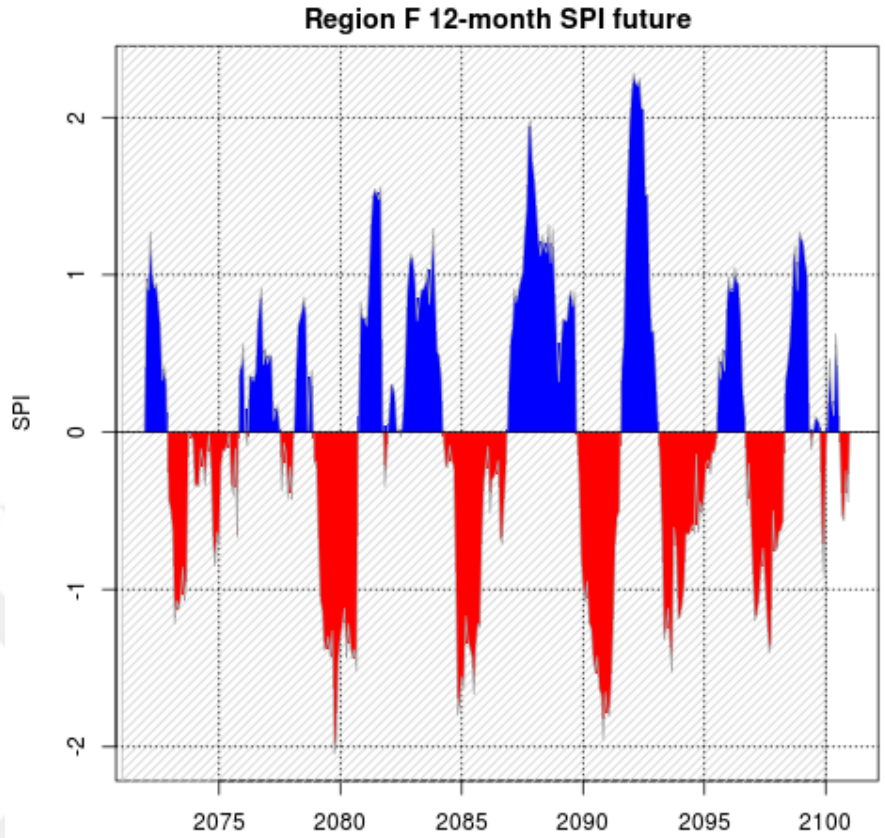


Figure 4.24. 2071-2100 period time series of 12-month SPI for Region F.

Figure 4.24 shows the 12-month SPI results of Region F for the future period. We see that the extremist event during the future period is the extremely wet event around 2092 and its SPI value exceeds 2. The longest event is between the years 2087-2090 and it is in the class of severely wet in the McKee drought classification. There are 3 severely dry events around the years 2080, 2085, 2091 and their durations seem comparable and around 2 years. This long periods and dry and wet conditions pose threat for all livings in the region.

## 4.2. SPEI

### 4.2.1. SPEI Results of Region A

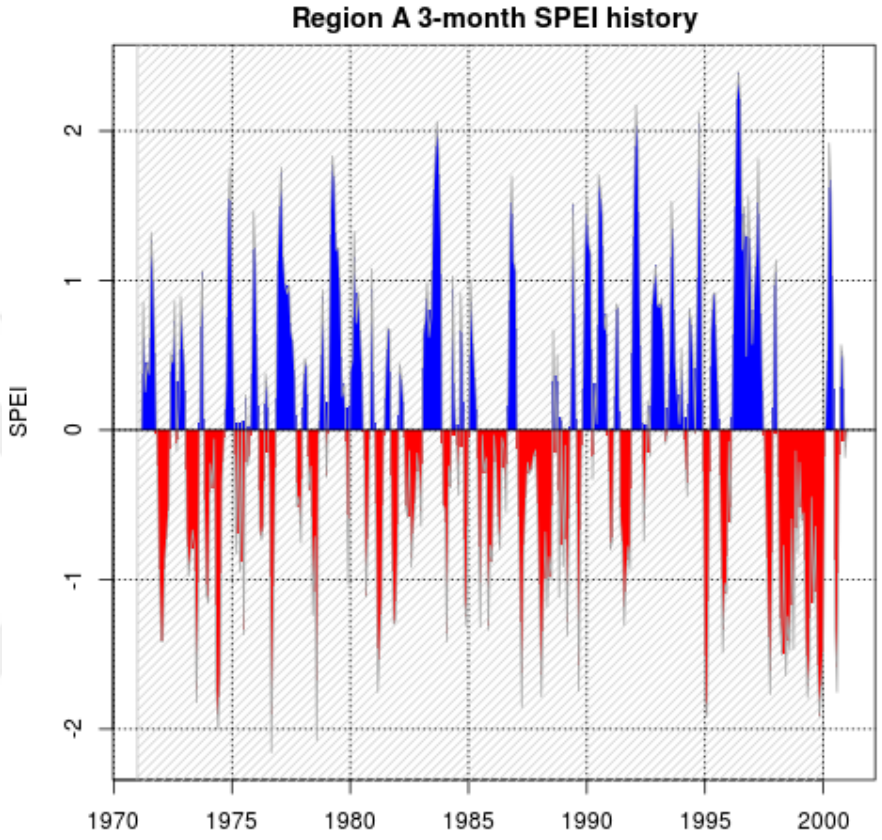


Figure 4.25. 1971-2000 period time series of 3-month SPEI for Region A.

In Figure 4.25, we see the 3-month SPEI results of Region A for the period 1970-2000. These results are very similar to 3-month SPI results. The first difference that captures the attention is that while the SPI value for the dry period around 1974 only a bit lower than -1, the SPEI value almost reaches to -2. The same characteristic is seen for the drought around 1987-1988. Moreover, SPI value for the wet period around the year 1997 reaches to 3, the SPEI value for the same period reaches to 2. This might mean that the SPEI measured the dry periods drier than the SPI. Also, it measured the wet periods less wet than the SPI.

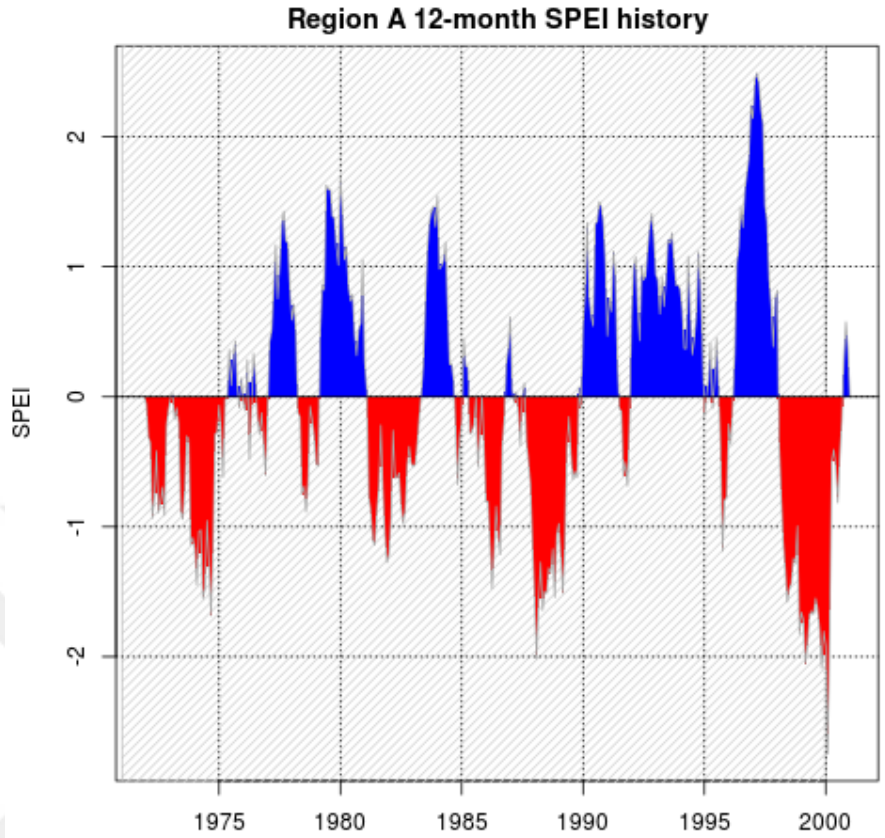


Figure 4.26. 1971-2000 period time series of 12-month SPEI for Region A.

Figure 4.26 shows the 12-month SPEI results of Region A for the historical period. Again we see the pattern is very similar with the 12-month SPI results. The first difference we see between the two graphs is the wet period around 1976. SPEI again measures the wet period less wet than the SPI. However, SPEI measures the wet period around 1980 wetter than SPI. The rest of the graphs are very comparable and the differences between the two results must be due to the fact that SPEI accounts for the evapotranspiration while SPI does not.

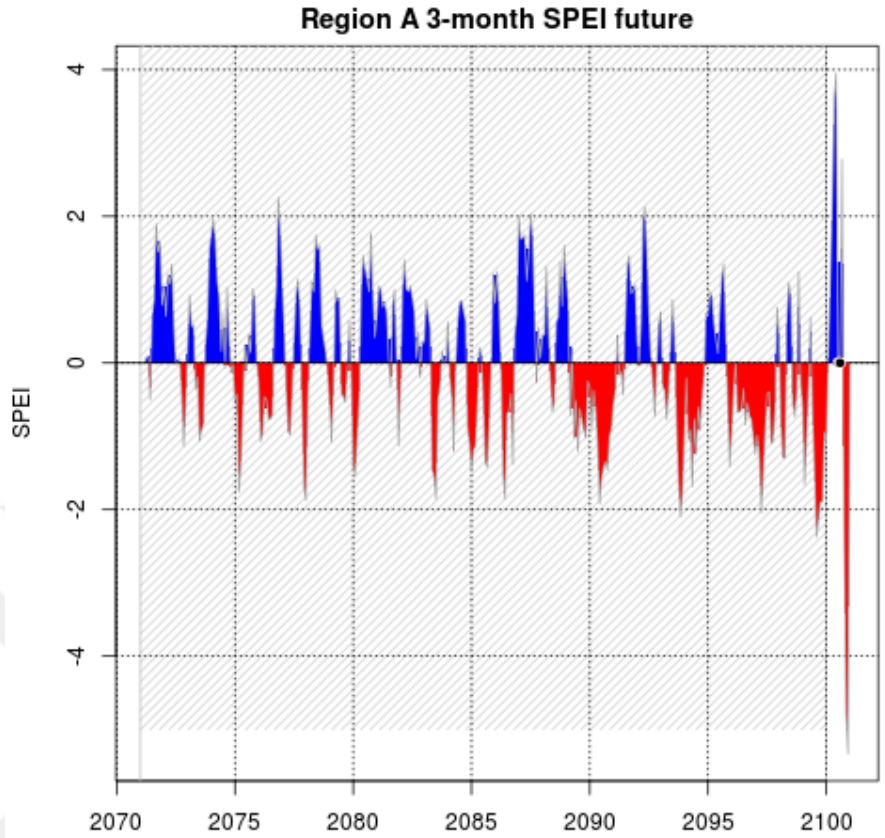


Figure 4.27. 2071-2100 period time series of 3-month SPEI for Region A.

In Figure 4.27, we see the 3-month SPEI results of Region A for the future period. When compared with the 3-month SPI results, we see SPEI value is lower than the SPI value for all the wet periods around the years 2074, 2088, 2093 and especially in 2098. That again means that SPI measures the wet periods wetter than SPEI, because SPI does not account for the evapotranspiration. When we look at the dry periods, we again see that SPEI measures the droughts around 2090, 2097, 2099 drier than SPI, however, SPI measures the drought around 2094 drier than SPEI.

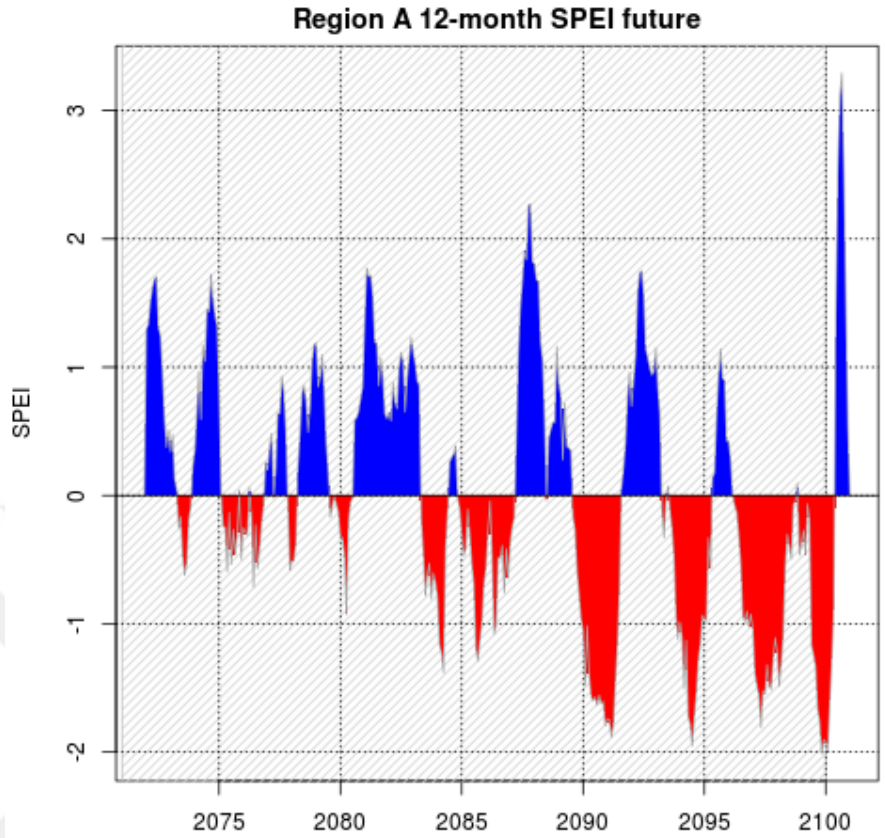


Figure 4.28. 2071-2100 period time series of 12-month SPEI for Region A.

In Figure 4.28, we see the 12-month SPEI results of Region A for the future period. Here, the first thing that captures the attention is that SPI measures the droughts around the years 2075 and 2085 drier than SPEI. The SPI value for the dry period around the years 2075-2076 is between -1 and -1.5 while the SPEI value is between 0 and -0.5. The dry period around the year 2085 is in the moderately dry class according to both of the results even if the SPI and SPEI values are a bit different. Plus, SPEI measures the wet period at the end of the century very much wetter than the SPI. These differences are due to the fact that SPEI accounts for evapotranspiration while SPI does not.

### 4.2.2. SPEI Results of Region B

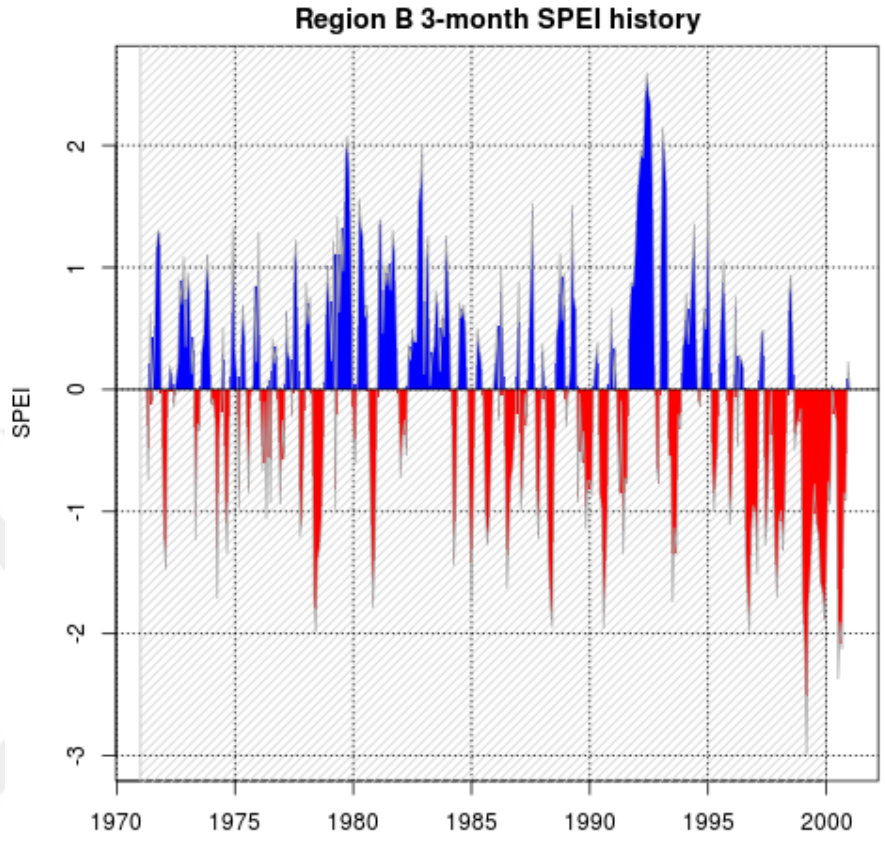


Figure 4.29. 1971-2000 period time series of 3-month SPEI for Region B.

In Figure 4.29, we see the 3-month SPEI results of Region B for the period 1970-2000. Again, the timing of the wet and dry periods are very consistent with the 3-month SPI results, however, there are some differences between the two graphs. One of the major differences is that SPI measures the wet period around 1989 a bit wetter than SPEI. The second is that while the SPI value exceeds 3 for the wet period around 1993, the SPEI value is only about 2.5. Thirdly, at the end of the century, SPI detects a moderately wet period while SPEI does not detect almost any wet period at all. Dry periods are a little bit more similar between the two graps except that at the end of the century the duration of the drought seems much longer in SPEI results than in SPI results.

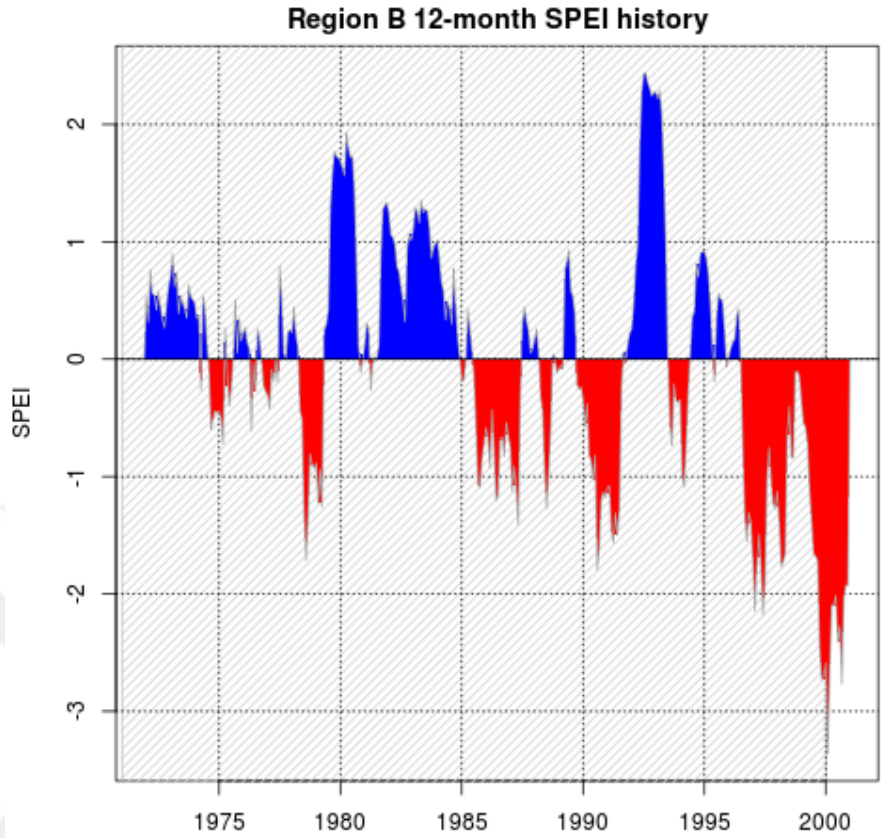


Figure 4.30. 1971-2000 period time series of 12-month SPEI for Region B.

Figure 4.30 shows the 12-month results of the Region B for the period 1970-2000. When compared with the 12-month SPI results, a few things draw the attention. In 1978, SPI measures the drought drier than SPEI, in 1993 SPI measures the wet period wetter than SPEI. The major difference between the two graphs, however, is that around 1997-1998 SPI detects a wet period while SPEI does not detect any wet period at all. Again, these differences are caused by the fact that SPEI accounts for the evapotranspiration in the region, while SPI does not.

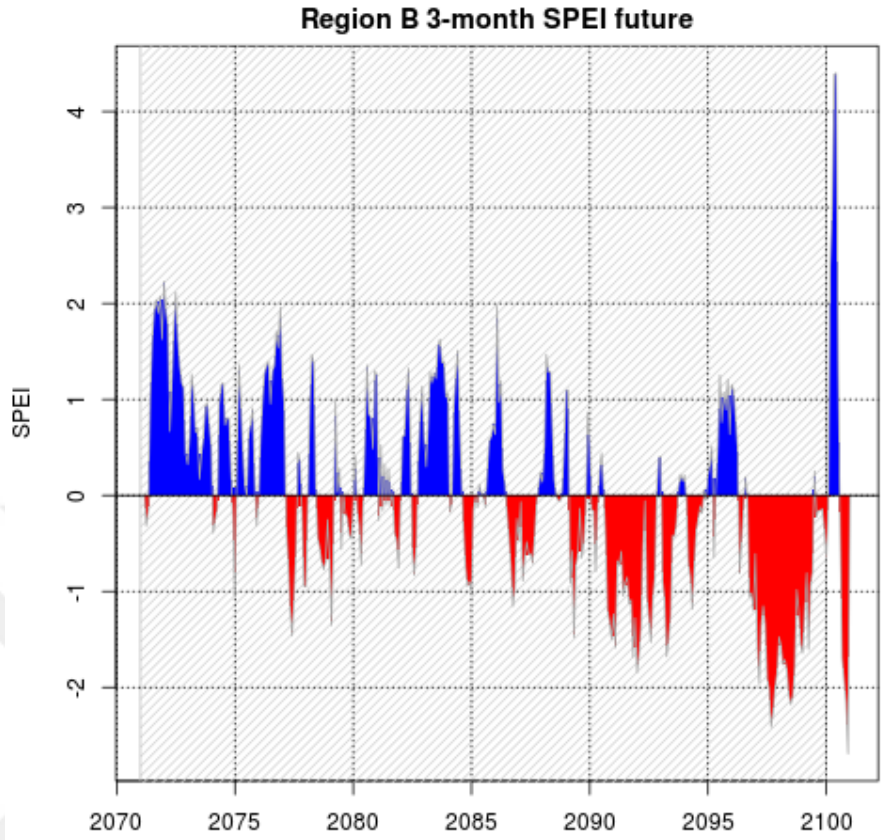


Figure 4.31. 2071-2100 period time series of 3-month SPEI for Region B.

In Figure 4.31, we see the 3-month SPEI results of Region B for the future period. When compared with the 3-month SPI results, we see 3 main differences. The first one is that SPEI detects almost no dry periods till the year 2077, however, SPI detects short-term, severely dry periods. The second one is that SPEI detects a long-term drought between the years 2091-2095, however, SPI detects a couple of severely wet periods in between. The third one is that SPEI detects another long-term drought between the years 2096-2099 while SPI again detects a couple of wet periods in between.

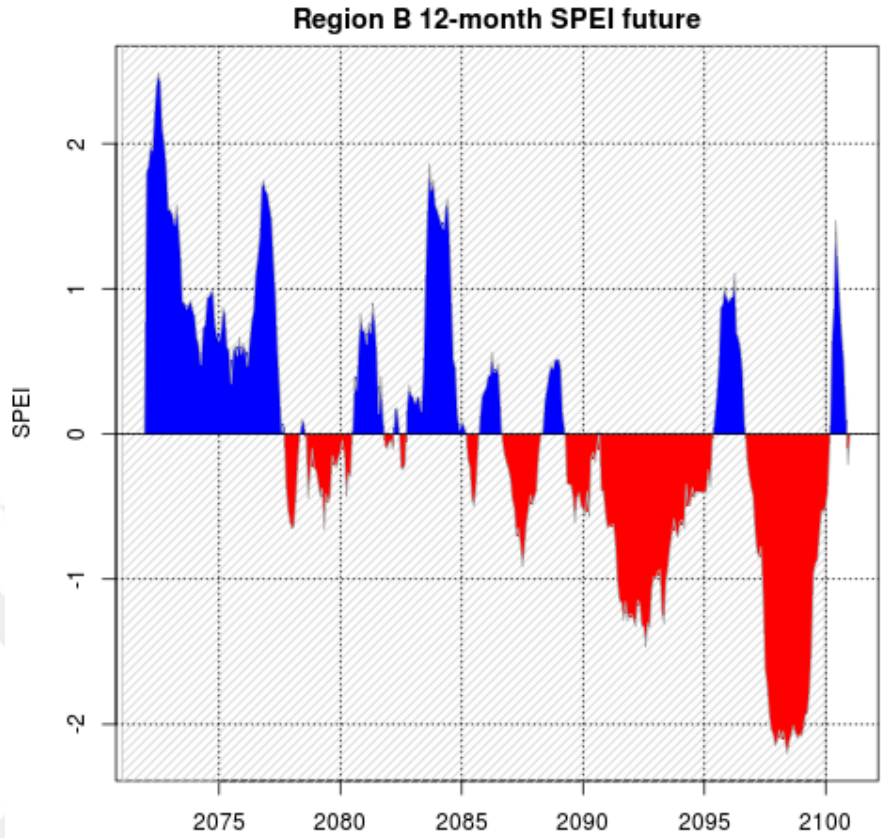


Figure 4.32. 2071-2100 period time series of 12-month SPEI for Region B.

Figure 4.32 shows the 12-month SPEI results of Region B for the future period. There are a few important differences with the 12-month SPI results for the region. Firstly, SPI results detect a near normal drought around the years 2075-2076, however, SPEI detects no such drought. Secondly, the drought around the year 2080 is severely dry according to the SPI results and it is moderately dry according to the SPEI results. Thirdly, during the long-term drought between the years 2089-2095 SPI detects some wet periods while SPEI does not. Finally, at the end of the century, SPI detects a severely wet period while SPEI detects only near normal wet period.

### 4.2.3. SPEI Results of Region C

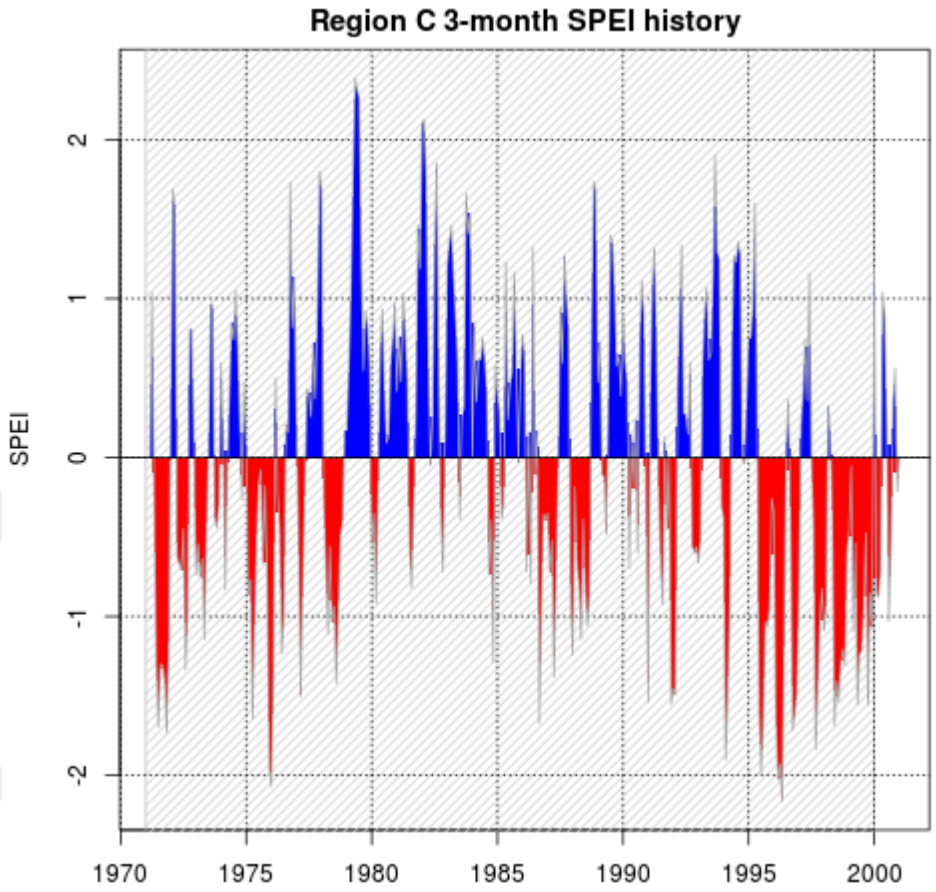


Figure 4.33. 1971-2000 period time series of 3-month SPEI for Region C.

In Figure 4.33 we see the 3-month SPEI results of Region C for the historical period. When compared with the 3-month SPI results, 2 major differences are seen. The first one is that during the long-term wet period seen in the SPEI results between the years 1979-1986, SPI detects moderately and severely dry periods. The second one is that the drought at the end of the century is shown drier in the SPEI results than the SPI results, and moreover the wet period around 1997 is almost extremely wet according to SPI while SPEI shows the same period as near normal.

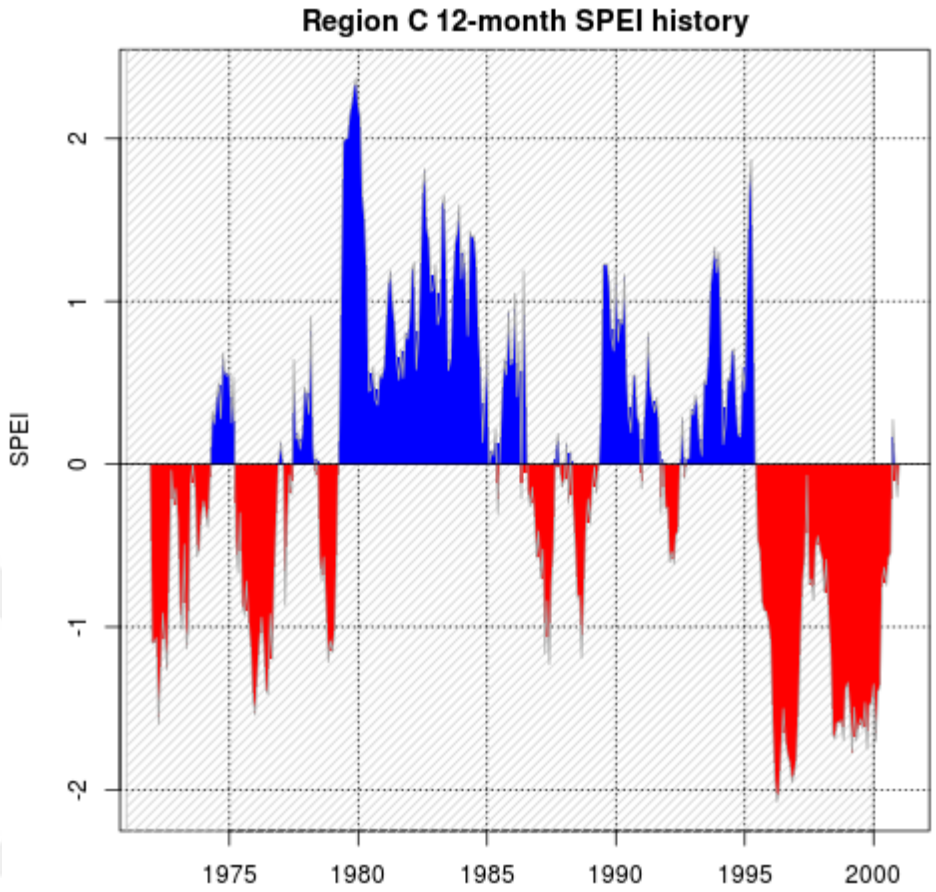


Figure 4.34. 1971-2000 period time series of 12-month SPEI for Region C.

In Figure 4.34, we see the 12-month SPEI results of Region C for the period 1970-2000. The 12-month SPI results show a few differences from 12-month SPEI results. Firstly, during the long-term wet period between the years 1979-1986 in the SPEI results, SPI shows near normal drought conditions. Secondly, during the long-term drought period between the years 1995-2000 seen in the SPEI results, SPI shows long-term severely wet period in the first years of the period. In the literature, it is stated in more than one source that Morocco had droughts in 1995, 1999, Algeria and Tunisia had a long-term drought during 1999-2000 [66]. There is no drought recorded in Northern Africa in 1996, 1997 and around these two years the drought severity in the SPEI results decreases. These informations may mean that the SPEI results reflect the truth better than SPI results for this region.

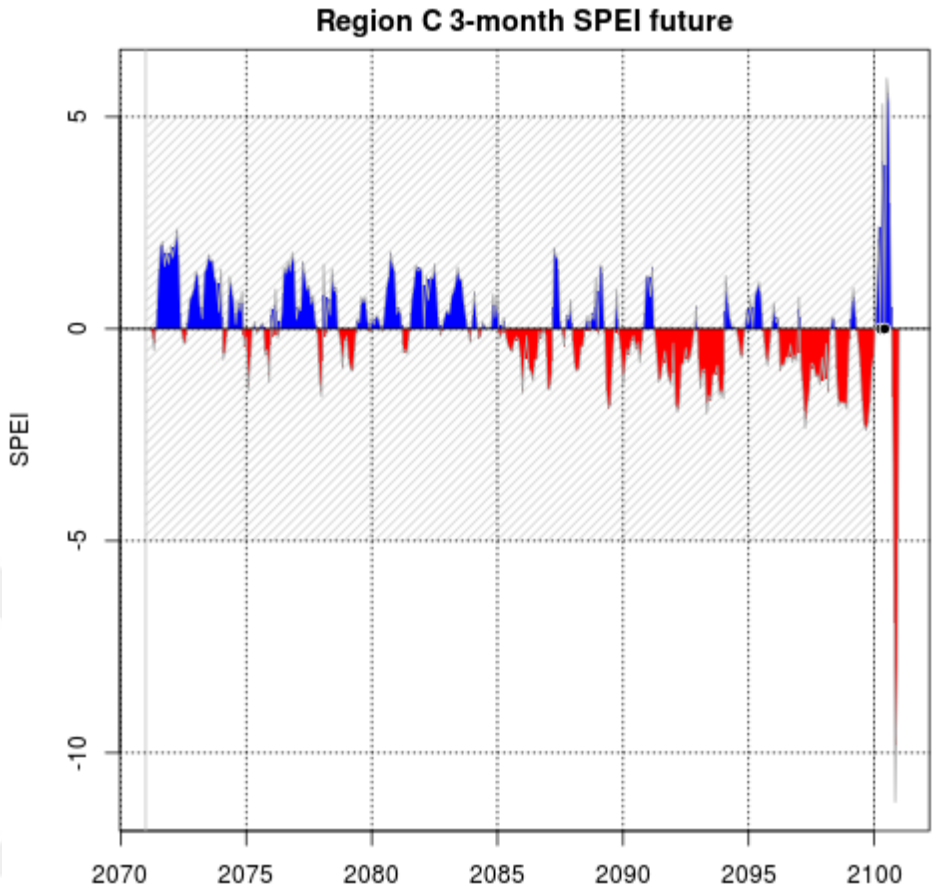


Figure 4.35. 2071-2100 period time series of 3-month SPEI for Region C.

Figure 4.36 shows the 12-month SPEI results of Region C for the period 2071-2100. When compared with the 12-month SPI results, we see that the two graphs are comparable except that during the first 15 years of the future period SPI detects more dry events than SPEI and they are not severe, and similarly during the last 15 years of the future period SPI detects more wet events than SPEI and they are not severe either. At the end of the century, we again see a peak in the wet and dry conditions which are both extremely extreme.

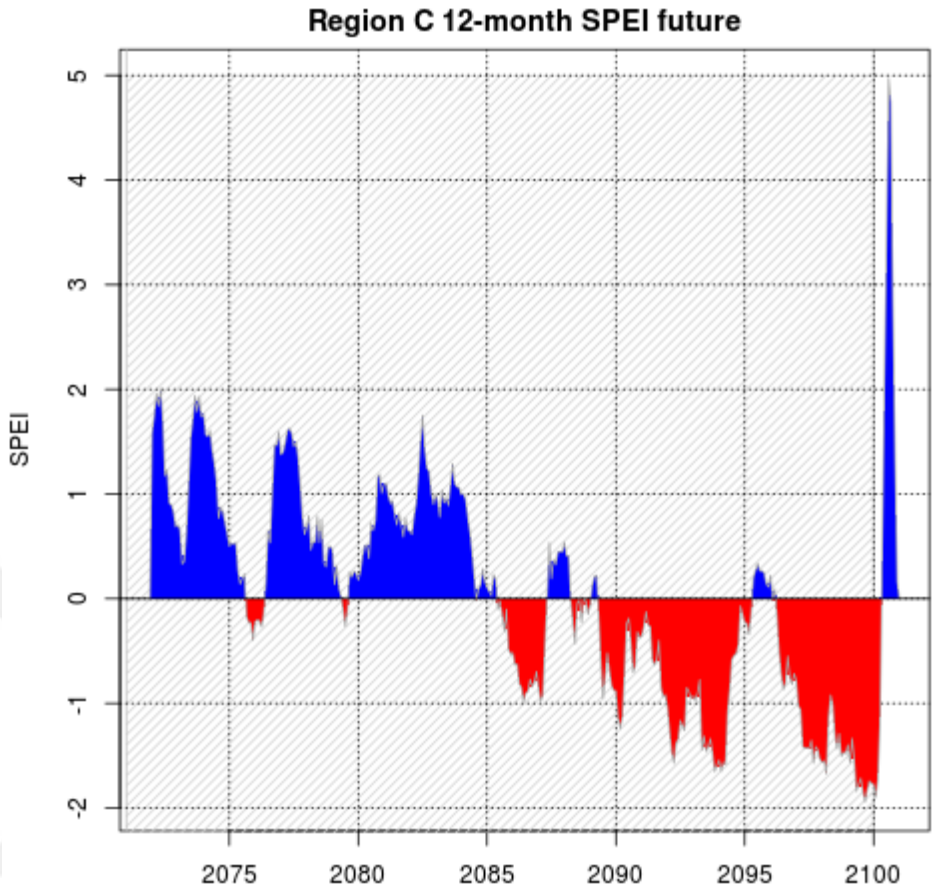


Figure 4.36. 2071-2100 period time series of 12-month SPEI for Region C.

Figure 4.36 shows the 12-month SPEI results of Region C for the future period. We see the same differences that we saw between the 3-month SPEI and 3-month SPI results here as well. During the first 15 years of the future period SPI detects more dry events than SPEI and they are not severe, and similarly during the last 15 years of the future period SPI detects more wet events than SPEI but this time they seem to be severely wet and extremely wet. Again, at the end of the century we see an extremely wet period and its value almost reaches to 5, which is very extreme.

### 4.2.4. SPEI Results of Region D

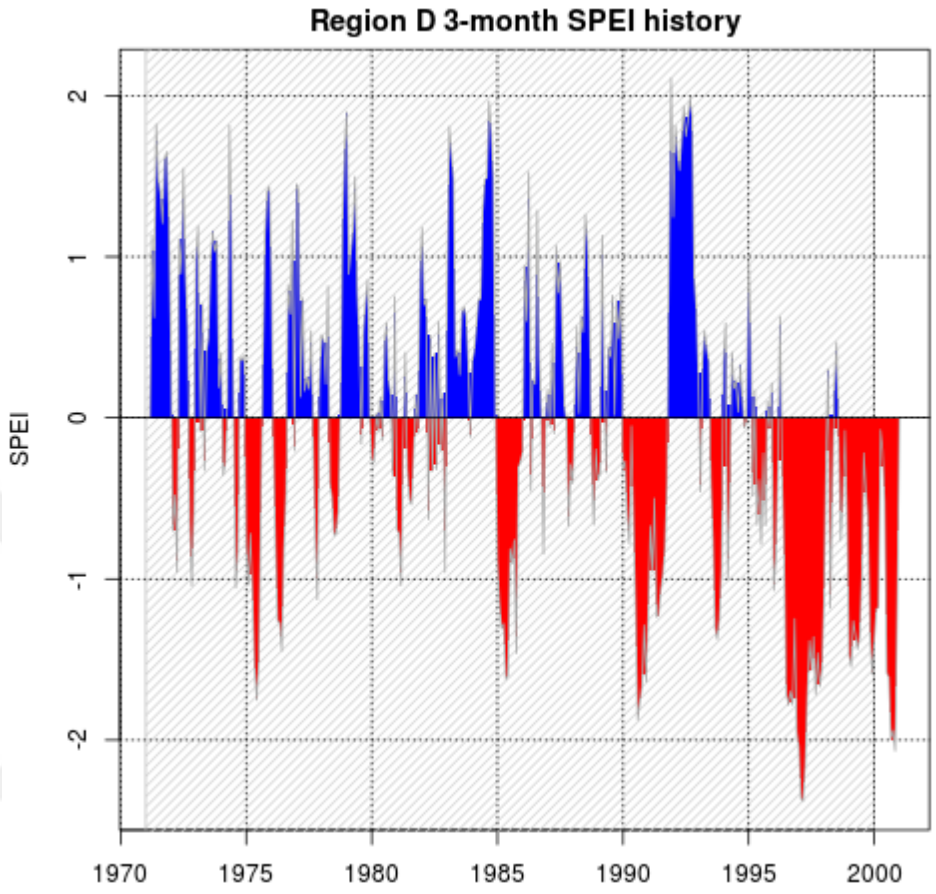


Figure 4.37. 1971-2000 period time series of 3-month SPEI for Region D.

Figure 4.37 shows the 3-month SPEI results of Region D for the historical period. When compared with the 3-month SPI results for Region D, the two graphs are very comparable and similar. The only difference is that SPI detects a couple of wet conditions during the last 5 years of the historical period, whose severities are in the class of near normal mostly and moderately wet rarely. At the end of the century, we see a very long dry period which seem to last around 5 years. This may be due to the 1997-1998 El Niño episode.

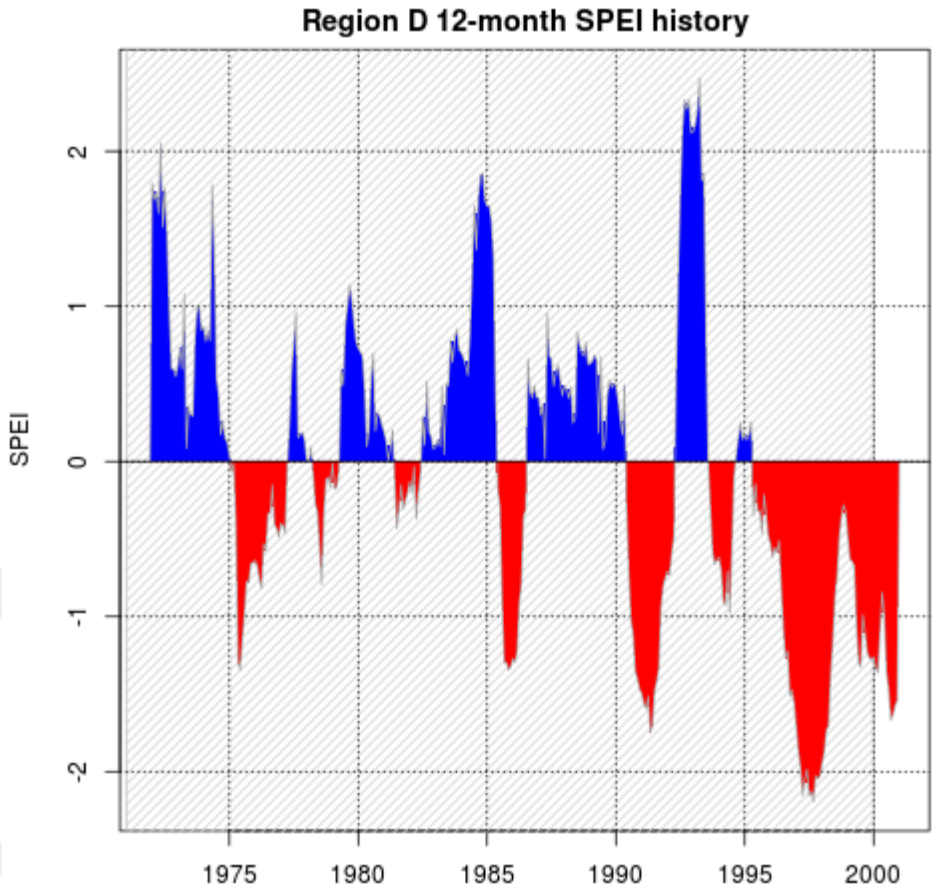


Figure 4.38. 1971-2000 period time series of 12-month SPEI for Region D.

Figure 4.38 shows the 12-month SPEI results of Region D for the historical period. We see the durations of the wet and dry periods in the 12-month SPEI more clearly than the 3-month SPEI results. Here, again the results are very comparable with the 12-month SPI results. The duration and the severity of the events are very similar. Only the long-term drought in the last 5 years of the period seems a little bit more severe in the SPI results, but still, both of the results show the drought in the severely dry class.

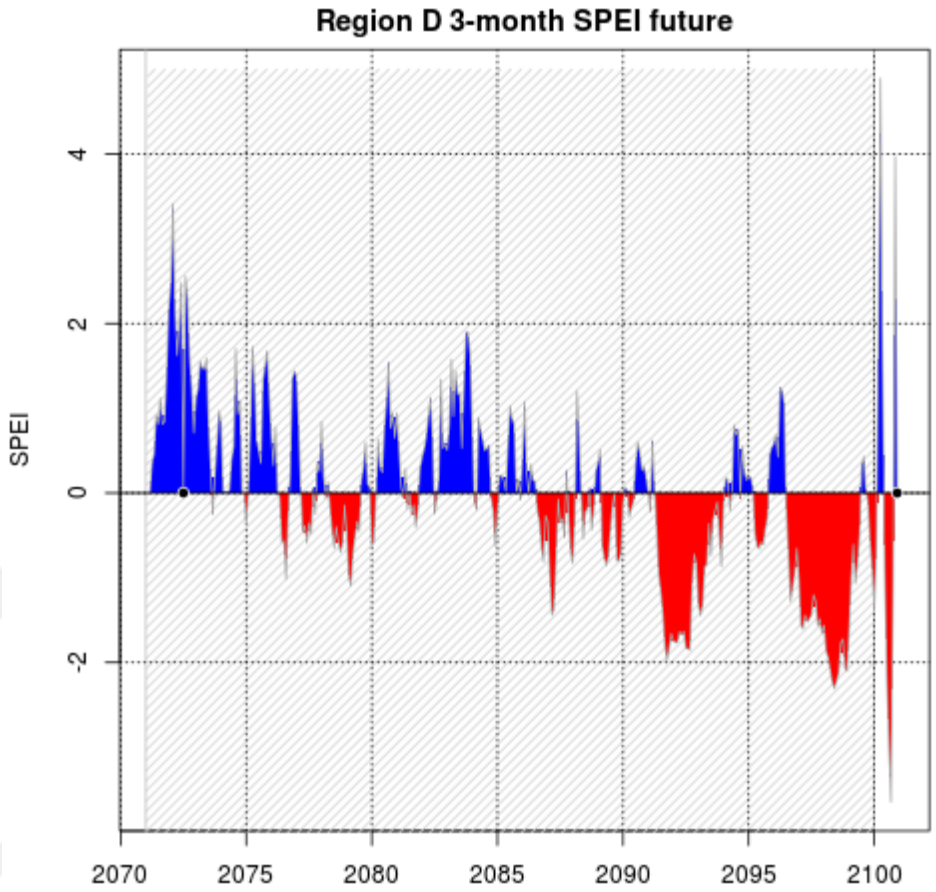


Figure 4.39. 2071-2100 period time series of 3-month SPEI for Region D.

Figure 4.39 shows the 12-month SPEI results of Region D for the future period. When compared with the 12-month SPI results, there are a few differences between the two results. The years between 2080-2085 seem wetter in the SPEI results. The duration of the wet period is longer. The years between 2091-2094 and 2096-2099 are measured drier by SPEI even though the durations of the drought periods are the same between the two results. We may expect an another El Niño event during these years since the effect of El Niño on the region is making it drier.

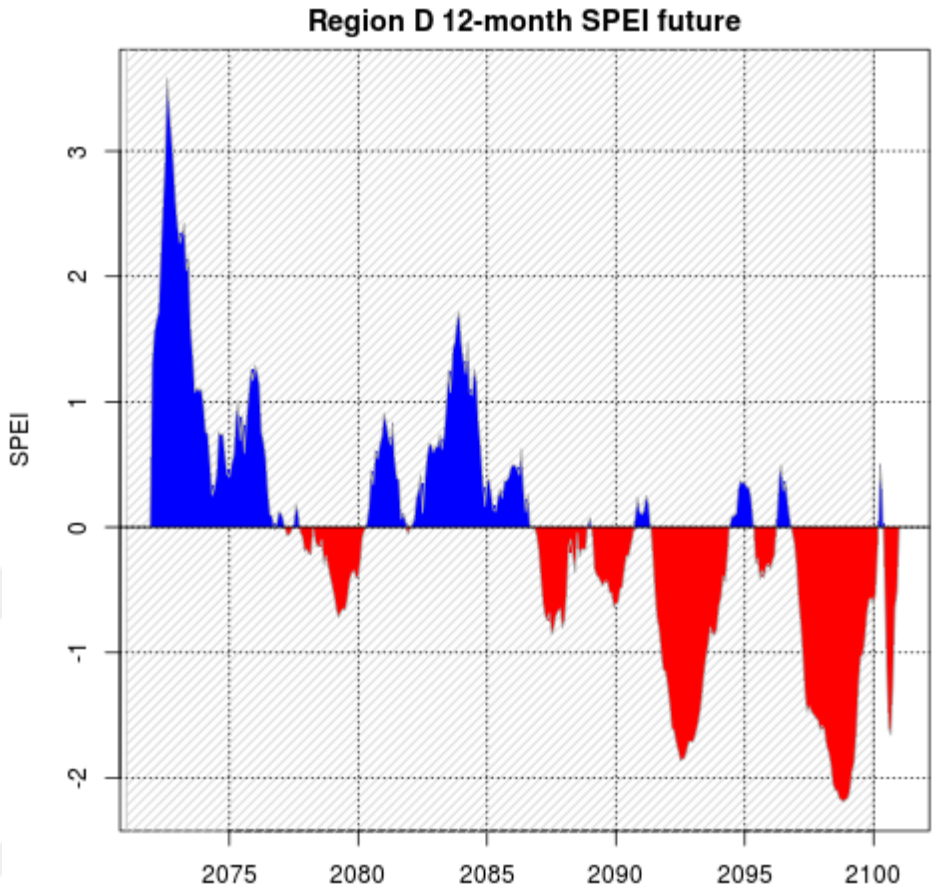


Figure 4.40. 2071-2100 period time series of 12-month SPEI for Region D.

Figure 4.40 shows the 12-month SPEI results of Region D for the future period. The first years of the period is extremely wet according to both results. Around the year 2075, SPI detects a near normal drought while SPEI detects no drought. Actually, SPEI foresees a very long wet period till the year 2086 with a 2-year near normal drought during the years 2078-2079. This drought seems to be in the severely dry class according to SPI results. At the end of the century, there are two droughts which are in the extremely dry class between the years 2092-2093 and 2096-2099.

### 4.2.5. SPEI Results of Region E

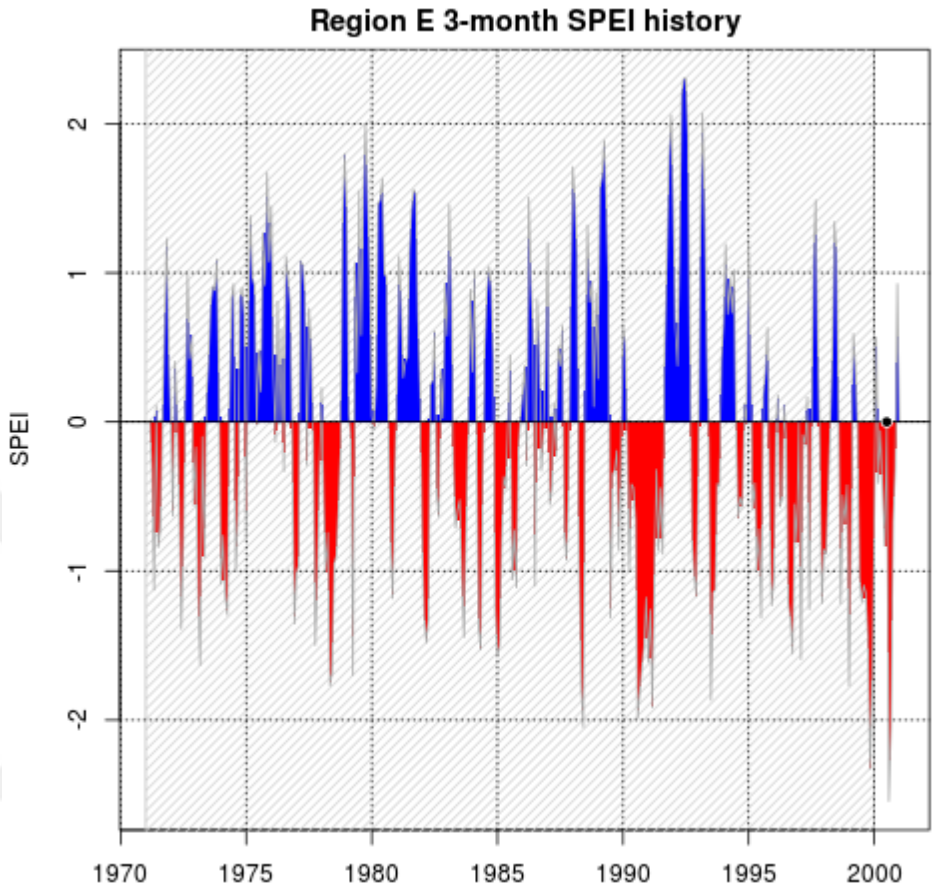


Figure 4.41. 1971-2000 period time series of 3-month SPEI for Region E.

Figure 4.41 shows the 3-month SPEI results of Region E for the historical period. Compared to the 3-month SPI results, the two graphs are very similar both in terms of the duration and the severity of the events. Even though the SPI and SPEI values are different a little bit, the difference is so small that the events are still in the same class of the McKee drought classification. We can see the droughts that Ethiopia had in 1989 and 1999, South Africa had in 1990, Somalia, Kenya, Uganda had in 1999 in the SPEI results as we did in SPI results.

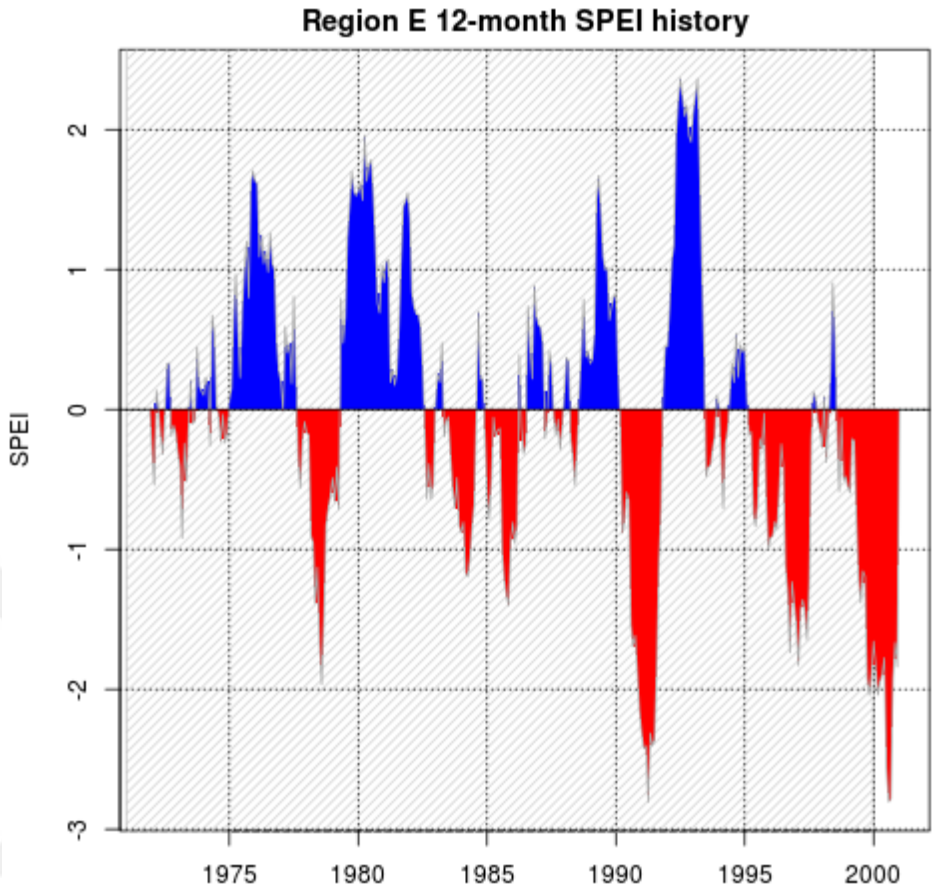


Figure 4.42. 1971-2000 period time series of 12-month SPEI for Region E.

In Figure 4.42 we see the 12-month SPEI results of Region E for the historical period. Compared with the SPI results, again there are lots of similarities in terms of the duration and the severity of the events, however there is one important difference. The wet period around the year 1998 is measured as moderately wet by SPI, while it is measured as near normal by SPEI. That is again due to the fact that SPEI adds the evapotranspiration in the region into account while SPI does not. The rest of the results are very similar between the SPI and SPEI graphs.

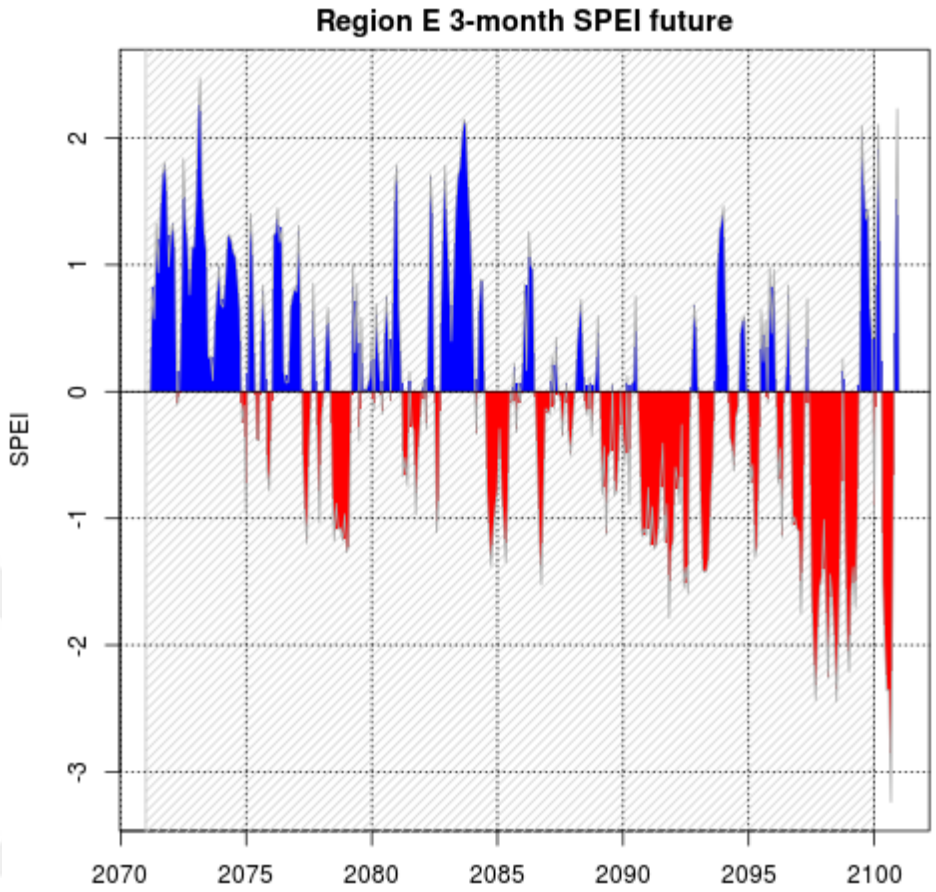


Figure 4.43. 2071-2100 period time series of 3-month SPEI for Region E.

In Figure 4.43 we see the 3-month SPEI results of Region E for the future period. Here in the results SPEI foresees a wet period till the year 2077. However, SPI detects a short term severely dry period around the year 2071. The latter half of the future period seems to be mostly moderately dry and severely dry with only short term interruptions around the year 2095 according to the SPEI results. On the other hand, according to SPI results wet and dry periods fluctuate till the end of the century. At the end of the century, both results show a peak for the drought with the values exceeding -2 for SPEI and reaching almost to -4 for SPI.

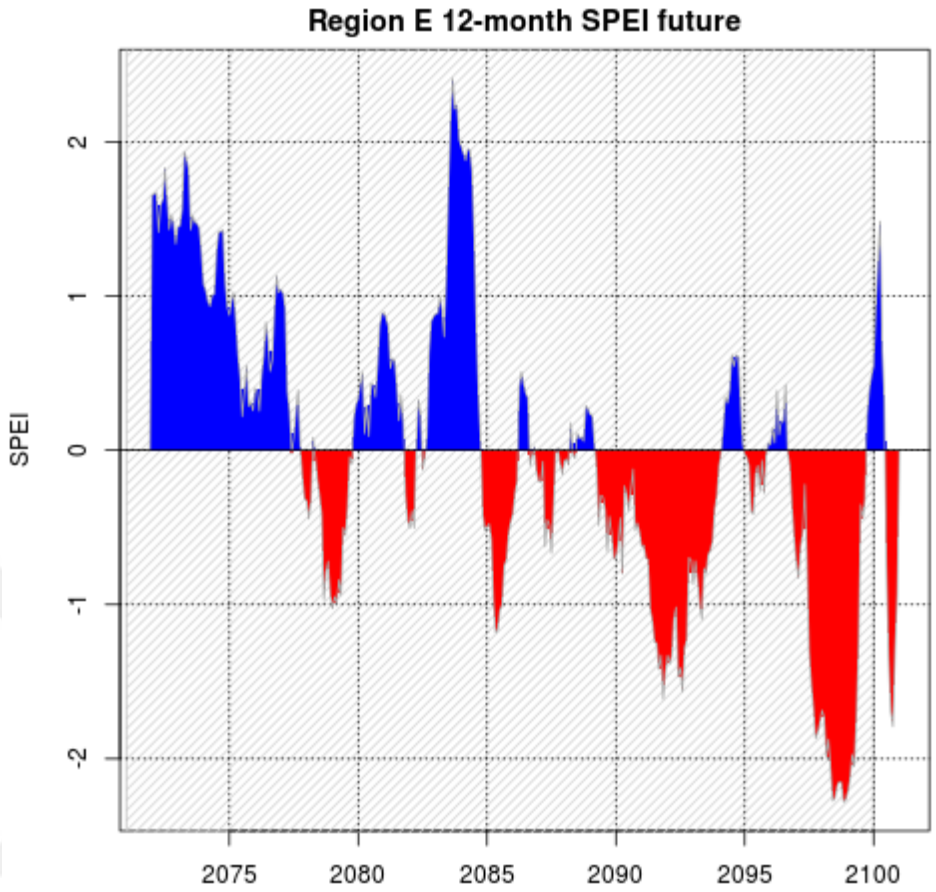


Figure 4.44. 2071-2100 period time series of 12-month SPEI for Region E.

In Figure 4.44 we see the 12-month SPEI results of Region E for the future period. For the first half of the future period, SPEI foresees wetter conditions for Region E. The drought around the years 2078-2079 is longer and it is more severe according to the SPI results. The same is valid for the drought around the years 2085-2086. For the latter half of the future period SPEI foresees drier conditions for the region than the SPI. At the end of the century SPEI value exceeds -3 and the duration of this extremely dry period is around 3 years, which would be very difficult for all livings in the region to adapt.

### 4.2.6. SPEI Results of Region F

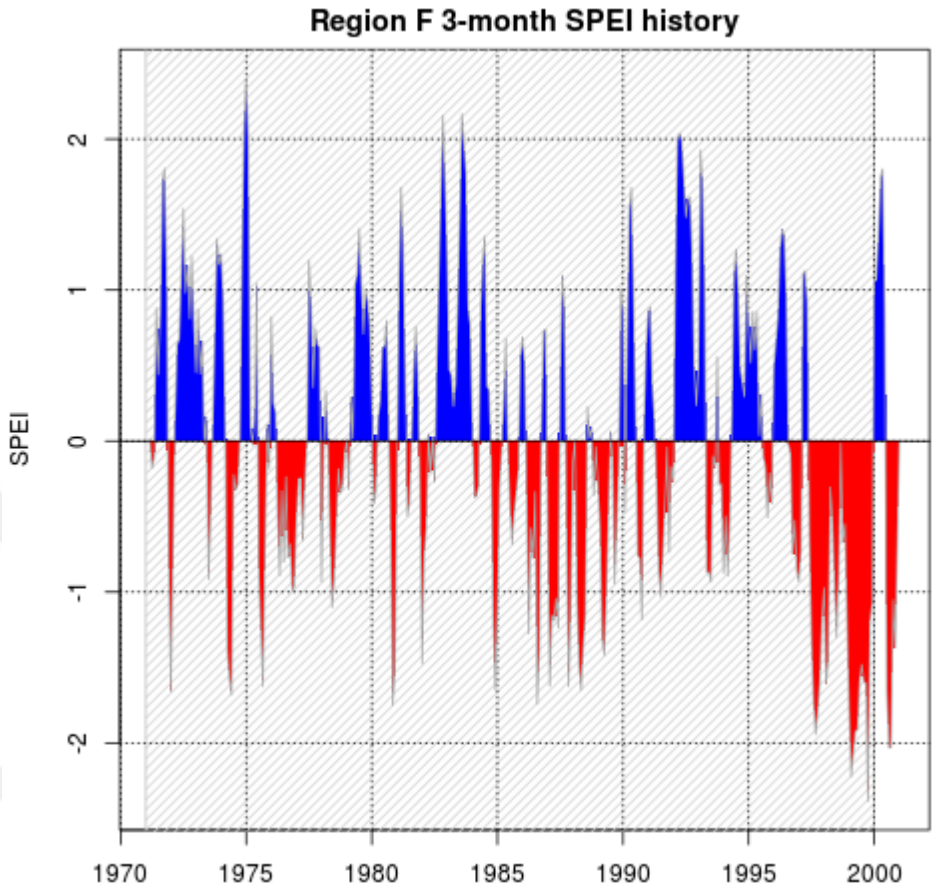


Figure 4.45. 1971-2000 period time series of 3-month SPEI for Region F.

Figure 4.45 shows the 3-month SPEI results of Region F for the period 1971-2000. When compared with the SPI results, the two results are similar and comparable. The main difference between SPI and SPEI results is that the drought events till the year 1995 are longer and more severe in the SPI results, on the other hand, the drought event at the end of the century is longer and more severe in the SPEI results. It should not be forgotten that the Region F contains Arabian Desert, therefore the duration and severity of the wet and dry events are affected by this desert.

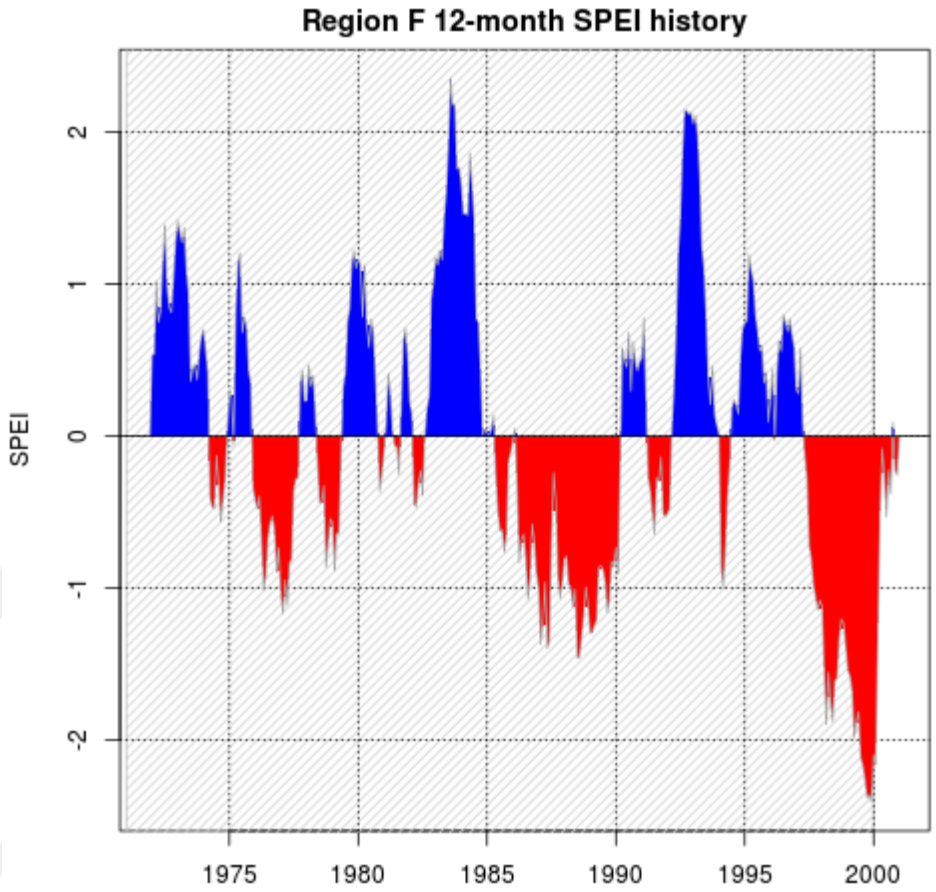


Figure 4.46. 1971-2000 period time series of 12-month SPEI for Region F.

Figure 4.46 shows the 12-month SPEI results of Region F for the period 1971-2000. In the SPI results, the 1975 wet period and 1976-1979 dry period seem longer and more severe. The dry period between the years 1985-1990 has the same duration in both of the results but is a bit more severe in the SPI results. Still, it seems very dangerous in both of the results. In year 1991, SPI detects no drought, instead it foresees a prolonged wet period. The drought around 1994 is severely dry according to SPI results. At the end of the century SPI shows a moderately wet period while there is no such period in the SPEI results.

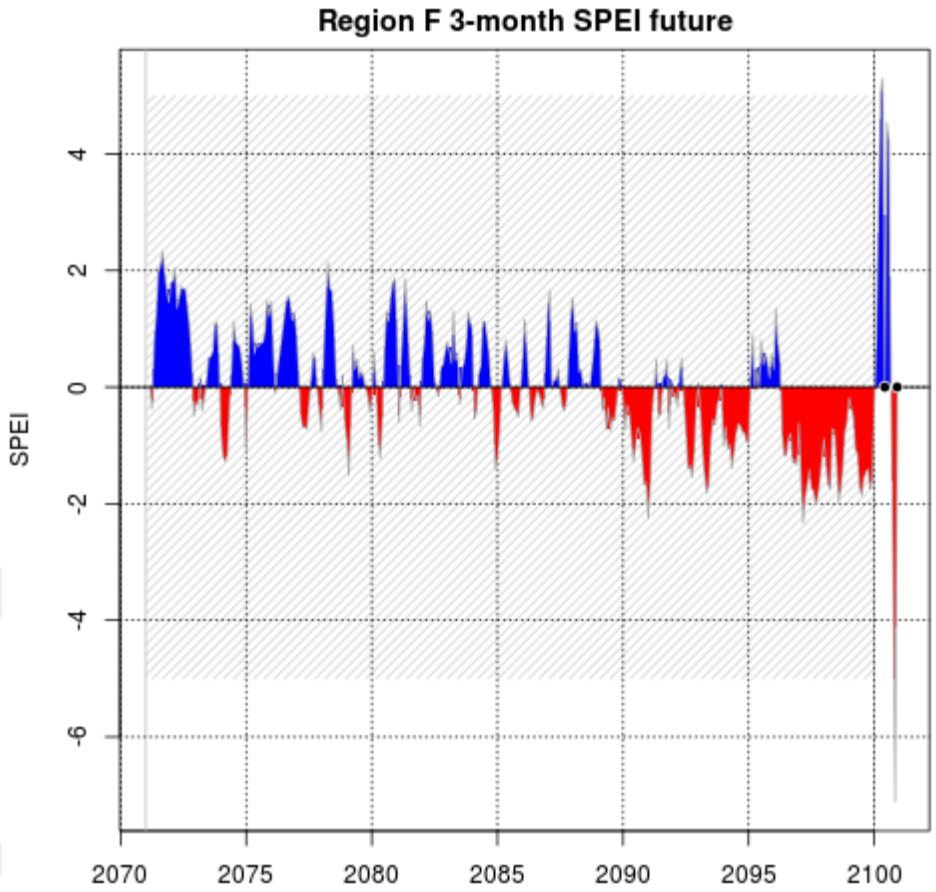


Figure 4.47. 2071-2100 period time series of 3-month SPEI for Region F.

Figure 4.47 shows the 3-month SPEI results of Region F for the period 2071-2100. Until the year 2090, the two results agree to some extent but SPEI shows more wet events compared to SPI. After the year 2090, SPEI shows longer and more severe drought events. The drought at the end of the century seems to last about 4 years and it is severely dry, which is very dangerous for the countries in Region F. In the year 2100, we see a peak, the SPEI value reaches to 4, which is again very dangerous for Region F.

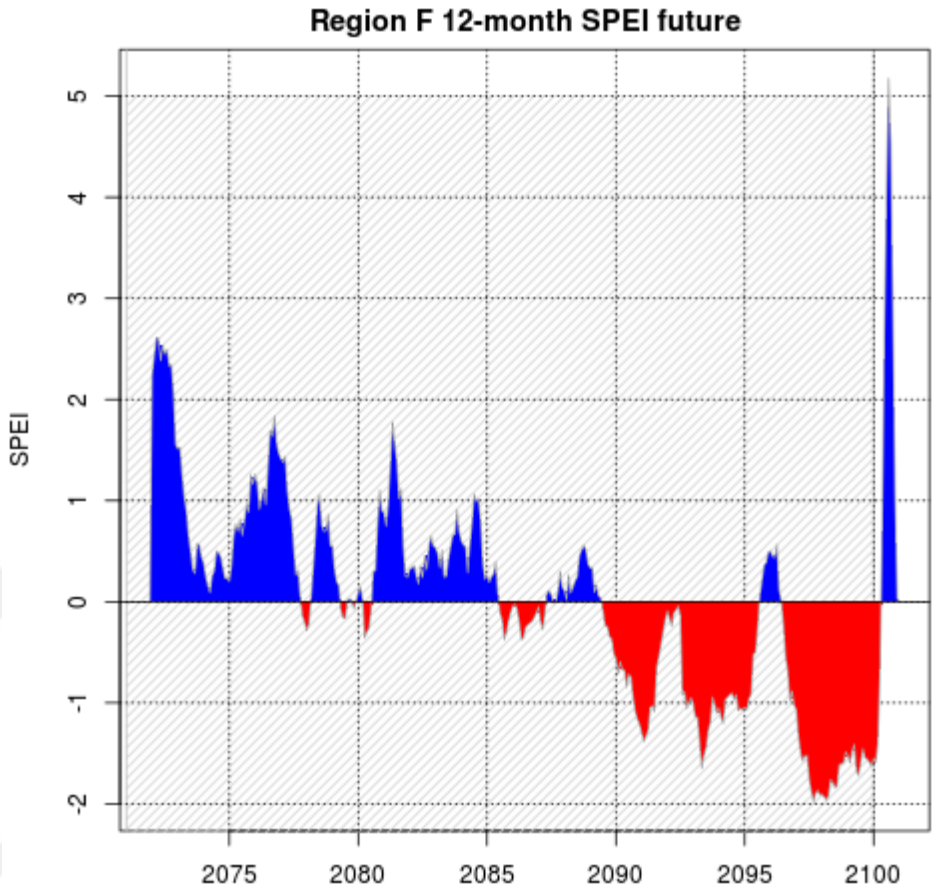


Figure 4.48. 2071-2100 period time series of 12-month SPEI for Region F.

Figure 4.48 shows the 12-month SPEI results of Region F for the future period. For the two results, it is hard to say they agree. For the first half of the future period, SPEI shows a very long wet period lasting for almost 15 years. Then, during the last 10 years of the future period SPEI shows moderately and severely dry periods almost without a break. This of course agrees with the 3-month SPEI results but not with the 12-month SPI results for the same region. SPI shows fluctuating wet and dry periods through the 30 years, almost all of which are long and severe.

# 5. CONCLUSION

In this study, it is aimed to determine the changes of drought occurrence in MENA region by the use of RegCM4. Therefore in the study, simulated data from RegCM4 has been used rather than the observed data. MENA region has been chosen since the region is more prone to drought. MENA has been divided into 6 subregions whose climates are comparable within themselves, and spatial averages of the subregions are taken to be able to draw the SPI and SPEI time series. SPI and SPEI are among the most useful indices to analyze and monitor the drought. SPI is advised by WMO to be used by the scientists, it is simple and uses only precipitation data. It does not account for the evapotranspiration. Therefore, among with SPI, SPEI is also used in this study to be able to see the effect of evapotranspiration. SPEI uses the basis of SPI, however, it takes temperature data as well as precipitation data as input, which ensures the index to account for the effect of temperature on drought development. By the Thornthwaite method PET is calculated and used in the calculation of the SPEI.

In the results of the historical periods, it is seen that SPI and SPEI are consistent with actual events. SPI and SPEI detected many events that caused many lives in the history with the data taken from RegCM. This concludes that the results for the future periods should be taken seriously as well.

In the results, it is seen that SPI and SPEI correlates well with each other most of the time. Since the SPEI accounts for evapotranspiration as well, drought periods were a a bit more drier and wet periods were a bit less wet in the SPEI results in general. The effects of El Niño and La Niña episodes were seen in both of the results. For the future periods, it is seen that MENA region's wet and dry conditions are hazardous, the region has already suffered many life-causing floods and drought conditions, and to be able to avoid more losses of lives, necessary studies have to be done and necessary precautions and measures have to be taken

immediately.

In conclusion, RegCM4 is a very trustworthy regional climate model to simulate future climates, and SPI and SPEI are two very useful indices that can be used by scientists in their studies to analyze and monitor droughts.

# REFERENCES


1. World Meteorological Organization, 7 bis, avenue de la Paix CH-1211 Geneva 2, Switzerland, *Standardized Precipitation Index User Guide*, 2012.

2. Trenberth, K. E., A. Dai, G. Schrier, P. D. Jones, J. Barichivich, K. R. Briffa and J. Sheffield, "Global Warming and Changes in Drought", *Nature Climate Change*, Vol. 4, pp. 17–22, 2014.

3. Guttman, N. B., "On the Sensitivity of Sample L Moments to Sample Size", *Journal of Climate*, Vol. 7, pp. 1026–1029, 1994.

4. Guttman, N. B., "Accepting the Standardized Precipitation Index: a calculation algorithm", *Journal of the American Water Resources Association*, Vol. 32, pp. 311–322, 1999.

5. Neves, J., *Compute SPI Index*, 2012, `https://cran.r-project.org/web/packages/spi/spi.pdf`, accessed at August 2017.

6. Vicente-Serrano, S. M., S. Begueria and J. I. Lopez-Moreno, "A Multiscalar Drought Index Sensitive to Global Warming: The Standardized Precipitation Evapotranspiration Index", *Journal of Climate*, Vol. 23, pp. 1696–1711, 2010.

7. MET Office, *What is Climate Change?*, 2015, `http://www.metoffice.gov.uk/climate-guide/climate-change`, accessed at June 2017.

8. Dahlman, L., *Climate Change: Global Temperature*, April 19, 2017, `https://www.climate.gov/news-features/understandingclimate/climate-change-global-temperature`, accessed at June 2017.

9. Carlowicz, M., "Annual Temperature Anomaly", https://earthobservatory.nasa.gov/Features/WorldOfChange/decadaltemp.php, accessed at May 2017.

10. NASA Climate, *Global Climate Change Vital Signs of the Planet, Sea Level*, https://climate.nasa.gov/vital-signs/sea-level/, accessed at June 2017.

11. NASA Climate, *Global Climate Change Vital Signs of the Planet, Arctic Sea Ice*, https://climate.nasa.gov/vital-signs/land-ice/, accessed at June 2017.

12. NASA Climate, *Global Climate Change Vital Signs of the Planet, Land Ice*, https://climate.nasa.gov/vital-signs/land-ice/, accessed at June 2017.

13. Houghton, J., *Global Warming The Complete Brief*, Cambridge university press, 1990.

14. "International Environmental Data Rescue Organization", http://iedro.org/articles/part-5-energy-for-life/, accessed at July 2017.

15. International Panel on Climate Change, *IPCC Second Assessment Report: Climate Change 1995 Synthesis Report*, 1995, https://www.ipcc.ch/pdf/climate-changes-1995/ipcc-2nd-assessment/2nd-assessment-en.pdf, accessed at June 2017.

16. International Panel on Climate Change, *IPCC Third Assessment Report: Climate Change 2001 Synthesis Report*, 2001, https://www.ipcc.ch/pdf/climate-changes-2001/synthesis-syr/english/front.pdf, accessed at June 2017.

17. International Panel on Climate Change, *IPCC Forth Assessment Report: Climate Change 2007 Synthesis Report*, 2007, https://www.ipcc.ch/pdf/assessment-report/ar4/syr/ar4-syr-full-report.pdf, accessed at June 2017.

18. International Panel on Climate Change, *IPCC Fifth Assessment Report: Climate Change 2007 Synthesis Report*, 2007, https://www.ipcc.ch/pdf/assessment-report/ar4/syr/ar4-syr-full-report.pdf, accessed at June 2017.

19. International Panel on Climate Change, *Sixth Assessment Report Cycle*, 2017, http://www.ipcc.ch/, accessed at June 2017.

20. *New Earth system model of Max Planck Institute for Meteorology*, https://www.mpimet.mpg.de/en/science/models/mpi-esm/, accessed at June 2017.

21. International Center for Theoretical Physics, *RegCM4*, 2010, https://www.ictp.it/research/esp/models/regcm4.aspx, accessed at June 2016.

22. Elguindi, N., X. Bi, F. Giorgi, B. Nagarajan, J. Pal, F. Solmon, S. Rauscher, A. Zakey, T. O'Brien, R. Nogherotto and G. Giuliani, *Regional Climate Model RegCM Reference Manual Version 4.5*, ICTP, 2014.

23. IPCC, *RCP Scenarios*, https://en.wikipedia.org/wiki/Representative_Concentration_Pathways, accessed at May 2017.

24. Riahi, K., A. Grübler and N. Nakicenovica, "Scenarios of long-term socio-economic and environmental development under climate stabilization", *Elsevier*, Vol. 74, pp. 887–935, 2007.

25. Rao, S. and K. Riahi, "The Role of Non-$CO_3$ Greenhouse Gases in Climate Change Mitigation: Long-term Scenarios for the 21st Century", *The Energy Journal*, Vol. 27, pp. 177–200, 2006.

26. Fujino, J., R. Nair, M. Kainuma, T. Masui and Y. Matsuoka, "Multi-gas Mitigation Analysis on Stabilization Scenarios Using Aim Global Model", *The Energy Journal*, Vol. 27, pp. 343–353, 2006.

27. Hijioka, Y., Y. Matsuoka, H. Nishimoto, M. Masui and M. Kainuma, "Global GHG emissions scenarios under GHG concentration stabilization targets", *Journal of Global Environmental Engineering*, Vol. 13, pp. 97–108, 2008.

28. Smith, S. J. and T. Wigley, "Multi-Gas Forcing Stabilization with Minicam", *The Energy Journal*, Vol. 27, pp. 373–391, 2006.

29. Clarke, L., J. Edmonds, H. Jacoby, H. Pitcher, J. Reilly and R. Richels, *Scenarios of Greenhouse Gas Emissions and Atmospheric Concentrations*, U.S. Climate Change Science Program and the Subcommittee on Global Change Research. Department of Energy, Office of Biological and Environmental Research, 2007.

30. Wise, M., K. Calvin, A. Thomson, L. Clarke, B. Bond-Lamberty, R. Sands, S. J. Smith, A. Janetos and J. Edmonds, "Implications of Limiting CO2 Concentrations for Land Use and Energy", *Science*, Vol. 324, pp. 1183–1186, 2009.

31. Van Vuuren, D., B. Eickhout, P. Lucas and M. den Elzen, "Long-Term Multi-Gas Scenarios to Stabilise Radiative Forcing — Exploring Costs and Benefits Within an Integrated Assessment Framework", *The Energy Journal*, Vol. 27, pp. 201–233, 2006.

32. Van Vuuren, D. P., M. J. G. Den Elzen, P. L. Lucas, B. Eickhout, B. J. Strengers, B. Van Ruijven, S. Wonink and R. Van Houdt, "Stabilizing green-

house gas concentrations at low levels: an assessment of reduction strategies and costs", *Climatic Change*, Vol. 81, pp. 119–159, 2007.

33. Riahi, K., S. Rao, V. Krey, C. Cho, V. Chirkov, G. Fischer, G. Kindermann, N. Nakicenovic and P. Rafaj, "RCP 8.5 - A scenario of comparatively high greenhouse gas emissions", *Climatic Change*, Vol. 109, pp. 33–57, 2011.

34. Mckee, T., N. Doesken and J. Kleist, "The Relationship of Drought Frequency and Duration of Time Scales", *8th Conference on Applied Climatology*, pp. 179–184, 1993.

35. Turkes, M. and H. Tatli, "A New Standardized Precipitation Index (New-SPI) For Determining Extreme Droughts and Wet Conditions: Application In Turkey", *Proceedings of the International Fourth Symposium on Atmospheric Sciences*, 2008.

36. Thom, H. C. S., "Some Methods of Climatological Analysis", *World Meteorological Organization Technical Note*, Vol. 81, p. 63, 1996.

37. Mckee, T., N. Doesken and J. Kleist, "Drought Monitoring with Multiple Time Scales", *9th Conference on Applied Climatology*, pp. 233–236, 1995.

38. Wilks, D., *Statistical Methods in the Atmospheric Sciences: An Introduction*, Academic Press, 1995.

39. Guttman, N. B., "Comparing the Palmer Drought Index and the Standardized Precipitation Index", *Journal of the American Water Resources Association*, Vol. 34, pp. 113–121, 1998.

40. Press, W. H., B. P. Flannery, S. A. Teukolsky and W. T. Vetterling, *Gamma Function, Beta Function, Factorials, Binomial Coefficients and Incomplete Gamma Function, Error Function, Chi-Square Probability Function, Cumula-*

*tive Poisson Function. Numerical Recipes in FORTRAN: The Art of Scientific Computing*, Cambridge University Press, 1992.

41. Gonzales, J. and J. B. Valdes, "New Drought Frequency Index: Definition and Comparative Performance Analysis", *Water Resources Research*, Vol. 42, p. W11421, 2006.

42. Keyantash, J. A. and J. A. Dracup, "An Aggregate Drought index: Assessing Drought Severity Based on Fluctuations in the Hydrologic Cycle and Surface Water Storage", *Water Resources Research*, Vol. 40, p. W09304, 2004.

43. Wells, N., S. Goddard and M. J. Hayes, "A Self-Calibrating Palmer Drought Severity Index", *Journal of Climate*, Vol. 17, pp. 2335–2351, 2004.

44. Tsakiris, G., D. Pangalou and H. Vangelis, "Regional Drought Assessment Based on the Reconnaissance Drought Index", *Water Resources Management*, Vol. 21, pp. 821–833, 2007.

45. Palmer, W. C., "Meteorological Droughts", *U.S. Department of Commerce*, Vol. Weather Bureau Research Paper 45, p. 58 pp., 1965.

46. Alley, W. M., "The Palmer Drought Severity Index: Limitations and Applications", *Journal of Applied Meteorology and Climatology*, Vol. 23, pp. 1100–1109, 1984.

47. Karl, T. R., "Some Special Characteristics of Drought Duration in the United States", *Journal of Applied Meteorology and Climatology*, Vol. 22, pp. 1356–1366, 1983.

48. Karl, T. R., "The Sensitivity of the Palmer Drought Severity Index and Palmer's Z-Index to Their Calibration Coefficients Including Potential Evapotranspiration", *Journal of Applied Meteorology and Climatology*, Vol. 25, pp. 77–86,

1986.

49. Alley, W. M., "Spatial Patterns of Drought Frequency and Duration in the contiguous USA Based on Multiple Drought Event Definitions", *International Journal of Climatology*, Vol. 12, pp. 11–24, 1992.

50. Weber, L. and L. C. Nkemdirim, "The Palmer Drought Severity Index Revisited", *Geografiska Annaler*, Vol. 80A, pp. 153–172, 1998.

51. Thornthwaite, C. W., "An Approach Toward a Rational Classification of Climate", *Geographical Review*, Vol. 38, pp. 55–94, 1948.

52. Abramowitz, M. and I. A. Stegun, *Handbook of Mathematical Functions, with Formulas, Graphs, and Mathematical Tables*, Dover Publications, 1965.

53. NASA Jet Propulsion Laboratory, *Regional Climate Model Evaluation System*, `https://rcmes.jpl.nasa.gov/content/cordex`, accessed at July 2017.

54. WCRP Cordex, *Mena Cordex Domain Specifications*, `http://mena-cordex.cyi.ac.cy/index.php/domain-specification`, accessed at July 2017.

55. World Bank, *DataBank World Development Indicators*, `http://databank.worldbank.org/data/reports.aspx?source=2country=MEA`, accessed at May 2017.

56. World Bank, *Annual Report 2016*, `http://www.worldbank.org/en/about/annual-report/regions/mena/`, accessed at May 2017.

57. Heathwaite, A. L., "Multiple stressors on water availabbility at global catchment scales: Understanding human impact on nutrient cycles to protect water quality and water availability in the long term.", *Freshwater Biology*, Vol. 55,

pp. 241–257, 2010.

58. World Bank, *Water in the Arab world: From droughts to flood, building resilience against extremes*, http://www.worldbank.org/en/news/feature/2014/03/20/floods-and-droughts-in-mena/, accessed at May 2017.

59. World Bank, *Water Resources Data*, http://siteresources.worldbank.org/INTMENA/Resources/App-all-Scarcity.pdf, accessed at July 2017.

60. Food and Agriculture Organization of the United Nations, *Total Renewable Water Resources per Capita*, http://www.fao.org/nr/water/aquastat/maps/TRWR.Capeng.pdf, accessed at July 2017.

61. Food and Agriculture Organization of the United Nations, *Aquastat database*, http://www.fao.org/nr/water/aquastat/data/query/index.html?lang=en, accessed at July 2017.

62. Ahrens, C. D., *Essentials of Meteorology*, Thomson Brooks Cole, 2008.

63. Meteoroloji Genel Müdürlüğü, *Türkiye Geneli Yıllık Alansal Yağışları*, https://www.mgm.gov.tr/veridegerlendirme/yillik-toplam-yagis-verileri.aspx, accessed at July 2017.

64. Vries, A. J., E. Tyrlis, D. Edry, S. O. Krichak, B. Steil and J. Lelieveld, "Extreme Precipitation Events in the Middle East: Dynamics of the Active Red Sea Through", *Journal of Geophsical Research*, Vol. 118, pp. 7087–7108, 2013.

65. Elagib, N. A. and M. M. Elhag, "Major Climate Indicators of Ongoing Drought in Sudan", *Journal of Hydrology*, Vol. 409, pp. 612–625, 2011.

66. Masih, I., S. Maskey, F. E. F. Mussa and P. Trambauer, "A Review of Droughts on the African Continent: A Geospatial and Long-Term Perspective", *Hydrology and Earth System Sciences*, Vol. 18, pp. 3635–3649, 2014.

67. Ouassou, A., T. Ameziane and M. Belghiti, "Application of the Drought Management Guidelines in Morocco", *Options Mediterraneennes*, Vol. 58, pp. 343–372, 2007.

68. Touchan, R., K. J. Anchukaitis, D. M. Meko, S. Attalah, C. Baisan and A. Aloui, "Long Term Context for Recent Drought in Northwestern Africa", *Geophysical Research Letters*, Vol. 35, 2008.

69. Food and Agriculture Organization, *Flood Monitoring*, `http://www.faoswalim.org/water/floods/flood-monitoring`, accessed at August 2017.

70. Dartmouth College, *1993 Flood Archive*, `http://www.dartmouth.edu/ floods /Archives/1993sum.htm`, accessed at August 2017.

71. Membery, D., "Monsoon Tropical Cyclones: Part 2", *Weather*, Vol. 57, pp. 246–255, 2002.

72. *List of Arabian Peninsula Tropical Cyclones*, `http://www.0wikipedia.org/index.php?q=aHR0cHM6Ly9lbi53aWtpcGVkaWEub3JnL3dpa2kvTGlzdF9vZl9BcmFiaWFuX1Blbmluc3VsYV90cm9waWNhbF9jeWNsb25lcyNjaXRlX25vdGUtZGF2aWQtMTk`, accessed at August 2017.

# APPENDIX A: R CODES

```
library(SPEI)
setwd("/media/sibel/S/MENA_SPEI_SPI/Sibel/MENA/HIST/output")
data(mena1)
attach(mena1)
names(mena1)
tho <- thornthwaite(TMED,39.00)
png(filename="mena13spei.png")
plot(spei(ts(mena1$PRCP-tho,freq=12,start=c(1971,1)),3,
ref.start=c(1971,1), ref.end=c(2000,1)),main="Region A 3-month SPEI history",)
dev.off()
library(SPEI)
setwd("/media/sibel/S/MENA_SPEI_SPI/Sibel/MENA/HIST/output")
data(mena2)
attach(mena2)
names(mena2)
tho <- thornthwaite(TMED,15.00)
png(filename="mena23spei.png")
plot(spei(ts(mena2$PRCP-tho,freq=12,start=c(1971,1)),3,
ref.start=c(1971,1), ref.end=c(2000,1)),main="Region B 3-month SPEI history",)
dev.off()
library(SPEI)
setwd("/media/sibel/S/MENA_SPEI_SPI/Sibel/MENA/HIST/output")
data(mena3)
attach(mena3)
names(mena3)
tho <- thornthwaite(TMED,30.00)
png(filename="mena33spei.png")
plot(spei(ts(mena3$PRCP-tho,freq=12,start=c(1971,1)),3,
ref.start=c(1971,1), ref.end=c(2000,1)),main="Region C 3-month SPEI history",)
dev.off()
library(SPEI)
setwd("/media/sibel/S/MENA_SPEI_SPI/Sibel/MENA/HIST/output")
data(mena4)
attach(mena4)
names(mena4)
tho <- thornthwaite(TMED,9.50)
png(filename="mena43spei.png")
plot(spei(ts(mena4$PRCP-tho,freq=12,start=c(1971,1)),3,
ref.start=c(1971,1), ref.end=c(2000,1)),main="Region D 3-month SPEI history",)
dev.off()
library(SPEI)
setwd("/media/sibel/S/MENA_SPEI_SPI/Sibel/MENA/HIST/output")
data(mena5)
attach(mena5)
names(mena5)
tho <- thornthwaite(TMED,3.50)
png(filename="mena53spei.png")
plot(spei(ts(mena5$PRCP-tho,freq=12,start=c(1971,1)),3,
ref.start=c(1971,1), ref.end=c(2000,1)),main="Region E 3-month SPEI history",)
dev.off()
```

Figure A.1. R codes for history.

```
library(SPEI)
setwd("/media/sibel/S/MENA_SPEI_SPI/Sibel/MENA/FUT/R")
data(mena1)
attach(mena1)
names(mena1)
tho <- thornthwaite(TMED,39.00)
png(filename="mena13spei.png")
plot(spei(ts(mena1$PRCP-tho,freq=12,start=c(2071,1)),3,
ref.start=c(2071,1), ref.end=c(2100,1)),main="Region A 3-month SPEI future",)
dev.off()
library(SPEI)
setwd("/media/sibel/S/MENA_SPEI_SPI/Sibel/MENA/FUT/R")
data(mena2)
attach(mena2)
names(mena2)
tho <- thornthwaite(TMED,15.00)
png(filename="mena23spei.png")
plot(spei(ts(mena2$PRCP-tho,freq=12,start=c(2071,1)),3,
ref.start=c(2071,1), ref.end=c(2100,1)),main="Region B 3-month SPEI future",)
dev.off()
library(SPEI)
setwd("/media/sibel/S/MENA_SPEI_SPI/Sibel/MENA/FUT/R")
data(mena3)
attach(mena3)
names(mena3)
tho <- thornthwaite(TMED,30.00)
png(filename="mena33spei.png")
plot(spei(ts(mena3$PRCP-tho,freq=12,start=c(2071,1)),3,
ref.start=c(2071,1), ref.end=c(2100,1)),main="Region C 3-month SPEI future",)
dev.off()
library(SPEI)
setwd("/media/sibel/S/MENA_SPEI_SPI/Sibel/MENA/FUT/R")
data(mena4)
attach(mena4)
names(mena4)
tho <- thornthwaite(TMED,9.50)
png(filename="mena43spei.png")
plot(spei(ts(mena4$PRCP-tho,freq=12,start=c(2071,1)),3,
ref.start=c(2071,1), ref.end=c(2100,1)),main="Region D 3-month SPEI future",)
dev.off()
library(SPEI)
setwd("/media/sibel/S/MENA_SPEI_SPI/Sibel/MENA/FUT/R")
data(mena5)
attach(mena5)
names(mena5)
tho <- thornthwaite(TMED,3.50)
png(filename="mena53spei.png")
plot(spei(ts(mena5$PRCP-tho,freq=12,start=c(2071,1)),3,
ref.start=c(2071,1), ref.end=c(2100,1)),main="Region E 3-month SPEI future",)
dev.off()
```

Figure A.2. R codes for future.